CRYSTALLIZATION OF HELIUM-3 AND NEUTRON MATTER FERMIONS IN CONDENSED MATTER PHYSICS

By

MURUNGA GODFREY S.W.,

SC/PH D/TP/004/13

A THESIS SUBMITTED TO THE DEPARTMENT OF PHYSICS AND THE SCHOOL OF SCIENCEUNIVERSITY OF ELDORET IN PARTIAL FULFILLMENT OF THE REQUIREMENTS FOR THE AWARD OF THE DEGREE OF DOCTOR OF PHILOSOPHY IN PHYSICS,UNIVERSITY OF ELDORET,KENYA.

JULY, 2017

DECLARATION

Declaration by the candidate:

This thesis is my original work and has not been presented in any other University. No part of this thesis may be reproduced in any form or by any means without my permission in writing from the author and/or University of Eldoret.

Murunga, Godfrey S. W.,

SC/PH D/TP/004/13

Signature……Date……

Declaration by supervisors:

This thesis has been submitted for examination with our approval as University supervisors.

Prof. Khanna M. Kapil (Professor of Physics, University of Eldoret)

Signature……Date……..

Prof. Tonui K. Joel (Associate Professor of Physics, University of Eldoret)

Signature……Date……

Department of Physics

University of Eldoret

P. O. Box 1125-30100

Eldoret, Kenya.

DEDICATION

This piece of work is dedicated to my ever caring parents: Mr. Mark Wakoli and Mrs. Ann Nakhumicha Wakoli for propping me up for this insurmountable task which has propelled me to achieve this coveted scholarly gains, I developed the right attitude and value for scholarly engagement. Mother and Father may the Almighty God grant you His abundant grace.

ABSTRACT

In this Thesis crystallization of a hard-sphere assembly of fermions with densities ranging from low to high values has been theoretically investigated, the fermions are very close to each other, and the interaction between a pair of fermions is assumed to be a hard-sphere one. The hard-sphere system is a useful first approximation of a many-body system interacting via a potential containing a short-ranged repulsive part, which happens to be even better at very low densities at which the particles experience weakly attractive potential tail surrounding the repulsion, or at very high densities where the repulsion is predominant. However, at intermediate densities, the attractive potential is assumed to play a significant role. Since fermions (degenerate Fermi gas or liquid) such as a gas or liquid ^3He or neutrons satisfy Pauli's exclusion principle which leads to repulsion between two fermions when they try to approach each other to occupy the same quantum (energy) state. A hard-sphere assembly of fermions of densities ranging from very low to very high values was considered to obtain an expression for the energy per particle, E/N. For an N-identical fermion hard-sphere system with ν intrinsic degrees of freedom for each fermion, the total energy, E in terms of other parameters, a generalized London equation was applied to obtain the total energy of the system, and to obtain the saturation density, ρ_s, leading to crystallization of the system. Particle number densities, ρ_s, for low and high densities were $7.11\text{x}10^{27}$ particles/cm^3 and $1.502\text{x}10^{29}$ particles/cm^3 respectively, at which the fermions close pack or crystallize. Transition Temperature T_c at crystallization of fermions was calculated whose value was 19.26K. These results are consistent with experimental and computer-simulated results whose value is 20.3K. Next, similar techniques were applied to neutron stars which were considered as reservoirs of high density fermions. The energy per neutron in a neutron star was calculated for low and high density neutron stars whose findings demonstrated that the energy per neutron for both low and high density of the neutron star increases for a given value of the scattering length, in agreement with experimental results, since increasing the density leads to strong interactions which in turn increase energy of the assembly. This also confirms that under high pressure, the system attains large density and huge amount of energy on crystallization.

Table of Contents

LIST OF TABLES

LIST OF FIGURES

LIST OF SYMBOLS

The following symbols have the defined meaning associated with them, unless otherwise defined in a particular section of this thesis:

H – Hamiltonian

h- Planck's constant

ħ=$\frac{h}{2\pi}$, which is reduced Planck's constant allowing conversion from energy to frequency units

μ - Chemical Potential

T_c - Critical Temperature

ξ_o - Coherence Length

LIST OF ABBREVIATIONS

The following Abbreviations have the defined meaning associated with them, unless otherwise defined in a particular section of this thesis:

ABM – Anderson, Brinkman and Morel

ARPES – Angle Resolved Photoemission Spectroscopy

BCS – Bardeen, Cooper and Shrieffer

BV- Bogoliubov-Valatin

BW- Balian and Wertharmer

DFT – Density Functional Theory

FQHE – Fractional Quantum Hall Effects

FR – Feshback Resonance

IUPAP – International Union of Pure and Applied Physics.

MIT – Massachusetts Institute of Technology, (USA)

MRI – Magnetic Resonance Imaging

NASA – National Aeronautic and Space Agency, (USA)

NMR – Nuclear Magnetic Resonance

QCD – Quantum Chrome-Dynamics

QCP – Quantum Critical Point

QMC- Quantum Monte Carlo

QPT- Quantum Phase Transition

STM – Scanning Tunneling Microscopy

ACKNOWLEDGEMENT

I am very grateful to Prof. K. M. Khanna for his valuable and impeccable guidance during my research work and for high level of patience in reading and offering corrections of the entire thesis. I am indebted to Prof. J. K. Tonui as co-supervisor for his extensive, and technical academic advice and valuable input, to the entire Physics Department fraternity for their encouragement.

Finally, I must appreciate the support, encouragement and enabling environment created and accorded to me by my family, led by my wife, Mrs. Rose Murunga followed by all our children.

CHAPTER ONE

INTRODUCTION

1.1: Background

1.1.1: Condensed Matter Physics

The field of Condensed Matter Physics (CMP) explores the macroscopic and microscopic properties of Matter. Condensed Matter Physicists study how Matter arises from a large number of interacting atoms and electrons, and what physical properties it has as a result of these interactions. Traditionally, CMP is split into "hard" CMP, which studies quantum properties of Matter, and "soft" CMP which studies those properties of Matter for which quantum mechanics plays no role.The Condensed Matter field is considered one of the largest and most versatile sub-fields of study in Physics, primarily due to the diversity of topics and phenomena that are available to study. Breakthroughs in the field of CMP have led to the discovery and use of liquid crystals, modern plastic and composite materials and the discovery of the Bose-Einstein Condensate (Taylor, 2002). Fig. 1.1 is a plot of variation of temperature with pressure depicting the quantum states of CMP system.

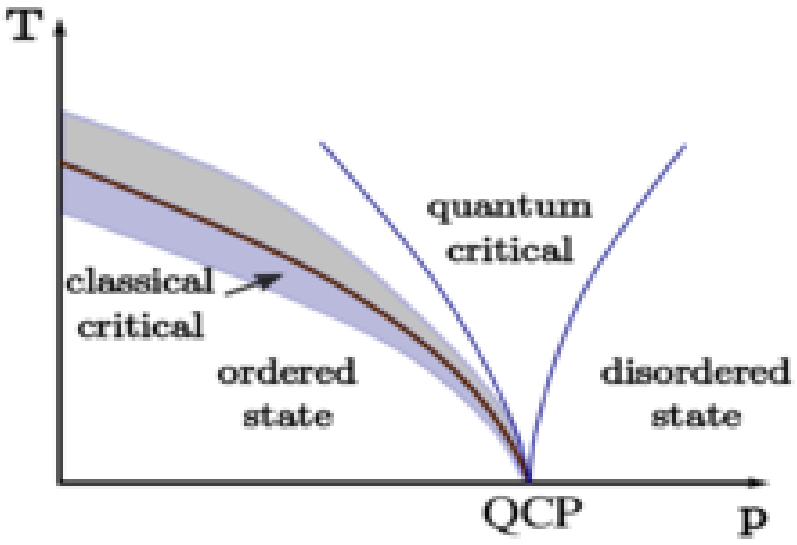

Fig. 1.1: Quantum Phase states of Matter (Kapitza, Allen & Miscener, 1937)

In disordered State, spins of the particles orient in all possible directions, in an ordered state spins of the particles have definite orientation. Classical critical refers to the state at the temperature when classical statistical mechanics is applicable. Quantum critical state is one which is a departure from the classical critical state in which quantum laws are applicable.

Condensed Matter Physics is the branch of Physics that studies the properties of the large collections of atoms that compose both ordinary and exotic materials. Because it deals with properties of Matter at ordinary chemical and thermal energy scales, CMP is the subfield of Physics that has the largest number of direct practical applications, and has a large overlap with chemistry, materials science, and electrical engineering. It is also an intellectually challenging field that is currently producing many advances in fundamental Physics.

The Condensed Matter Physics is particularly strong in the study of quantum materials, which reveals unexpected and exotic behaviour when subjected to extreme conditions such as low temperature and/or high pressure. Physical properties of these materials are studied using various theoretical methods and experimental techniques, such as Scanning Tunneling Microscopy (STM), quantum oscillations, neutron/x-ray scattering.

CMP is a branch of Physics that deals with the physical properties of Condensed phases of Matter (Taylor, 2002). Condensed Matter Physicists seek to understand the behavior of these phases by using physical laws. In particular, they include the laws of Quantum Mechanics, Electromagnetism and Statistical Mechanics.

The most familiar Condensed phases are solids and liquids while more exotic Condensed phases include the superconducting phase exhibited by certain materials at low temperature, the ferromagnetic and anti-ferromagnetic phases of spins on atomic lattices, and the Bose–Einstein condensate found in cold atomic systems. The study of CMP involves measuring various material properties via experimental probes along with

using techniques of Theoretical Physics to develop mathematical models that help in understanding physical behavior.

The diversity of systems and phenomena available for study makes CMP the most active field of contemporary Physics: one third of all American Physicists identify themselves as Condensed Matter Physicists (Cohen, 2008), and the Division of CMP is the largest division at the American Physical Society. The field overlaps with chemistry, materials science, and nanotechnology, and relates closely to Atomic Physics and Bio Physics. Theoretical CMP shares important concepts and techniques with theoretical particle and nuclear Physics (Cohen, 2008).

A variety of topics in Physics such as crystallography, metallurgy, elasticity, magnetism, etc., were treated as distinct areas until the 1940s, when they were grouped together as *Solid State Physics*. Around the 1960s, the study of physical properties of liquids was added to this list, forming the basis for the new, related specialty of CMP. According to Physicist Philip Warren Anderson, the term was coined by him and Volker Heine, when they changed the name of their group at the Cavendish Laboratories, Cambridge from "Solid state theory" to "Theory of Condensed Matter" in 1967, as they felt it did not exclude their interests in the study of liquids, nuclear Matter and so on. Although (Anderson & Heine, 1967) helped popularize the name "Condensed Matter", it had been present in Europe for some years, most prominently in the form of a journal published in English, French, and German by Springer-Verlag titled *Physics of Condensed Matter*, which was launched in 1963. The funding environment and Cold War politics of the 1960s and 1970s were also factors that lead some Physicists to prefer the name "CMP", which emphasized the commonality of scientific problems encountered by Physicists working on solids, liquids, plasmas, and other complex Matter, over "Solid State Physics", which was often associated with the industrial applications of metals and semiconductors. The Bell Telephone Laboratories was one of the first institutes to conduct a research program in CMP.

References to "Condensed" state can be traced to earlier sources. For example, in the introduction to his 1947 book "Kinetic Theory of Liquids" (Frenkel, 1947). Yakov

Frenkel proposed that "The kinetic theory of liquids must accordingly be developed as a generalization and extension of the kinetic theory of solid bodies. As a Matter of fact, it would be more correct to unify them under the title of 'Condensed bodies'. By 1908, (Dewar & Kamerlingh, 1908) were successfully able to liquefy hydrogen and then newly discovered helium, respectively.

One of the first studies of Condensed states of Matter was by English chemist Humphry Davy, in the first decades of the nineteenth century. Davy observed that of the forty chemical elements known at the time, twenty-six had metallic properties such as lustre, ductility and high electrical and thermal conductivity. This indicated that the atoms in Dalton's atomic theory were not indivisible as Dalton claimed, but had inner structure. Davy further claimed that elements that were then believed to be gases, such as nitrogen and hydrogen could be liquefied under the right conditions and would then behave as metals (Davy, 1839).

(Faraday, 1823) then an assistant in Davy's lab, successfully liquefied chlorine and went on to liquefy all known gaseous elements, with the exception of nitrogen, hydrogen and oxygen. Shortly after, in 1869, Irish chemist Thomas Andrews studied the phase transition from a liquid to a gas and coined the term critical point to describe the condition where a gas and a liquid were indistinguishable as phases, and Dutch Physicist Johannes van der Waals supplied the theoretical framework which allowed the prediction of critical behavior based on measurements at much higher temperatures (Atkins, 2009). Paul Drude in 1900 proposed the first theoretical model for a classical electron moving through a metallic solid (Cohen, 2008). Drude's model described properties of metals in terms of a gas of free electrons, and was the first microscopic model to explain empirical observations such as the Wiedemann–Franz law (Kittel & Hoddeson, 1996). However, despite the success of Drude's free electron model, it had one notable problem, in that it was unable to correctly explain the electronic contribution to the specific heat and magnetic properties of metals, as well as the temperature dependence of resistivity at low temperatures (Kragh, 2002).

In 1911, three years after helium was first liquefied, Onnes working at University of Leiden discovered superconductivity in mercury, when he observed the electrical resistivity of mercury to vanish at temperatures below a certain value T_c. The phenomenon completely surprised the best theoretical Physicists of the time, and it remained unexplained for several decades (Slichter, 2012). Albert Einstein, in 1922, said regarding contemporary theories of superconductivity that "with our far-reaching ignorance of the quantum mechanics of composite systems I am very far from being able to compose a theory out of these vague ideas".

1.1.2: Fermions

There are two types of particles in nature; one type is known as fermions and the other type is called bosons.Bosons give rise to the classical Maxwell- Boltzmann gas of distinguishable particles, whereas fermions lead to either Bose-Einstein or Fermi-Dirac statistics depending upon the physical properties of the system such as spin.The basic building blocks of an atom (electron, neutron, photon) are all fermions.

The atom as a whole can be either a boson or a fermion, depending on the total number of electrons and nucleons. Fermionic superfluidity has been achieved using the attractive interaction required for Cooper pairing, and the attractive interaction is provided by direct scattering between fermions in different spin states.

Fermions obey anti-commutation relations and have total spin equal to ½; they obey Pauli Exclusion Principle.

1.1.3: Crystallization of fermions

Crystallization refers to a fermionic system in which the fermions are close to each other and the interaction between a pair of fermions is intense. In general reduction of temperature followed by the application of large external pressure can lead to freezing and or crystallization of fermions.

1.1.4: Modern Many Body Physics

Today some Physicists are working to understand high-temperature superconductivity using the Anti-desitter Space/ Conformal Field Theory (AdS/ CFT) correspondence (Merali, 2011), which has provided a new tool to investigate strongly correlated systems in CMP. The Sommerfeld model and spin models for ferromagnetism illustrated the successful application of quantum mechanics to Condensed Matter problems in the 1930s. However, there still were several unsolved problems, most notably the description of superconductivity and the Kondo effect (Coleman, 2003). After World War II, several ideas from quantum field theory were applied to Condensed Matter problems. These included recognition of collective modes of excitation of solids and the important notion of a quasiparticle. Russian Physicist Lev Landau used the idea for the Fermi liquid theory wherein low energy properties of interacting fermion systems were given in terms of what are now known as Landau-quasiparticles (Coleman, 2003). Landau also developed a mean field theory for continuous phase transitions, which described ordered phases as spontaneous breakdown of symmetry. The theory also introduced the notion of an order parameter to distinguish between ordered phases (Kadanoff, 2009). Eventually in 1957, John Bardeen, Leon Cooper and John Schrieffer developed the so-called BCS theory of superconductivity, based on the discovery that arbitrarily small attraction between two electrons of opposite spin and momenta mediated by phonons in the lattice can give rise to a bound state called a Cooper pair (Coleman, 2011). The coherence length, ξ of the Cooper pair gives the length of the Cooper pair state in space. It refers to the physical size of the single Cooper pair. Fig 1.2 shows components of the Hall resistivity as a function of the external magnetic field

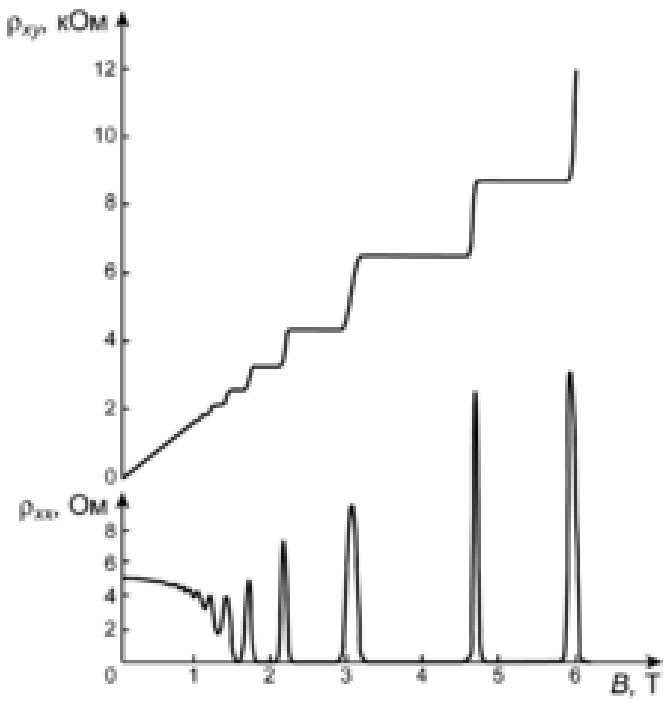

Fig. 1.2: The quantum Hall effect: (Von, 1985).

The study of phase transition and the critical behavior of observables, known as critical phenomena, was a major field of interest in the 1960s (Fisher, 1998). Leo Kadanoff, Benjamin Widom and Michael Fisher developed the ideas of critical exponents and scaling. These ideas were unified by Kenneth Wilson in 1972, under the formalism of the renormalization group in the context of quantum field theory (Fisher, 1998).

The quantum Hall Effect was discovered by Klaus von Klitzing in 1980 when he observed the Hall conductance to be integer multiples of a fundamental constant. The effect was observed to be independent of parameters such as the system size and impurities (Von, 1985). In 1981, (Laughlin proposed a theory explaining the unanticipated precision of the integral plateau. It also implied that the Hall conductance can be characterized in terms of a topological invariable called Chern number (David, 1998). Shortly after, in 1982, Horst Störmer and Daniel Tsui observed the fractional quantum Hall effect where the conductance was now a rational multiple of a constant. Laughlin, in 1983, realized that this was a consequence of quasiparticle interaction in the

Hall states and formulated a variational solution, known as the Laughlin wave function (Wen, 1992). The study of topological properties of the fractional Hall effect remains an active field of research.

In1986, Karl Müller and Johannes Bednorz discovered the first high temperature superconductor, a material which was superconducting at temperatures as high as 50 Kelvin. It was realized that the high temperature superconductors are examples of strongly correlated materials where the electron–electron interactions play an important role (Quintanilla, *et. al.,* 2012). A satisfactory theoretical description of high-temperature superconductors is still not known and the field of strongly correlated materials continues to be an active research topic.

In 2009, David Field and researchers at Aarhus University discovered spontaneous electric fields when creating prosaic films of various gases. This has more recently expanded to form the research area of spontelectrics (Field, *et. al.*, 2013).

In 2012 several groups released preprints which suggest that samarium hexaboride has the properties of a topological insulator in accordance with the earlier theoretical predictions (Dzero, 2009). Since samarium hexaboride is an established Kondo insulator, i.e. a strongly correlated electron material, the existence of a topological surface state in this material would lead to a topological insulator with strong electronic correlations.

1.1.5: Theoretical Condensed Matter Physics

Theoretical CMP involves the use of theoretical models to understand properties of states of Matter. These include models to study the electronic properties of solids, such as the Drude model, the Band structure and the density functional theory. Theoretical models have also been developed to study the Physics of phase transitions, such as the Ginzburg–Landau theory, critical exponents and the use of mathematical techniques of quantum field theory and the renormalization group. Modern theoretical studies involve the use of numerical computation of electronic structure and mathematical tools to understand phenomena such as high-temperature superconductivity, topological phases and gauge symmetries.

1.1.6: Emergence

Theoretical understanding of CMP is closely related to the notion of emergence, wherein complex assemblies of particles behave in ways dramatically different from their individual constituents (Coleman, 2011). For example, a range of phenomena related to high temperature superconductivity are not well understood, although the microscopic Physics of individual electrons and lattices is well known. Similarly, models of Condensed Matter systems have been studied where collective excitations behave like photons and electrons, thereby describing electromagnetism as an emergent phenomenon. Emergent properties can also occur at the interface between materials: one example is the lanthanum-aluminate-strontium-titanate interface, where two non-magnetic insulators are joined to create conductivity, superconductivity, and ferromagnetism.

1.1.7: Electronic theory of solids

The metallic state has historically been an important building block for studying properties of solids (Neil & Mervin, 1976). The first theoretical description of metals was given by Paul Drude in 1900 with the Drude model, which explained electrical and thermal properties by describing a metal as an ideal gas of then-newly discovered electrons. He was able to derive the empirical Wiedemann-Franz law and get results in close agreement with the experiments (Hoddeson, 1992). This classical model was then improved by Arnold Sommerfeld who incorporated the Fermi–Dirac statistics of electrons and was able to explain the anomalous behavior of the specific heat of metals in the Wiedemann–Franz law (Hoddeson, 1992). In 1912, The structure of crystalline solids was studied by Max von Laue and Paul Knipping, when they observed the X-ray diffraction pattern of crystals, and concluded that crystals get their structure from periodic lattices of atoms (Hoddeson, 1992). In 1928, Swiss Physicist Felix Bloch provided a wave function solution to the Schrödinger equation with a periodic potential, called the Bloch wave (Han, 2010).

Calculating electronic properties of metals by solving the many-body wave function is often computationally hard, and hence, approximation techniques are necessary to obtain

meaningful predictions (Perdew, 2010). The Thomas–Fermi theory, developed in the 1920s, was used to estimate system energy and electronic density by treating the local electron density as a variational parameter. Later in the 1930s, Douglas Hartree, Vladimir Fock and John Slater developed the so-called Hartree–Fock wave function as an improvement over the Thomas–Fermi model. The Hartree–Fock method accounted for exchange statistics of single particle electron wave functions. In general, it's very difficult to solve the Hartree–Fock equation. Only the free electron gas case can be solved exactly (Neil, 1976). Finally in 1964–65, Walter Kohn, Pierre Hohenberg and Lu Jeu Sham proposed the density functional theory which gave realistic descriptions for bulk and surface properties of metals. The density functional theory (DFT) has been widely used since the 1970s for band structure calculations of variety of solids (Perdew, 2010).

1.1.8: Phase transition

Phase transition refers to the change of phase of a system, which is brought about by change in an external parameter such as temperature. Classical phase transition occurs at finite temperature when the order of the system was destroyed. For example, when ice melts and becomes water, the ordered crystal structure is destroyed. In quantum phase transitions, the temperature is set to absolute zero, and the non-thermal control parameter, such as pressure or magnetic field, causes the phase transitions when order is destroyed by quantum fluctuations originating from the Heisenberg uncertainty principle. Here, the different quantum phases of the system refer to distinct ground states of the Hamiltonian. Understanding the behavior of quantum phase transition is important in the difficult tasks of explaining the properties of rare-earth magnetic insulators, high-temperature superconductors and other substances.

There are two classes of phase transitions: first-order transitions and continuous transitions. For the continuous transitions, the two phases involved do not co-exist at the transition temperature, also called critical point. Near the critical point, systems (undergo) display critical behavior, wherein several of their properties such as correlation length, specific heat and susceptibility diverge exponentially. These critical phenomena pose serious challenges to Physicists because normal macroscopic laws are no longer

valid in the region and novel ideas and methods have to be invented to find the new laws that can describe the system.

The simplest theory that can describe continuous phase transitions is the Ginzburg–Landau theory, which works in the so-called mean field approximation. However, it can only roughly explain continuous phase transition for ferroelectrics and type I superconductors which involves long range microscopic interactions. For other types of systems that involve short range interactions near the critical point, a better theory is needed (Malcolm, 2013).

Near the critical point, the fluctuations happen over broad range of size scales while the feature of the whole system is scale invariant. Renormalization group techniques successively average out the shortest wavelength fluctuations in stages while retaining their effects into the next stage. Thus, the changes of a physical system as viewed at different size scales can be investigated systematically. The techniques, together with powerful computer simulation, contribute greatly to the explanation of the critical phenomena associated with continuous phase transition.

1.1.9: Experimental Condensed Matter Physics

Experimental CMP involves the use of experimental probes to try to discover new properties of materials. Experimental probes include effects of electric and magnetic fields, measurement of response functions, transport properties and thermometry (Richardson,1988). Commonly used experimental techniques include spectroscopy, with probes such as X-rays, infrared light and inelastic neutron scattering; study of thermal response, such as specific heat and measurement of transport via thermal and heat conduction.

1.1.10: Scattering

Several Condensed Matter experiments involve scattering of an experimental probe, such as X-ray, optical photons, neutrons, etc., on constituents of a material. The choice of scattering probe depends on the observation energy scale of interest. Visible light has energy on the scale of 1 eV and is used as a scattering probe to measure variations in

material properties such as dielectric constant and refractive index. X-rays have energies of the order of 10 keV and hence are able to probe atomic length scales, and are used to measure variations in electron charge density (Chaikin & Lubensky, 1995).

Neutrons can also probe atomic length scales and are used to study scattering of nuclei and electron spins and magnetization (as neutrons themselves have spin but no charge). Coulomb and Mott scattering measurements can be made by using electron beams as scattering probes (Chaikin & Lubensky, 2012). Similarly, positron annihilation can be used as an indirect measurement of local electron density. Laser spectroscopy is an excellent tool for studying the microscopic properties of a medium, for example, to study forbidden transitions in media with nonlinear optical spectroscopy.

1.1.11: External magnetic fields

In experimental CMP, external magnetic fields act as thermodynamic variables that control the state, phase transitions and properties of material systems (Committee IUPAP, 2004). Nuclear magnetic resonance (NMR) is a technique by which external magnetic fields can be used to find resonance modes of individual electrons, thus giving information about the atomic, molecular and bond structure of their neighborhood. NMR experiments can be made in magnetic fields with strengths up to 60Tesla. Higher magnetic fields can improve the quality of NMR measurement data (Moulton, 2006). Quantum oscillations is another experimental technique where high magnetic fields are used to study material properties such as the geometry of the Fermi surface (Doiron, 2007). High magnetic fields will be useful in experimentally testing of the various theoretical predictions such as the quantized magneto-electric effect, image magnetic monopole, and the half-integer quantum Hall effect (National Research Council, ME, 2013).

1.1.12: Cold Atom Trapping

Cold atom trapping in optical lattices is an experimental tool commonly used in Condensed Matter as well as atomic, molecular, and optical Physics. The technique involves using optical lasers to create an interference pattern, which acts as a "lattice", in which ions or atoms can be placed at very low temperatures. Cold atoms in optical

lattices are used as "quantum simulators", that is, they act as controllable systems that can model behavior of more complicated systems, such as frustrated magnets (Buluta & Nori, 2009). In particular, they are used to engineer one-, two- and three-dimensional lattices for a Hubbard model with pre-specified parameters, and to study phase transitions for anti-ferromagnetic and spin liquid ordering (Greiner & Jaksch, 2008).

In 1995, a gas of rubidium atoms cooled down to a temperature of 170 nK was used to experimentally realize the Bose–Einstein condensate, a novel state of Matter originally predicted by S. N. Bose and Albert Einstein, wherein a large number of atoms occupy a single quantum state; or zero-momentum state (ZMS) is macroscopically occupied.

1.1.13: Solid-state Physics

Solid-state Physics is the study of rigid Matter, or solids, through methods such as quantum mechanics, crystallography, electromagnetism, and metallurgy. It is the largest branch of CMP. Solid-state Physics studies how the large-scale properties of solid materials result from their atomic-scale properties. Thus, solid-state Physics forms a theoretical basis of materials science. It also has direct applications, for example in the technology of transistors and semiconductors.

Solid materials are formed from densely packed atoms, which interact intensely. These interactions produce the mechanical e.g. hardness and elasticity), thermal, electrical, magnetic and optical properties of solids. Depending on the material involved and the conditions in which it was formed, the atoms may be arranged in a regular, geometric pattern (crystalline solids, which include metals and ordinary water ice) or irregularly (an amorphous solid such as common window glass).

The bulk of solid-state Physics, as a general theory, is focused on crystals. Primarily, this is because the periodicity of atoms in a crystal — its defining characteristic — facilitates mathematical modeling. Likewise, crystalline materials often have electrical, magnetic, optical, or mechanical properties that can be exploited for engineering purposes.

The forces between the atoms in a crystal can take a variety of forms. For example, in a crystal of sodium chloride (common salt), the crystal is made up of ionic sodium and chlorine, and held together with ionic bonds. In others, the atoms share electrons and form covalent bonds. In metals, electrons are shared amongst the whole crystal in metallic bonding. Finally, the noble gases do not undergo any of these types of bonding. In solid form, the noble gases are held together with van der Waals forces resulting from the polarization of the electronic charge cloud on each atom. The differences between the types of solid result from the differences between their bonding.

The physical properties of solids have been common subjects of scientific inquiry for centuries, but a separate field going by the name of solid-state Physics did not emerge until the 1940s, in particular with the establishment of the Division of Solid State Physics (DSSP) within the American Physical Society. The DSSP catered to industrial Physicists, and solid-state Physics became associated with the technological applications made possible by research on solids. By the early 1960s, the DSSP was the largest division of the American Physical Society (Hoddeson, 1992).

Large communities of solid state Physicists also emerged in Europe after World War II, in particular in England, Germany, and the Soviet Union (Hoffman, 2013). In the United States and Europe, solid state Physics became a prominent field through its investigations into semiconductors, superconductivity, nuclear magnetic resonance, and diverse other phenomena. During the early Cold War, research in Solid State Physics was often not restricted to solids, which led some Physicists in the 1970s and 1980s to found the field of CMP, which organized around common techniques used to investigate solids, liquids, plasmas, and other complex Matter.

Today, solid-state Physics is broadly considered to be the subfield of CMP that focuses on the properties of solids with regular crystal lattices.

1.1.14: Crystal structure and properties

Many properties of materials are affected by their crystal structure. This structure can be investigated using a range of crystallographic techniques, including X-ray crystallography, neutron diffraction and electron diffraction.

The sizes of the individual crystals in a crystalline solid material vary depending on the material involved and the conditions when it was formed. Most crystalline materials encountered in everyday life are polycrystalline, with the individual crystals being microscopic in scale, but macroscopic single crystals can be produced either naturally (e.g. diamonds) or artificially.

Real crystals feature defects or irregularities in the ideal arrangements, and it is these defects that critically determine many of the electrical and mechanical properties of real materials.

1.1.15: Electronic properties

Properties of materials such as electrical conduction and heat capacity are investigated by Solid State Physics. An early model of electrical conduction was the Drude model, which applied kinetic theory to the electrons in a solid. By assuming that the material contains immobile positive ions and an "electron gas" of classical, non-interacting electrons that are mobile, the Drude model was able to explain electrical and thermal conductivity and the Hall effect in metals, although it greatly overestimated the electronic heat capacity.

Arnold Sommerfeld combined the classical Drude model with quantum mechanics in the free electron model (or Drude-Sommerfeld model). Here, the electrons are modelled as a Fermi gas, a gas of particles which obey the quantum mechanical Fermi–Dirac statistics. The free electron model gave improved predictions for the heat capacity of metals, however, it was unable to explain the existence of insulators.

The nearly free electron model is a modification of the free electron model which includes a weak periodic perturbation meant to model the interaction between the conduction electrons and the ions in a crystalline solid. By introducing the idea of

electronic bands, the theory explains the existence of conductors, semiconductors and insulators.

The nearly free electron model rewrites the Schrödinger equation for the case of a periodic potential. The solutions in this case are known as Bloch states. Since Bloch's theorem applies only to periodic potentials, and since unceasing random movements of atoms in a crystal disrupt periodicity, this use of Bloch's theorem is only an approximation, but it has proven to be a tremendously valuable approximation, without which most solid-state Physics analysis would be intractable. Deviations from periodicity are treated by quantum mechanical perturbation theory.

1.1.16: Superconductivity

Superconductivity is the property of complete disappearance of electrical resistance in solids when they are cooled below a characteristic temperature. This temperature is called transition temperature or critical temperature, T_c, and at this temperature a material changes from normal state to the superconducting state when the specific heat and entropy also change.

1.1.17: No scattering, no resistance

The formation of collective state of Cooper pairs takes place at $T < T_c$. In the collective bound state the Cooper pairs do not scatter from the lattice and the conductivity of superconductor is infinitely large. Scattering of electrons from the lattice atoms require a change of state of electron. In the superconductive state the current carrying species is the electron pair. For the Cooper pair to scatter it would have to change its state (like an electron in normal metal). However, the Cooper pair is coupled to a large number of other Cooper pairs and so the whole collective of Cooper pairs would have to be involved in scattering at once. This does not happen, and therefore there is no scattering of Cooper pairs, there is no resistance and therefore the conductivity is infinite, fig. 1.3

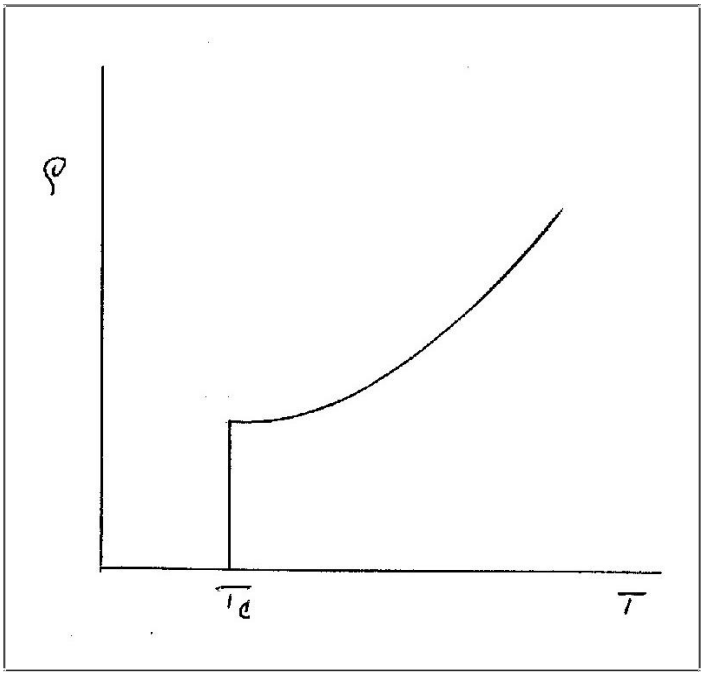

Fig1.3: Graph of conductivity against absolute temperature for a superconductor (Subraanyam, & Raja, 1989)

Superconductive state of mercury (T_c=4.15 K) was discovered by the Dutch physicist Heike Kamerlingh Onnes in 1911, several years after the discovery of liquid helium.

1.1.18: Cooper pairs and BCS theory

As a prelude to the description of the superfluid phases of ^{3}He, I briefly review the theory of conventional superconductivity in metals Bardeen, Cooper and Schrieffer (Bardeen, et.al., 1957). Cooper showed that a pair of electrons of opposite momenta lying outside the Fermi surface in the presence of (even weak) attractive interactions is unstable towards the formation of a bound state known as Cooper pairs. In the full BCS theory, this idea is exploited to variationally find the ground state of such a system with pairs of electrons of opposite spin (spin singlet) and opposite momenta. The attractive interaction is provided by coupling between electrons and lattice vibrations (phonons).

The ground state of the BCS superconductor is characterized by the formation of an energy gap at the Fermi level in the superconducting state which means that quasi-particle excitations of the ground state have a finite lower bound in energy. The gap is thus a measure of the strength of the superconducting pairing. The quasi-particle energy spectrum is given by

$$E(k) = [\varepsilon^2(k) + \Delta^2]^{1/2} \quad (1.1)$$

where ε(k) is the kinetic energy of the electron measured with respect to the Fermi level and Δ is the superconducting energy gap.

1.1.19: Mechanism of superconductivity

Isotope effect, T_c depends on the mass of atoms

$$T_c \alpha \frac{1}{\sqrt{mass\ of\ atoms\ constituting\ the\ crystal\ lattice}}$$

Interaction between electrons and lattice atoms is critical for the existence of superconductive state. Good conductors (weak scattering from the lattice) are poor superconductors (low T_c).

Electrons on their flight through the lattice cause lattice deformation (electrons attract the positively charged lattice atoms and slightly displace them) which results in a trail of positively charged region, as illustrated in fig. 1.4. This positively charged region of lattice atoms attracts another electron and provides for electron-electron coupling.

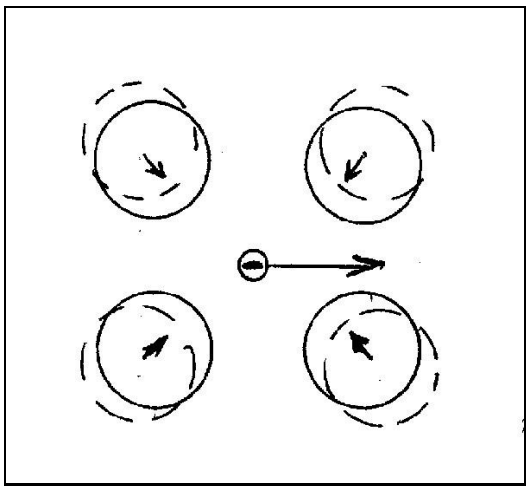

Fig. 1.4: Mechanism of superconductivity

Electron pairs, and not single electrons, are charge carriers in superconductors. As an electron moves through the crystal, it affects the positions of the ions producing a potential which is attractive to a second electron moving in the opposite direction to the first, fig. 1.5

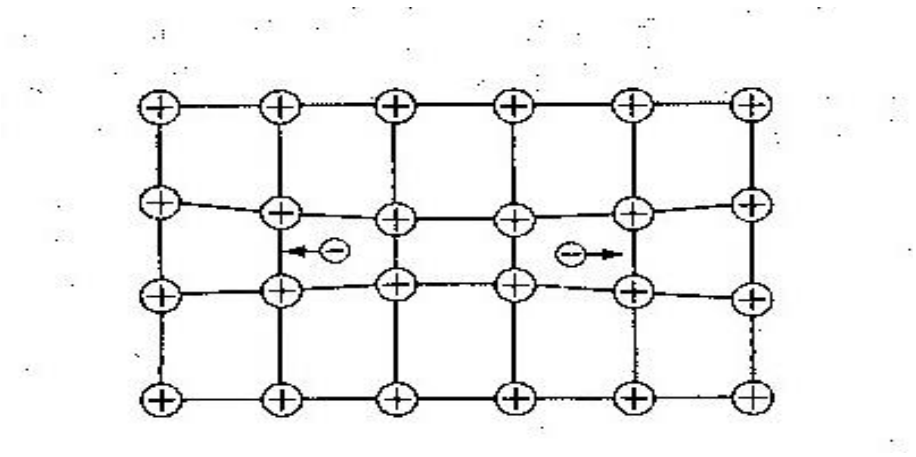

Fig.1.5: the formation of a Cooper pair.

The electron-electron coupling is weak and can be destroyed by thermal motion of the lattice. For this reason, the BCS type superconductivity exists only at low temperatures.

The electron-electron coupling results in electron pairing - formation of Cooper pairs. The Cooper pairs do not have spin 1/2 and therefore do not follow Pauli's principle (1 electron per state). Large number of Cooper pairs can populate one collective state. This state is stable and requires some additional energy input (thermal energy) to be destroyed.

The binding energy of Cooper pairs in the collective state is several meV. Note that in the superconductor, there is a gap between the highest field states and the lowest vacant states, fig. 1.6b

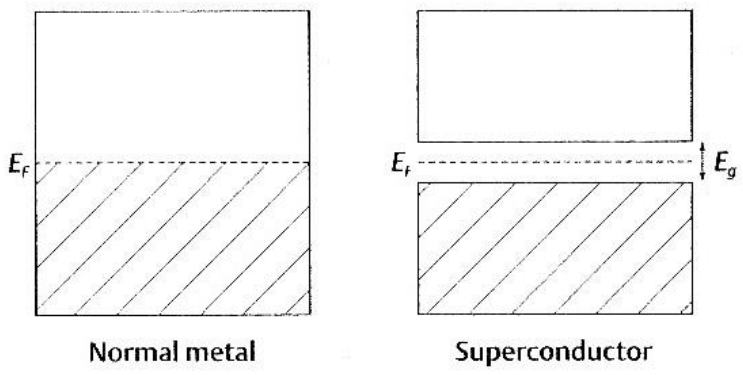

(a) (b)

Fig. 1.6: occupation of energy levels at absolute zero in (a) a normal metal and (b) a superconductor. E_F denotes the Fermi energy.

Formation of Cooper pairs is a spontaneous process resulting in lower energy state of electrons in the superconductor. In superconductors, the filled states are occupied by Coopers pairs, and the empty band, above E_g, is occupied by "broken" Cooper pairs. The band gap E_g is a measure of binding energy of Cooper pairs, the greater binding energy, the greater T_c

$$E_g = 3.53 k_B T_c \qquad (1.2)$$

E_g is confirmed from absorption spectra. For, $hc/\lambda > E_g$, electromagnetic radiation can be absorbed.

1.1.20: Crystallization of Neutron Matter (Neutron Stars)

A neutron star is the collapsed core of a large (10 – 29 solar masses) stars. Neutron stars can be considered as reservoirs of high-density fermions, as these systems can be assumed to be the largest of its type in the universe. Neutron stars are the smallest and most dense stars of the size of 10Km radius, and their mass is roughly twice or more of

the sun. I have calculated the energy per neutron in a neutron star for low and high density neutron stars. It is found that the energy per neutron increases as the density of the neutron star increases for a given value of the scattering length.

In the past, calculations (Canuto & Chitre, 1974) showed that the solidification pressure of the order of 5×10^{27} atmospheres can lead to the solidification of neutron matter in the vicinity of the density of neutron matter, $\rho_n = 5\times10^{14}\, gcm^{-3}$. As such, crystallization of neutron matter has been studied for high values of ρ_n as compared to density of high mass nuclei-assuming different types of inter - particle interactions, and different spin states, such as the singlet states, $^1S_0$, $^1P_1$, $^1D_2$ and triplet states $^3s_1$, $^3p_0$, $^3p_1$, $^3p_2$, $^3D_1$, $^3D_2$, in which the two interacting particles can exist and also assuming solid ordered structures, such as body centred cubic (BCC), face centred cubic (FCC) and values of the neutron density in the range $\rho_n = 1.4X10^{15} gcm^{-3} to\ 5.237\ X10^{15} gcm^{-3}$. In general, the calculations showed that for densities $\rho_n = 1.5\ X\ 10^{15} gcm^{-3}$ or more, solid phase for cold matter can exist. The energies per particle (E/N) vary from structure to structure. For pure neutron matter for $\rho_n = \ 5.237\ X10^{15} gcm^{-3}$, the E/N for BCC is 1194.0 MeV, for HCP, E/N = 884.7 Mev; and E/N =864.6 MeV for FCC. The saturation density of a nucleus ≈ 2.84 x 10^{14} gcm$^{-3} = \rho_s$. Thus for the crystallization of neutron matter, the density should be roughly ten times, i.e, $\rho_n = 10\rho_s$.

It is by now known that neutron stars can be considered as reservoirs of high-density fermions, and these systems are perhaps the largest of its type in the universe. A neutron star is the collapsed core of a large (10-29 solar masses) star. Neutron stars are the smallest and most dense stars known to exist, typical size of a neutron star is 10km radius, but the mass could be twice or more than that of the sun (Wikipedia, 2017). Since the volume of the neutron star being small and its mass is very large, the density of such neutron stars is almost ten times ($\rho_n \cong 10\rho_s$), the saturation density of a heavy nucleus, there exist strong nucleon-nucleon interactions between the neutrons, and consequently a number of different phases can occur.

Temperatures in the interior of the neutron stars fall below a billion degrees Kelvin in less than one year after the birth of the star (Gezerlis et.al., 2015). Such temperatures may look high, but they are low compared with the characteristic energies such as the Fermi energy, which for neutron density are of the order of 10-100 MeV, and this energy corresponds to temperatures of the order of $10^{11} - 10^{12}$ K (kT=energy). It is now understood that in the inner crust of neutron stars, the neutrons paired in a $^1S_0$ state co-exist with a lattice of a neutron-rich nuclei; in fact superfluid neutrons co-exist with a crystal lattice of neutron-rich nuclei and an electron gas. To understand the properties of such systems, interaction between individual nucleons must be accurately known. As a first step a simple nucleon-nucleon interaction can be chosen to study the state of crystallization of neutron stars.

Another important property of matter is the density that determines the state of matter from gaseous to crystalline state. In the case of neutron star crust, it is well known that it is in a crystal state for a wide range (Rogers, 1964) of mass densities and temperatures.

1.1.21: Characteristics of neutron stars

Some of the important physical quantities that are associated with the neutron stars are, velocity of sound(C_s) in the neutron star, the radius R of the star, maximum spin rate of the star which is the number of rotations of the star around its own axis of rotation per second (σ), and the surface speed of the star.

i. Velocity of sound in a Neutron star(C_s)

The velocity of sound in the star is given by:

$$C_s^2 = \frac{\partial p}{\partial \epsilon} \quad (1.3)$$

Where p is the pressure given by

$$p = \rho^2 \left(\frac{\partial E}{\partial \rho}\right) = \rho^2 \left[\frac{\partial E(\rho_n)}{\partial \rho}\right] \quad (1.4)$$

Knowing the value of E(ρ_n) from the equation of state, I can calculate p from equation (1.4),and then equation (1.3) gives C_s^2,where ϵ=Energy density=$\rho(E+m_N)$,Where m_N is the neutron mass, here ρ=Particle number density.

Another expression for the velocity of sound is,

$$C_s=\sqrt{\frac{Y}{\rho_m}} \quad (1.5)$$

Where Y=Young's modulus in the neutron star

$Y=5.3x10^{30}$ Pa (1.6)

ρ_m=Mass density of the neutron star=$5.9x10^{17}kgm^{-3}$ (1.7)

Between equations (1.5),(1.6) and (1.7), gives

$$C_s=3.0\ x10^6 ms^{-1}=\frac{C}{100} \quad (1.8)$$

Where c=velocity of light=$3.0x10^8 ms^{-1}$

ii. The radius R of the neutron star

The Tolman-Oppenheimer-Volkoff(TOV)equation (arxiv:1307.5815vI, nucl-Th, 22 July 2013,EPJ manuscript by S. Gandolfi, S. Reddy) gives the value of P(r) in terms of ϵ, ρ and the function radius r. The total radius of the neutron star is given by the condition that P(r)=0 at r=R, i.e., P(R)=0,

where P(r) is the pressure at the radius, r.

iii. Surface speed of the neutron star

Experimentally it has been observed that a star of radius R=10km rotates 716 times/sec around an axis passing through it, i.e., the star rotates or spins 716 times s^{-1}.The surface speed of this star is V, i.e.,

$V=2\Pi R\ x\ 716kms^{-1}=44987.28kms^{-1}$ (1.9)

and this is a very large speed.

Surface speed can also be calculated by using the fact that the maximum spin rate of the star corresponds to a point on the surface of the star where the surface gravity, g, is equal to centrifugal force. Now the surface gravity g is

$$g=\frac{GM_n m}{R^2} \quad (1.10)$$

and the centrifugal force F_C is,

$$F_c=\frac{mV^2}{R} \quad (1.11)$$

Equating g and F_c yields,

$$V^2=\frac{GM_n}{R} \text{ or } V=\sqrt{\frac{GM_n}{R}} \quad (1.12)$$

Now $M_n = mass\ of\ the\ star = 1.9885\ x\ 10^{30} Kg$

$G = Gravitational\ constant$

$$=6.67408\ x10^{-11}m^3kg^{-1}s^{-2} \quad (1.13)$$

R=12km.

equation(1.12) now gives,

$$V=1.5\ x\ 10^8 ms^{-1} = 0.5\ c \quad (1.14)$$

Which is a large velocity.

Hence the velocities involved in Neutron stars are relativistic.

It should be mentioned that the speed c_s of acoustic waves in a neutron star is also very large. The speed of sound in solids is,

$$C_s = \sqrt{\frac{E}{\rho}}, \quad (1.15)$$

$where\ \rho = density\ of\ neutron\ star = 5.9x10^{17} Kgm^{-3}$, and its Young's modulus $E = 5.3x10^{30} Pa$, and thus on calculation, it yields C_S=3.0 x$10^6$$ms^{-1}$.which is very large. It is still not known whether the elastic properties or due to a nuclear interactions n-n and

q-q, or it is just due to gravitational force. It is also found that the pressure in the neutron star can vary from 3 x10^{33} Pa to 1.6 x 10^{35} Pa from the inner crust to the center.

Also the equation of state of neutron star at such high densities is not precisely known. However, some properties of neutron stars are similar to the properties of atomic nuclei, including density and composition. But a nucleus is held together by strong nuclear interactions, whereas a neutron star is held together by gravity. It is still not clear whether both nuclear interactions and gravity hold the neutron star together, and if that be so, then a new equation of state will have to be proposed(Togashi, Hiyama, Yamamoto & Takano 2016) & (Zdunik, Fortin & Haema, 2017)

Two systems of fermions chosen for this study are ^{3}He and Neutron matter.

1.2: Justification

Helium-3 is light, non-radioactive, with two protons and one neutron (unlike common Helium Nuclide having two protons and two neutrons), occurs as a *primordial* nuclide, escaping from the Earth's crust into the atmosphere and into the outer space over millions of years, hence, it is readily available in the Earth's atmosphere. Helium-3 is also thought to be a natural *nucleogenic and cosmogenic* nuclide, which is produced when Lithium is bombarded by natural neutrons, which can be released by spontaneous *fission* and by nuclear reactions with cosmic rays. Helium-3 is touted to be a future energy source, since the *fusion* of Helium-3 atoms releases large amount of energy without causing surrounding material to become *radioactive.* Their microscopic physical properties are mainly determined by their Zero-point energy which is higher than Helium-4, hence, Helium-3 can overcome *dipole-dipole* interactions with less thermal energy than Helium-4.

Neutron Stars (NS) have high density and display strong magnetic fields. They display many types of behaviour, including *pulsing* (in radio, IR, optical, UV, X-ray, gamma-rays and gravitational wave emission). In their interior, they are superconducting and superfluid, with transition temperatures around a billion degrees kelvin, hence, their study enables one to push the envelope of fundamental theories about gravity, magnetic fields and high density matter, which is associated with Fermi energy. Crystallization (Hard-

sphere assembly) creates dense environment of momentum, hence an energy associated with the confinement (crystalline phase); hence, squeezing the system increases total energy and this Fermi energy acts as degeneracy pressure and degeneracy stars are smaller at higher masses. Superconductivity and superfluidity effects observed in neutron stars could tell us about the pairing and hence inform us about aspects of nuclear Physics that are mighty difficult to obtain from normal laboratories.

1.3: Statement of the problem

Quantum correlations in fermionic many-body systems, though central to many of the most fascinating effects of CMP, are poorly understood from a theoretical perspective. Even the notion of "paired" fermions which is widely used in the theory of superconductivity and has a clear physical meaning therein, is not a concept of systematic and mathematical theory so far, and more so as applies hard-sphere system of fermions that involve pair potential. Applying concepts and tools/techniques from BV diagonalization of the particle interaction Hamiltonian, a first approximation to many-body system pair potential containing a short-ranged repulsive part, which is influenced by the density of the hard-sphere system, and which in turn determines the total energy, E, of the system. Using Heisenberg's uncertainty principle to obtain energy per particle, E/N, and the saturation density, ρ_s, which leads to crystallization. Such techniques address the question/problem under consideration by closing the identified gap. Properties of fermions at ultra-cold temperatures leading to crystallization of fermions as well as magnitude of total energy of the assembly addresses the ambiguity that characterizes role of fermions in determining some of the properties of superconductors.

1.4: General objective

Theoretical investigation of properties of crystallization of a hard-sphere assembly of fermions (^{3}He and neutron matter).

1.5: Research questions

This study has sought to answer the following questions:

1) At what transition temperature does crystallization of fermions (Helium-3) take place?
2) How is the variation of energy per particle, E/N with density, ρ, both for low and high density for an assembly of fermions (helium-3 and neutrons)?
3) How is the variation of saturation density with hard-sphere diameter, C, both for low and high density fermionic system?
4) How does the energy per neutron, E/N, vary with low/high density in a neutron star?

1.6: Objectives of the study

1) To determine the transition Temperature, T_c, at which crystallization of fermions takes place.
2) To investigate the variation of E/N with density both for low and high density for an assembly of fermions.
3) To establish the variation of saturation density with hard-sphere diameter, C, both for low and high density fermionic system.
4) To investigate the variation between the energy per neutron, E/N, and low/high density in a neutron star.

1.7: Significance of the study

It is hoped that the study of Helium-3 will be useful to nuclear energy sector since helium-3 can be produced by low temperature fusion of Helium-2 isotope and a proton; the reaction produces a high energy alpha particle which captures an electron producing a stable light Helium ion which can be utilized directly as source of electricity without producing dangerous neutrons. Helium-3 is used in fusion reactions as well as in neutron detection. The study is also expected to improve practice in domestic front where Helium-3 is used in refrigeration to achieve temperatures of 0.2 to 0.3K. Also, in the health sector, since Helium-3 has total spin of ½, effectively aligns the nuclear spins with the magnetic field in order to enhance NMR signal. Upon inhalation, gas mixtures containing the *hyperpolarized* Helium-3 gas can be imaged with an MRI scanner to produce *anatomical* and functional images of lung *ventilation,* produce images of the

airway tree, locate unventilated defects, etc; this technique is critical for the diagnosis and treatment management of chronic respiratory ailments such as chronic obstructive pulmonary disease (COPD), emphysema cystic fibrosis, and asthma.

Since fermion anti-commutation behavior allows for carbon-based life forms such as mankind to exist and fermions being the building blocks of matter, interacting in a multitude of permutations to give rise to the elements of the periodic table, the study seeks to propose an elegant method for transmutation, i.e., making bosons act like fermions through quasiparticle excitations which is a key component concept in Condensed Matter Physics.

For neutron stars, they are the best clocks in the universe, the most stable since they are thousands of times more stable in the short term than the best atomic clocks. Their high density is associated with high Fermi energy.

CHAPTER TWO

THEORY AND LITERATURE REVIEW

2.1: Introduction

Helium was first liquefied by Kammerlingh Onnes in Leiden in 1908. During the late 1920s and early1930s it was noticed that the liquid had some strange properties, but it was not until 1938 that it was discovered independently by Allen, Misener and Kapitza that it exhibited frictionless flow and was what I now call a superfluid. Shortly afterwards Fritz London suggested that superfluidity could have some connection with Bose-Einstein condensation, which was known as a theoretical possibility in an ideal Bose gas. London also realized that there might be a strong connection with superconductivity, which had been discovered many years before and which could be seen as superfluidity in the electron as in a metal. With impressive intuition he also suggested that both superfluidity and superconductivity were "quantum mechanisms on a macroscopic scale", although the significance of this idea did not become really clear until the late 1950s or early 1960s (Kapitsa, & Misener, 1937)

Shortly after London produced these seminal ideas he and Tisza(London, & Tisza, 1964) suggested that the superfluid phase of the liquid could be described by a two-fluid model, the Condensed and non-Condensed atoms being identified respectively with the superfluid and normal components. In 1941 Landau wrote a remarkable paper in which he suggested that superfluidity can be understood in terms of the special nature of the thermally excited states of the liquid: the well-known phonons and rotons. This idea led Landau also to the idea of a two-fluid model, but with a microscopic interpretation that was different from that of London and Tisza. Indeed, Landau expressed the view that superfluidity has no obvious connection with Bose condensation, although, as I shall see, this view was certainly proved wrong. Nevertheless, the basic ideas in Landau's paper were correct, and his interpretation of the two-fluid model showed brilliant intuition.

After the Second World War the two-fluid model was placed on a firm experimental basis, especially with the experiment of Andronikashvili and the discovery of second sound. At the same time the properties of the normal fluid (the gas of phonons and rotons) were explored in great theoretical detail by Khalatnikov, with parallel confirmatory experiments (Andronikashvin, 1946).

A theoretical proof that Bose condensation does occur in a liquid such as superfluid helium was provided by Onsager and Penrose. Feynman wrote a number of important papers in the 1950s, exploring how the properties of liquid helium were strongly related to the fact that the atoms obey Bose statistics (Feynman, 1972)

The quantization of superfluid circulation and the existence of free quantized vortices were proposed theoretically and independently by Onsager and Feynman, and the first experimental confirmation came from the work of Hall and Vinen with the discovery of mutual friction in rotating helium and with the direct observation in a macroscopic experiment of the quantization of circulation. These works led to an appreciation for the first time of the full significance of London's "quantum mechanism on a macroscopic scale", and of the underlying importance of Bose condensation in superfluidity (Vinen, 1957).

In 1957 Bardeen, Cooper and Schrieffer wrote their famous paper on the theory of superconductivity (Bardeen, Cooper, & Shrieffer, 1957). In due course this led to a better appreciation of the connection between superfluidity and superconductivity, and the discovery of the quantization of flux and of free flux lines in type II superconductors demonstrated clearly the analogies between the two systems. As far as I know all superfluids and superconductors have one basic feature in common: their properties derive from the existence within them of some type of Bose condensation, involving atoms or pairs of atoms or pairs of electrons.

Liquid ^{3}He exhibits no superfluid behaviour at the relatively high temperatures involved in superfluid ^{4}He, thus confirming the importance of particle statistics in this behaviour. The discovery of superfluidity in liquid ^{3}He by Osheroff, Richardson and Lee in 1973 at a temperature of about 2mK completed the story, showing that BCS pairing can occur in an

uncharged Fermi liquid; the pairs are now pairs of atoms, but the pairing is unconventional in that it involves relative p-states rather than the s-states of the conventional BCS theory. Unconventional pairing is now known to occur in exotic superconductors, such as the heavy-fermion metals and the high-temperature materials. What follows is the focus on superfluidity in liquid ^{4}He, emphasizing the underlying physical principles, including those associated with macroscopic quantum phenomena (Henshaw and Woods, 1961).

2.2: Excitation

Fig. 2.1 shows a plot of excitation energy as a function of wave function in a superfluid. It is evident from this graph that there are two types of excitations in the superfluid, which are associated to phonons and rotons.

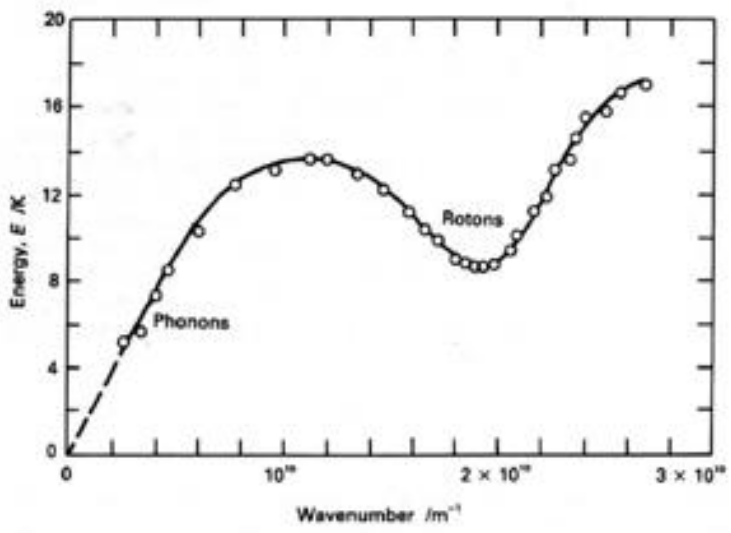

Fig 2.1: Dispersion curve of excitations in helium-II, as deduced from neutron scattering experiments (Henshaw and Woods, 1961).

The dispersion relationships for these excitations are given as:

$$E_{ph} = C_1 P \tag{2.1}$$

and

$$E_{rot} = \Delta + \frac{(p - p_o)^2}{2\mu} \qquad (2.2)$$

Where C_1 = 23.9 m/s = speed of sound, Δ/k_B = 8.65 = energy gap, μ = 0.16m$_4$= effective mass, and $p_o / \eta = 19.1/nm$ = wave number.

2.3: The Phase Diagram of ^{4}He

Fig. 2.2 presents a phase diagram for ^{3}He, where one observes two anomalous features. The liquid phase exists over a range of pressure up to about 25 atm even at the absolute zero temperature; and there are two liquid phases, helium I, which is conventional in its properties, and helium II, which is superfluid.

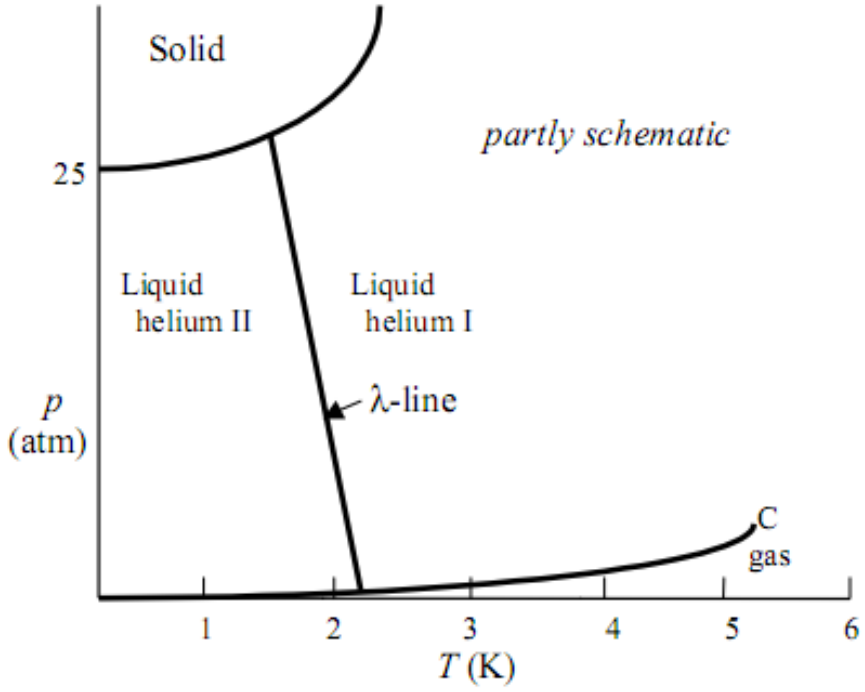

Fig. 2.2: The phase diagram of ^{4}He (London, 1954).

The existence of a liquid over a range of pressures at T = 0 must be a quantum effect. It arises from quantum mechanical zero-point energy: the fact that a confined particle must have kinetic energy, this energy increasing as the particle is more strongly confined. In the absence of a high pressure, the atoms cannot become sufficiently closely spaced to allow the formation of an ordered crystal, without the penalty of too large zero-point

energy. The Third Law of Thermodynamics requires that the entropy of a system in equilibrium should vanish at T = 0. Therefore, the liquid must be in some sense completely ordered at T = 0. This ordering must be quantum mechanical in origin, as in the ordering of particles among quantum mechanical energy levels rather than in position. It seems reasonable to suppose that superfluidity is a consequence of this ordering.

Helium is the only substance that does not liquefy at zero temperature. The Helium atom is confined by its neighboring atoms in a volume *V*, with the radius $R \sim V^{1/3}$**.** From Heisenberg's uncertainty principle in momentum, the uncertainty is given by:~

$$\Delta p \sim \frac{\hbar}{R},$$

$$E_0 \sim \frac{\Delta p^2}{2m_4} \approx \frac{\hbar^2}{2m_4 V^{\frac{2}{3}}} \tag{2.3}$$

The potential energy is attractive due to van der Waal`s forces, and repulsive due to "hard core", and Lenard Jones potential

$$E_{LJ} \sim \left[\left(\frac{\sigma}{R}\right)^6 - \left(\frac{\sigma}{R}\right)^{12}\right] \sim \left[\frac{1}{V^2} - \frac{1}{V^4}\right] \tag{2.4}$$

The thermal fluctuations have to be reduced substantially to make Helium-4 liquefy at 4.2 K, and even at zero temperature. The zero point fluctuations keep Helium-4 from solidifying. By applying pressure to the liquids, the atoms can be brought close enough to form a solid, and this happens at P≈25 bar for ^{4}He (Hall, & Vinen, 1956) The total energy is the sum of potential energy and zero-point energy as shown in Fig. 2.3.

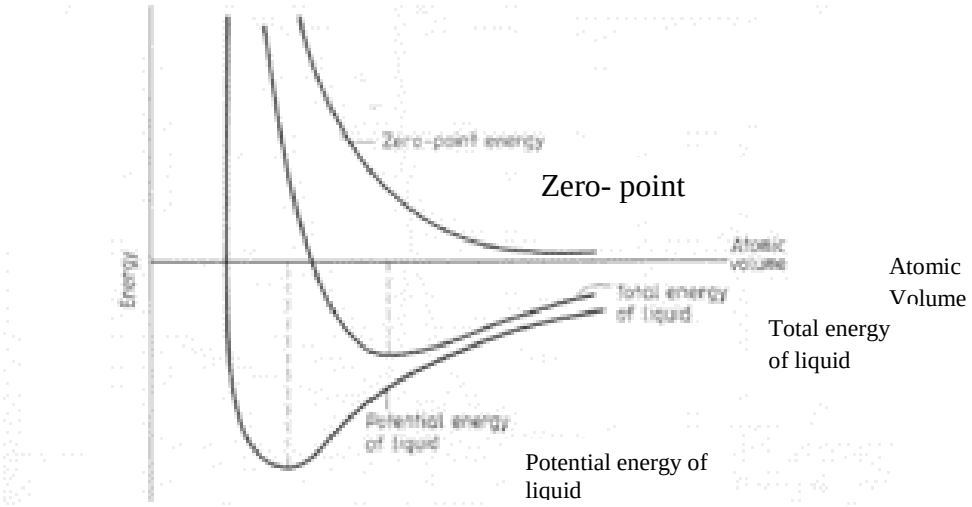

Fig 2.3 Energy of liquid Helium(Hall, & Vinen, 1956)

Helium-3 has even lower mass increasing the zero-point fluctuations even more. The Helium-3 liquefies at somewhat lower temperature 3.4 K, and solidifies at somewhat higher pressure ~32 bar (Hall, & Vinen, 1956). Whereas He-3 solidifies at higher pressure, hydrogen solidifies due to stronger van der Waal forces.

2.4: The Heat Capacity

The variation of heat capacity, *C*, with temperature is shown in Fig. 2.4, for the case when the helium is under its own vapor pressure. It is seen that the transition to superfluidity is accompanied by a large peak in the heat capacity. There is no latent heat, but the heat capacity tends to infinity at the transition, so that the transition can be classified as strictly second-order. The shape of the variation heat capacity near the transition is like a Greek letter lambda (λ), hence the term λ-point to describe the transition. The type of anomaly depicted in Fig. 2.4 is quite common in nature, and it is characteristic of a system that exhibits an order-disorder transition; an example is the ferromagnetic transition. Hence, a clear confirmation that superfluidity must be associated with a (quantum mechanical) ordering in the liquid. A similar anomaly in the heat capacity appears at the transition temperature of a superconductor, although in this case it has more nearly the character of a strictly second order transition. Notice that,

although the heat capacity becomes rather small at low temperatures, it is quite large just below the λ-point; for example, at 1.8 K. This feature can be useful in applications; He at $T < T_\lambda$ can be used for the study of superconducting transition temperatures of conducting materials, alloys and heavy fermion superconductors.

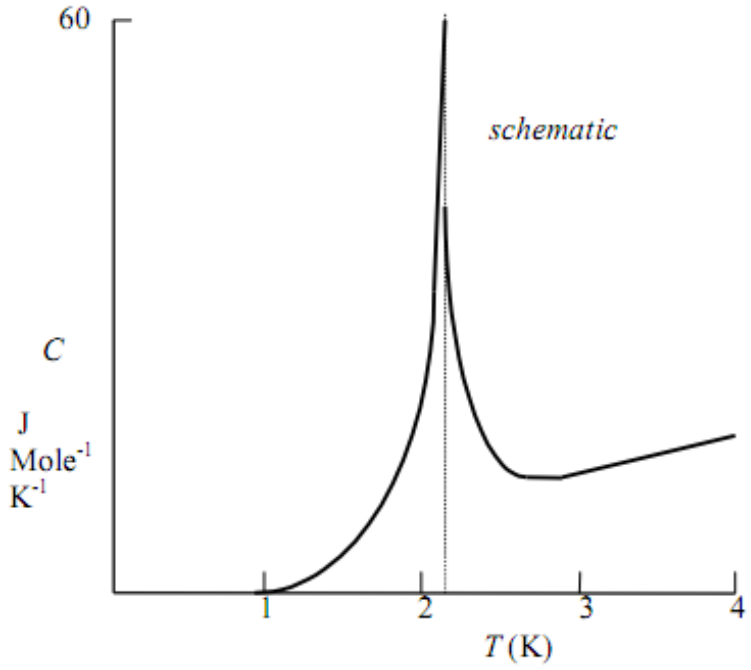

Fig. 2.4: The heat capacity of liquid ^{4}He, T_λ=2.176K (Atkins, 1959).

2.5: Mixtures of Helium-4 and Helium-3

Increasing the concentration of He-3 decreases the transition temperatures. Below 0.8 K, the liquid can separate into two phases; one Helium-4 rich and one Helium-3 rich as depicted in Fig. 2.5. The ^{3}He rich phase will float on top of the He-4 rich phase. At zero temperature the He-3 rich phase becomes "pure" i.e 100% He-3, whereas the He-4 rich phase always contains some He-3 (6.4% or more).

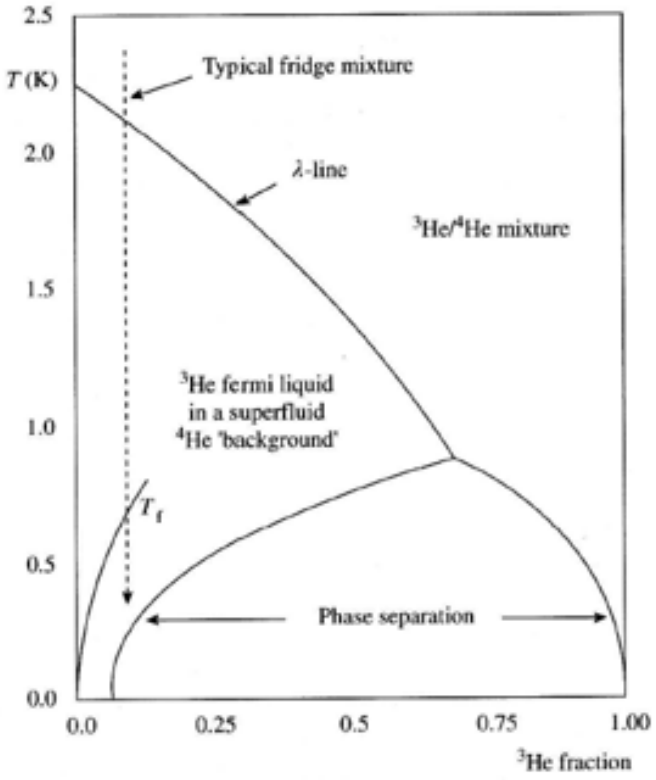

Fig 2.5: The schematic phase diagram of liquid helium mixtures (Kapitza, 1938).

2.6: The Two-Fluid Model of Superfluid ^4He

At first sight these properties present a confusing picture, but they make sense in terms of the two-fluid model, regarded as a purely phenomenological description. The essential features of this model have been described, and examples given of properties that can be described in terms of it. The superfluid phase can be regarded as a mixture of two fluids, which can support different velocity fields. The normal fluid, with density n, flow velocity field v_n, and conventional viscosity η, carries all the thermal energy and entropy in the system. The superfluid component, with density n_s and flow velocity field v_s, n_s, can flow without friction and carries no thermal energy. The densities, n and n_s vary with temperature in the way shown in Fig. 2.6.

A pressure gradient will tend to drive both fluids in the same direction. An increase in temperature increases η but decreases n_s, so a temperature gradient tends to drive the

superfluid component in one direction (towards high temperature) and the normal fluid in the opposite direction.

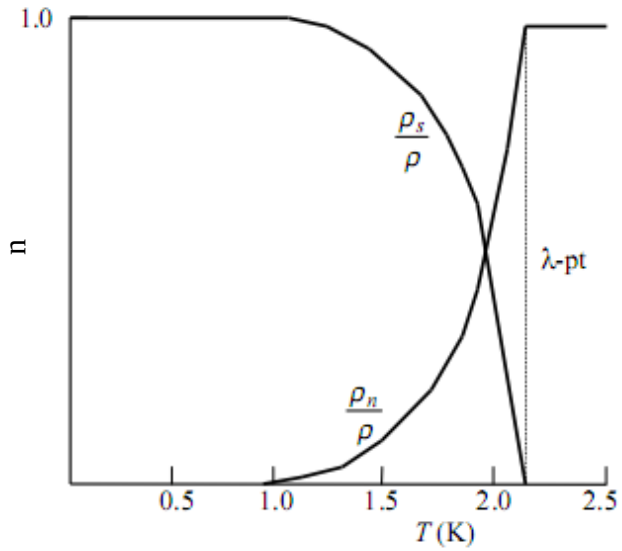

Fig. 2.6: The observed dependence of n and n_s on temperature (Atkins, 1959).

The superfluid component can flow without friction through even very narrow channels, so narrow that the normal fluid is rendered completely immobile by its viscosity. A striking example is provided by "film flow". Any solid surface in contact with the liquid is covered by a film of liquid, about 30 nm in thickness, as a result of van der Waals attraction between the helium atoms and the substrate. This is true in principle for any liquid, but in helium flow of the superfluid component through the very thin film becomes possible, with the result illustrated in Fig. 2.7.

If an empty beaker is immersed halfway into superfluid He, a thin film of helium condenses on the walls of the beaker (Fig 2.7a). This film can fill the beaker even if it is immersed halfway into the superfluid. The thin helium film is about 30nm thick and it actually flows upwards and fills the beaker until the levels are equal inside and outside the beaker (Fig 2.7b). The film acts as a siphon. This can be explained by the fact that it would cost energy to break the film and it costs less energy for the film to flow upwards. If the beaker is then lifted out of the superfluid the reverse process occurs, and small

droplets can be seen from the bottom of the beaker as it empties (Fig 2.7c). The flow velocity of the film is about 0.2 m/s.

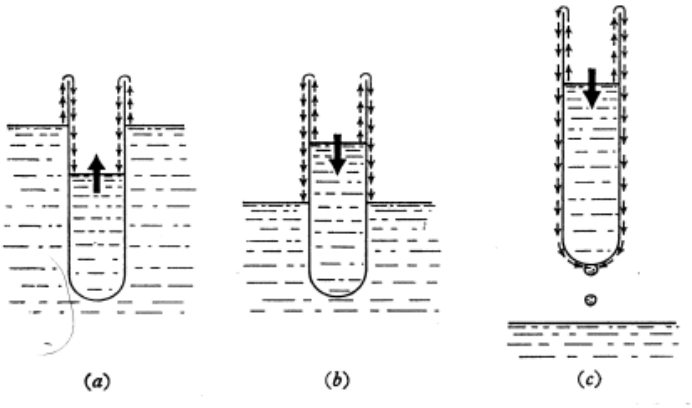

Fig. 2.7: Film flow of He II over the walls of a beaker (Viviani, 1957).

A famous experiment was performed by (Andronikashvin, 1946).. He constructed a pile of discs, which he suspended in helium by a torsion fiber, as shown in Fig. 2.8. He measured the period of torsional oscillation as a function of temperature. The spacing between the discs was such that at the period of oscillation the normal fluid was completely coupled to the disc system. However, the superfluid component was not coupled, so that only the normal fluid contributed to the moment of inertia of the disc system. These measurements provided the first evidence for the dependence of normal fluid density on temperature shown in Fig. 2.6.

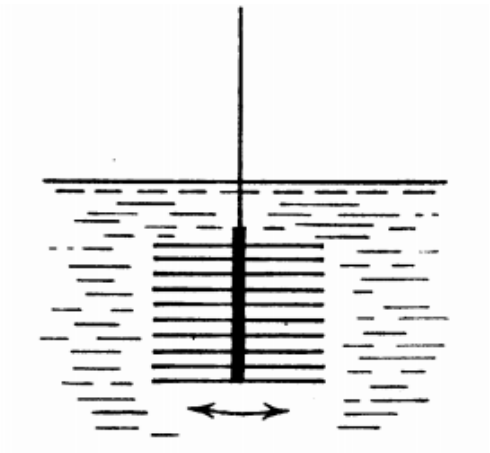

Fig. 2.8: The Andronikashvili experiment (Andronikashvili, 1946).

Heat transport in superfluid helium takes place by counter flow of the two fluids, the superfluid component moving towards the source of heat and the normal fluid away from it, as shown in Fig. 2.9. Only the normal fluid carries thermal energy, at a rate per unit area,

$$Q = \rho S T v_n \tag{2.5}$$

where S is the entropy of the helium per unit mass. This leads to very effective thermal transport, at a rate limited only by the small viscosity of the normal fluid. In practice the thermal transport is not quite as effective as is suggested by this idea, as will be explained later.

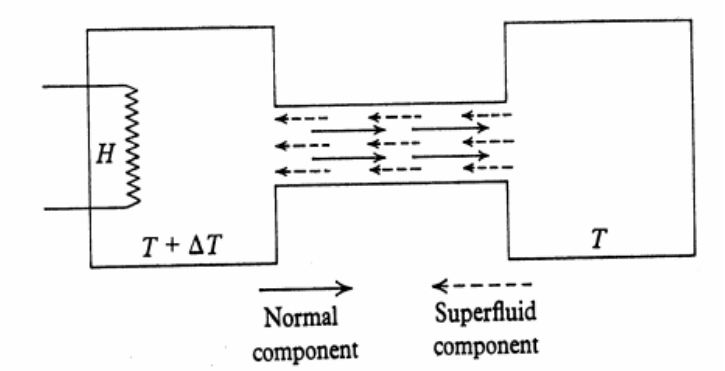

Fig. 2.9: Illustrating thermal transport by counterflow (Zhang & Van Sciver, 2005).

The existence of two fluids allows two modes of longitudinal wave propagation. The two fluids can oscillate in phase, giving rise to first sound, or they can oscillate in anti-phase, giving rise to second sound. The first sound is an isentropic pressure or density wave, analogous to ordinary sound in a fluid; it propagates at a speed of

$$c_1 = \left(\frac{\partial p}{\partial \rho}\right)_s^{1/2} \simeq 240 m/s \tag{2.6}$$

The second sound involves to a good approximation no change in density, but only a change in the proportions of the two fluids; it is therefore a temperature wave, but one that obeys the wave equation rather than the diffusion equation. The speed of second sound is given by:

$$C_2^2 = \frac{TS^2\rho_s}{C\rho_n} \tag{2.7}$$

The value of C_2 is roughly 20 ms^{-1} over the temperature range from 1 K to 2 K (Zhang & Van Sciver, 2005). Transient thermal effects in superfluid helium can therefore be very different from those in a conventional fluid, and discussion of them must allow for the existence of second sound. The examples of two-fluid behavior that I have described apply in their simplest form only if the flow velocities do not exceed certain critical values, which are often quite small (~few mm s^{-1}). The two-fluid model applies also to superconductors. The resistive loss that occurs in a rapidly oscillating electric field is due to motion of the normal fluid.

Suppose these excitations are set into motion with a drift velocity v, leaving the fluid otherwise at rest. Given the properties of the excitations (in particular their energy-momentum relationship, which can be determined experimentally by neutron scattering) Landau calculated the momentum density $\boldsymbol{J}_e$, associated with the drifting excitations. He found that

$$J_e = \rho_e v < \rho v, \tag{2.8}$$

where the inequality holds at sufficiently low temperatures, which turn out to be temperatures below the λ-point. Thus, the drifting excitations do not cause the whole fluid to drift, in the sense that they carry an effective density that is less than the total density of the helium. Identifying the gas of excitations with the normal fluid, then

$$\rho_e = \rho_n \tag{2.9}$$

Where ρ_e is effective density and ρ_n is density of the normal component, and can be calculated, and it can be shown to be equal to the observed normal-fluid density.

The superfluid component in Landau's picture is what is left over after the thermal excitations have been taken into account. Landau also considered what would happen if this background were to move. He showed that it could not slow up by creating or

scattering excitations if its velocity were less than a critical value, which is about 60 ms^{-1}. This picture of the superfluid component is not wholly satisfying, and it is certainly not the whole story, not least because observed critical velocities are typically very much less than 60 ms^{-1}. The nature of the superfluid component shall now be examined in more detail to demonstrate its connection with Bose condensation.

To understand the real nature of the superfluid component I must start by looking at the phenomenon of Bose-Einstein condensation. Bose condensation plays a crucial role in superfluidity, contrary to Landau's original opinion. Consider an ideal gas formed from Bose particles: i.e. particles such as ^{4}He atoms that are quantum-mechanically indistinguishable, but are not subject to the exclusion principle (i.e. there can be any number of particles in one quantum state). Calculation of the way in which the particles of the gas are distributed over the quantum states determined by the shape and size of the containing vessel, has yielded an interesting result: below a critical temperature, T_0, a finite fraction of the particles is "Condensed" into the lowest quantum state. The way in which this fraction varies with temperature is shown in Fig. 2.10(a), and the calculated heat capacity is shown in Fig. 2.10(b). The heat capacity reflects the ordering of the particles into a single quantum state below the temperature T_o. Very recently, such Bose condensation has been observed directly in weakly-interacting gases formed from alkali-metal atoms levitated magnetically and trapped in a vacuum, the gas being cooled below the temperature T_0 (typically in the range 0.1-1 K) by a combination of laser and evaporative cooling (Enrico, *et.al*., 1999).

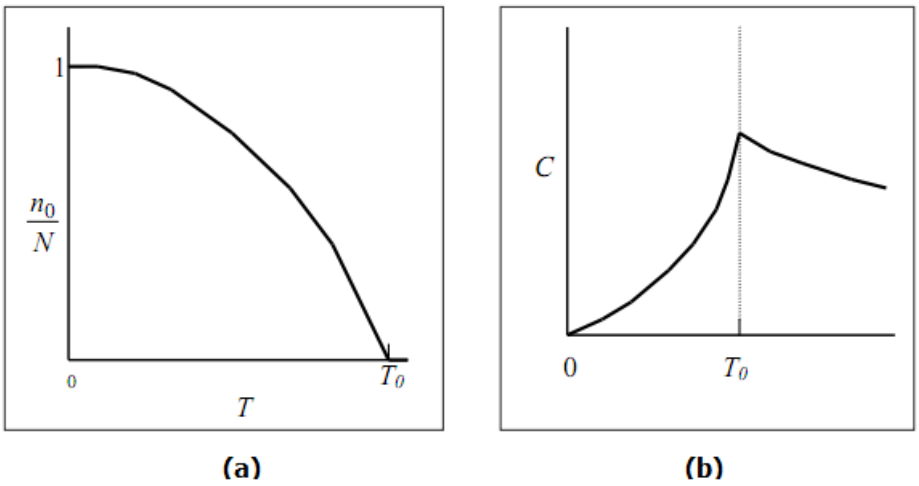

Fig. 2.10: The predicted behavior of an ideal Bose gas, (a) The temperature dependence of the Condensed fraction of particles; (b) the predicted heat capacity (Penrose & Onsager, 1947)

For an ideal hypothetical gas of non-interacting helium atoms with the same density as liquid helium the condensation temperature, T_0 is,

$$T_0 \sim 3.14K \qquad (2.10)$$

An obvious question is whether a similar type of ordering occurs in real liquid helium, albeit modified in some way by the strong interactions between the helium atoms. The answer is that it does, as shown first by Penrose and Onsager. The fraction of Condensed particles is smaller than in the ideal gas; even at T = 0 it is only about 10%.

But it remains the case that a macroscopic fraction, and a very large absolute number, of the atoms does condense into what is effectively a single quantum state, and it turns out that at T = 0 the non-Condensed atoms are effectively locked to the Condensed atoms. It is now understood that this is indeed the ordering process taking place below the λ-point, and that ultimately it is this ordering that is responsible for superfluidity. It is a remarkable process, because it is closely analogous to the formation of a coherent electromagnetic wave in a laser, which can be viewed as a condensation of photons into a single quantum state. In helium there is a coherent Matter wave. A similar process occurs in a superconductor, except that the coherent wave is formed from Cooper pairs.

A coherent Matter wave lies at the heart of both superfluidity and superconductivity. The assembly of Condensed atoms is called the condensate, and the associated wave function is called the condensate wave function (CWF). If the Condensed atoms are at rest then CWF is just a constant ψ_0, where ψ_0^2 is a measure of the number of Condensed atoms. If they are moving, each with momentum $m_4 v_s$ along the x-axis, the CWF becomes

$$\psi = \psi_0 exp\left(\frac{im_4 vx}{\hbar}\right) \tag{2.11}$$

For a more general motion of the condensate, it can be written as

$$\psi = \psi_0 \exp\big(iS(\boldsymbol{r})\big), \tag{2.12}$$

where the local velocity of the Condensed atoms is equal to $(\hbar/m_4)\nabla S$. This velocity is identified with the velocity of the superfluid component

$$v_s = \left(\frac{\hbar}{m_4}\right)\nabla S \tag{2.13}$$

One can ask how this view of superfluidity relates to that proposed by Landau, which was very successful in accounting for two-fluid behaviour. It is known that the two approaches are intimately connected, in the sense that the form of the spectrum of the thermal excitations, which underlies Landau's calculation showing that $\rho_n/\rho < 1$ below the λ-point, is intimately connected with the existence of the condensate. Without the condensate the spectrum would have the wrong form. Note especially that I now have a clear view of the meaning of the velocity of the superfluid component, which was not provided by Landau. A condensate exists also in a superconductor, formed from the Cooper pairs. In a superconductor, due to Cooper pairs of electrons, the mass m_4 is replaced by 2m, where m is the electron mass.

2.7: Quantum Restrictions on Superfluid Flow

The macroscopic occupation of a single quantum state in the Bose Condensed helium gives rise to macroscopic quantum effects (London, 1954), as London had foreseen.

Taking the curl of equation (2.13), it follows that the superfluid velocity is:

$$curl\boldsymbol{v}_s = 0 \tag{2.14}$$

This means that there can be no local rotational motion of the superfluid component. This is really a consequence of the quantization of angular momentum, as it is seen more clearly in a moment. But there can be a finite hydrodynamic circulation, defined as

$$\kappa = \oint_C v_s . dr \tag{2.15}$$

This equation shows that the closed circuit cannot vanish while remaining in the fluid. For example, a closed circuit around a solid cylinder passing through the fluid as shown in Fig. 2.11. However, the circulation cannot take any value.

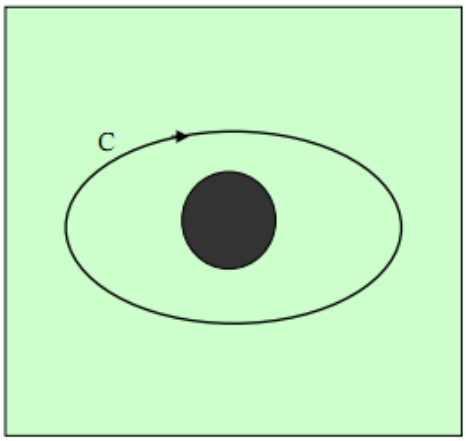

Fig. 2.11: Illustration of a circuit round which there can be a finite superfluid circulation (London, 1954).

To understand superfluid circulation, substitute for v_s from equation (2.13) into equation (2.15) to get

$$\kappa = \frac{\hbar}{m_4}\oint_C \boldsymbol{\nabla S}. d\boldsymbol{r} = n\frac{2\pi\hbar}{m_4}, \tag{2.16}$$

where n must be an integer in order to satisfy the condition that the CWF be single-valued. This means that the superfluid circulation must be quantized in units of $2\pi\hbar/m_4$. This circulation is macroscopically large (it can be measured in a macroscopic mechanical experiment), and this fact provides the clearest evidence that superfluidity is indeed a "quantum mechanism on a macroscopic scale". It arises from the quantization of angular momentum, combined with the fact that all the particles in the condensate must have the same angular momentum. In the absence of any quantized circulation there can be no local angular momentum, as it can be noted in connection with equation (2.14). The quantization of circulation has its analogue in superconductivity, where it is observed as the quantization of trapped flux.

As has been mentioned, Landau showed that the flowing superfluid component cannot decay into excitations unless the velocity is very large. With the idea of the condensate, greater insight into this frictionless flow can be gained. Suppose that there is a persistent superflow round a torus as shown in Fig. 2.12.

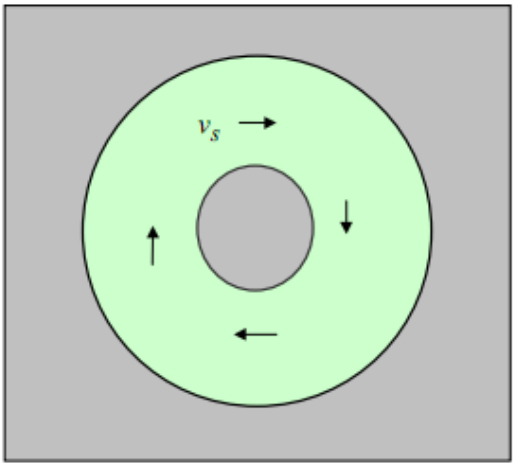

Fig. 2.12: Persistent superflow round a torus (Landau, 1999).

This flow can be only metastable, because a state with no flow has a smaller (free) energy. Why is it metastable? The condensate contains a macroscopic number of atoms. Interaction of these atoms with the walls of the torus will cause scattering, and some atoms may as a result be knocked out of the condensate. This will reduce the amplitude of the CWF, but it will not alter its coherent phase. Therefore, the superfluid velocity

does not change, although the superfluid density may decay a little, which would correspond to the creation of more normal fluid in the form of excitations. Putting it in another way, it can be observed that the destruction of superflow would require a transition that takes a macroscopic number of atoms from one state to another simultaneously, and such a process has very low probability. But superflow can decay through a mechanism that is yet to be considered: the creation of free vortex lines, to which the attention is now focused.

2.8: Quantized Vortex Lines on Superfluid Helium

It is seen that a quantized superfluid circulation can exist round a solid cylinder running through the helium. A free quantized vortex line in the superfluid component is a quantum of circulation round a tiny cylindrical hole in the helium. Such a line always has one quantum of circulation, and the hole then has a natural size, determined by a balance between the kinetic energy of flow and the surface energy of the hole, that is less than an inter-atomic spacing.

Such vortex lines can exist in superfluid helium, and they play an important role in its behavior. Most obviously, perhaps, they allow the superfluid component to rotate if the helium is placed in a rotating vessel; otherwise such rotation would be forbidden by equation (2.14). A parallel array of lines, as shown in Fig. 2.13, gives rise to a flow field that minimizes uniform rotation on length scales larger than the line spacing, which is about 0.2 mm at $\Omega = 1s^{-1}$.

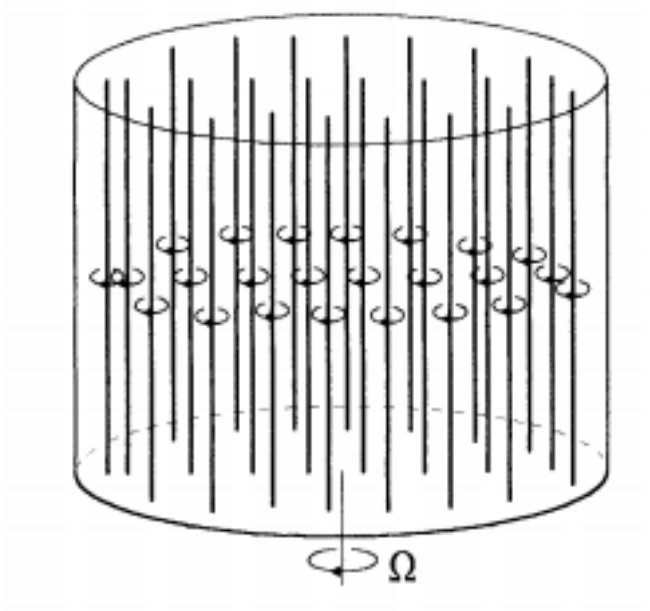

Fig. 2.13: Vortex lines in the uniformly rotating superfluid component (Hall, & Vinen, 1956).

This array is analogous to the array of fluxlines in the mixed state of a type II superconductor. Vortex lines scatter the excitations that constitute the normal fluid, and therefore they give rise to a frictional force between the two fluids, called mutual friction. This is observed as an attenuation of second sound when it propagates in the uniformly rotating helium. The observation of this attenuation provided the first experimental evidence for the existence of vortex lines. Vortex lines provide a new mechanism by which a persistent superflow can decay as shown in Fig. 2.14.

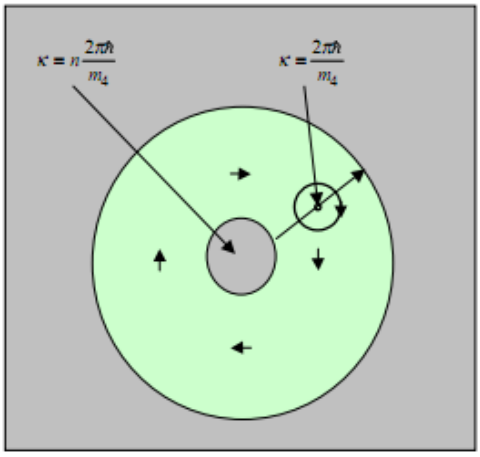

Fig. 2.14: Decay of a persistent current by vortex motion (Hall, & Vinen, 1956).

Consider again a persistent superflow in a torus. Let the persistent current consist of n quanta of circulation. If a free vortex, with the appropriate sign, crosses the channel, this value of n falls to n- 1. Does this mean that the current simply decays? It does not, because the movement of the free vortex across the channel is opposed by a potential barrier. This barrier arises because a vortex is attracted to a solid boundary by its image. The barrier is quite large in cases of practical interest, and it can be overcome only at high velocities ($>\sim$1-10 ms^{-1}) either thermally or by quantum tunneling. Without this barrier there would be no superflow. The barrier exists only because a vortex has a finite quantized circulation, so it is quantum in origin. The barrier exists also in a superconductor, where it is usually called the Bean-Livingston barrier. In practice frictionless superflow usually breaks down at velocities much less than 1 ms^{-1} This is due to a few remnant vortices, which can expand and multiply, and then cross the channel (cf remnant dislocations in a solid allowing the solid to deform much more easily than might have been expected). Remnant vortices seem always to be created when the helium is cooled through the λ-point. This expansion and multiplication leads to a type of turbulence in the superfluid component: a kind of tangle of vortex lines (Fig. 2.15).

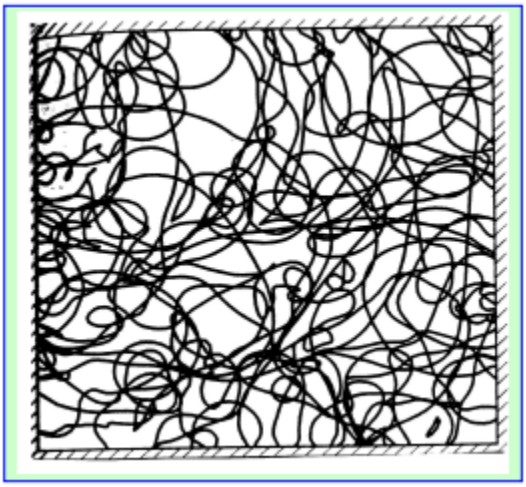

Fig. 2.15: A turbulent tangle of vortex lines (Kapitza, 1938).

Superfluid turbulence is very common. It seems always to be generated when the flow velocity exceeds a critical value that depends on channel size and is often as small as 1 mm s^{-1}

2.9: Practical Consequences of Superfluid Turbulence

Superfluid turbulence plays an important role in limiting heat transport in superfluid helium by counterflow. The counterflowing fluids cause remnant vortices to multiply (through the action of mutual friction), and this leads to a self-sustaining regime of homogeneous turbulence. The vortices thus generated lead to a steady average force of mutual friction per unit volume between the two fluids, given by

$$F_{sn} = A\rho_s\rho_n|v_s - v_n|^3, \qquad (2.17)$$

which limits the heat transport rate, Q per unit area, in a way that is generally much more important than normal-fluid viscosity. The parameter A is about 800 m s kg^{-1} at 1.8K. Q becomes a non- linear function of the temperature gradient, which is given by

$$\nabla T = \frac{A\rho_n}{\rho_s^3 S^4 T^3} Q^3, \qquad (2.18)$$

where S is again the entropy per unit mass of the helium. Although mutual friction becomes the dominant dissipative process limiting the heat flow, the effective thermal conductivity remains generally very high. Superfluid helium can be forced to flow down a tube or past an obstacle, just as can any conventional fluid. Except at very small velocities or in very narrow channels both the superfluid component and the normal component become turbulent. It turns out that this turbulence is surprisingly similar to that in a conventional fluid at high Reynolds number. The reasons are complicated, but they seem to be connected with two facts: on a scale large compared with the spacing between the vortex lines even the superfluid component looks like a classical fluid flowing at high Reynolds number; and the mutual friction associated with the vortex lines serves to lock the two velocity fields together. Thus the flow of the superfluid phase of liquid helium at high velocities in situations having a classical analogue is described quite well by classical formulae describing the flow of a conventional fluid, with density equalto the total helium density and viscosity similar to that of the normal fluid (Vinen & Niemela, 1999).

2.10: The Kapitza Thermal Boundary Resistance

As it can be seen, the effective thermal conductivity of superfluid helium is very high, but often it is necessary to transfer heat out of a solid body into the helium, or vice versa. Then taking into account of a high thermal boundary resistance between the solid and the helium (the Kapitza resistance), this resistance arises from the fact that it is generally difficult for a thermal excitation in the solid to convert to one in the helium. This can be seen most easily when both the excitations are quantized sound waves or phonons. When a sound wave approaches a change of medium, some is transmitted and some is reflected, the relative amounts being determined by the characteristic impedances ($Z = \rho c$) of the two media. For liquid helium Z has a value that is much smaller than for any solid, and the resulting serious acoustic mismatch at the boundary leads to the high thermal boundary resistance. Its value is typically of order 2×10^{-4} KW^{-1} m^2.

The superfluid phase of liquid ^{4}He behaves in strange ways, which can be summarized as follows. It shows “two-fluid” behavior; a normal fluid coexisting with a superfluid component. The superfluid component can exhibit frictionless flow at low velocities and

in narrow channels. Rotational motion in the superfluid component is severely restricted by quantum effects, associated with the quantization of circulation (essentially the quantization of angular momentum). This unconventional behavior has its origin in quantum effects and especially in the formation of a coherent Matter field within the liquid, associated with the phenomenon of Bose-Einstein condensation. At high flow velocities, ideal superfluid behavior, involving frictionless flow, breaks down through the generation of a form of quantum turbulence, which leads to a frictional interaction between the superfluid and normal components. Quantum turbulence is likely to be important in many situations of practical importance.

2.11: The superfluid phases of ^{3}He

Helium being a principal constituent of stellar Matter is the second most abundant element in the universe after hydrogen. It has dominated the scene in cryogenics as the most important refrigerant for attaining very low temperatures ever since it was liquefied for the first time in 1908 by Kamerlingh Onnes when at 0.9 K he was also able to attain the lowest temperature ever reached before that time. It exists in two isotopic forms namely ^{3}He and ^{4}He.

The small mass of the He atom is primarily responsible for many of its very interesting and unusual physical properties. It is extremely difficult to solidify Helium due to the fact that it has significant zero-point motion even at absolute zero since it is extremely light. This makes it possible to have He in the liquid phase up to very low temperatures. Hence the liquid state of He is a very good example of a quantum liquid whose phase diagrams demonstrate richness in their variety of physical properties, as shown in fig. 2.16.

Out of the two isotopes of He, only the heavier isotope ^{4}He had been in the focus of attention of Physicists for a long time. The reason for this is that ^{4}He shows a transition to the superfluid phase on cooling below 2.17 K which is known as the lambda transition one of whose signatures is a characteristic peak in the specific heat. The superfluid phase, along with other strikingly unusual properties has the ability to flow without friction.^{3}He on the other hand shows no such interesting property even at temperatures close to 1K. It

is only at much lower temperatures (of the order of a few mK) that liquid ^{3}He undergoes transition to the superfluid state

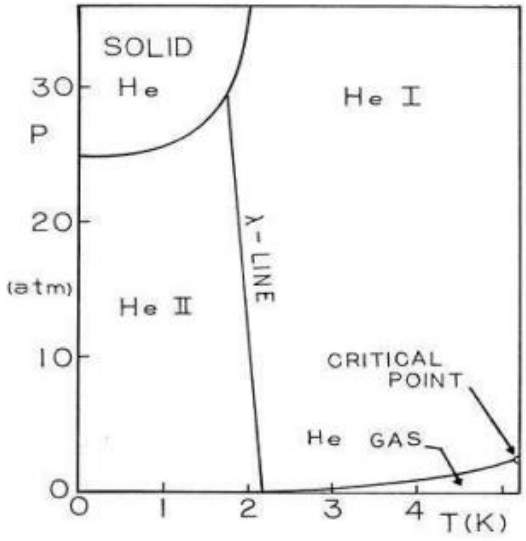

Fig. 2.16: Phase diagram of ^{4}He (Shiladitya, 2010)

That the two isotopes of He are strikingly different in their properties has to do with the fact that ^{4}He is a boson since it has an even number of spin ½ particles (electrons and nucleons) while ^{3}He being deficient of one neutron has an odd number of nucleons in its nucleus and hence behaves like a fermion. While in ^{4}He superfluidity is associated with Bose – Einstein Condensation (BEC) of the bosonic atoms, in ^{3}He the fermionic atoms form Cooper pairs very similar to how electrons pair up in a conventional BCS superconductor (Bardeen, *et.al.*, 1957).

2.11.1: Normal state behaviour of liquid ^{3}He

The physical properties of the normal' phase of liquid ^{3}He have been considered in detail. Experiments reveal that between 100mK and 3mK the liquid behaves like a weakly interacting degenerate Fermi gas. Two of the notable features in the experimental data are: 1) specific heat being linear in temperature, and 2) spin susceptibility being independent of temperature as pointed out by (Leggett, 1975). Given that the hard core radius is about 70% of the inter-atomic spacing, it is expected that the liquid be strongly interacting.

Landau's Fermi liquid theory seems to provide a good description of the normal phase of liquid ^{3}He. Although the theoretical details of Landau's theory shall not be explored here, the essential physical idea is the following: as a result of the inter –particle interaction, each atom is 'dressed' by a screening cloud around it. Such dressed states called quasiparticles take over the role of the bare particles. The effect of interactions appears as a renormalization of the effective mass of the particles. Thus the ground state of such a gas is a filled Fermi sea of quasiparticles of effective mass m* which differs from m, the mass of the bare particle. An important point to note here is that apart from the change in effective mass, the interactions are also responsible for introducing an effective interaction between quasiparticles themselves via a parameter f(p,F,;p`,F`) which is a measure of the interaction energy between quasiparticles of momenta p, p`and spins F and F`, respectively.

2.11.2:Inter-atomic interaction potential in liquid ^{3}He

The inter-atomic interaction potential in liquid ^{3}He is characterized by a strongly repulsive hard core at small distances (less than 2 Å) and an attractive Van der Waals interaction at larger distances as shown in the Fig. 2.17.

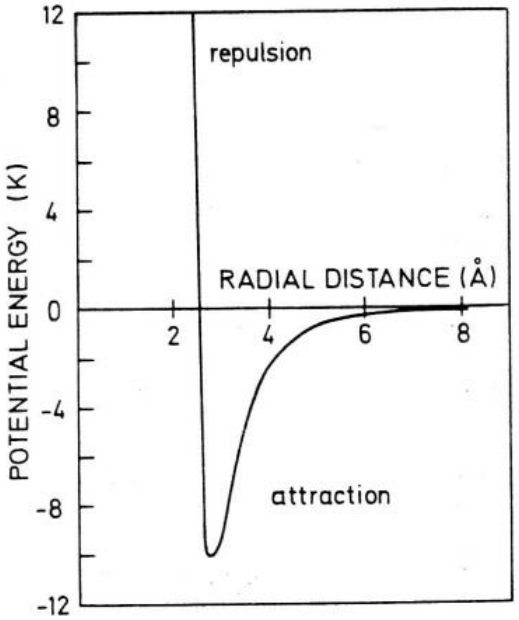

Fig. 2.17: The inter-atomic potential in liquid 3He (Vollhardt & Wolfle, 1990).

Shortly after BCS theory was developed (Bardeen, *et. al*., 1957), and applied successfully to the metallic superconductors, attempts towards applying the theory to other fermionic systems were initiated. The first thing that was noticed about ^{3}He was that the atoms could not possibly pair up in the s-wave state (zero angular momentum) since the hard core repulsion ensures that the wave function vanishes for small inter-atomic distances. One of the earliest works was done by (Brueckner *et. al*., 1960), who stated that the l = 2 state in ^{3}He can form a condensate at a temperature less than 0.07 K. Later, the work of (Anderson *et. al*., 1961), predicted an even lower upper bound of 0.02K. It was clear that ultra-low temperatures were needed to be attained in order to observe condensation in ^{3}He.

At this point it would be worthwhile to mention few of the advances made in the experimental scene as well. In the late sixties and early seventies active experimental research was conducted on ^{3}He and its mixture with ^{4}He, along with important advances in refrigeration techniques, as (Wheatley, 1975) points out. Dilution refrigeration was perhaps the most significant development. This technique enabled providing temperatures of as low as 10mK with further reduction possible by using other techniques. The other refrigeration techniques that were developed included nuclear refrigeration and adiabatic compressional cooling. It did not take too long for successful observation of superfluid condensation in ^{3}He to happen.

2.11.3: Experimental observation of superfluid condensation in ^{3}He

In 1972, (Osheroff, *et. al*., 1972) reported some interesting observations regarding liquid ^{3}He at temperatures below 3 mK. In their first experiment, they had Helium in a Pomeranchuk cell which is essentially a compressional cooling cell. Inside the cell they cooled ^{3}He under pressure so that they had the solid phase coexisting with the liquid phase. They observed two distinctive features on the pressure Vs time curve (also known as the pressurization curve) tunneling below 3mK. They called these features A and B. At point A the rate of change of pressure with time (dp/dt)) fell discontinuously by a factor of 1.8 at a temperature of about 2.65 mK. At point B another singularity was observed at a temperature of less than 2mK. This was initially attributed to nuclear spin effects in the solid phase until subsequent NMR experiments showed that the A and B features had to

do with dynamic magnetic effects in the liquid phase. In Fig. 2.18, the zero field phase diagram of ^{3}He is shown.

The new phases A and B are the superfluid phases that are achieved at very low temperatures under pressure. In this phase diagram there are two transition lines that are of concern in the light of the present discussion. The first is the T_c that separates the normal and superfluid phases. As pointed out by (Wheatley, 1975), the transition is second order. The other transition is the A to B transition which is first order.

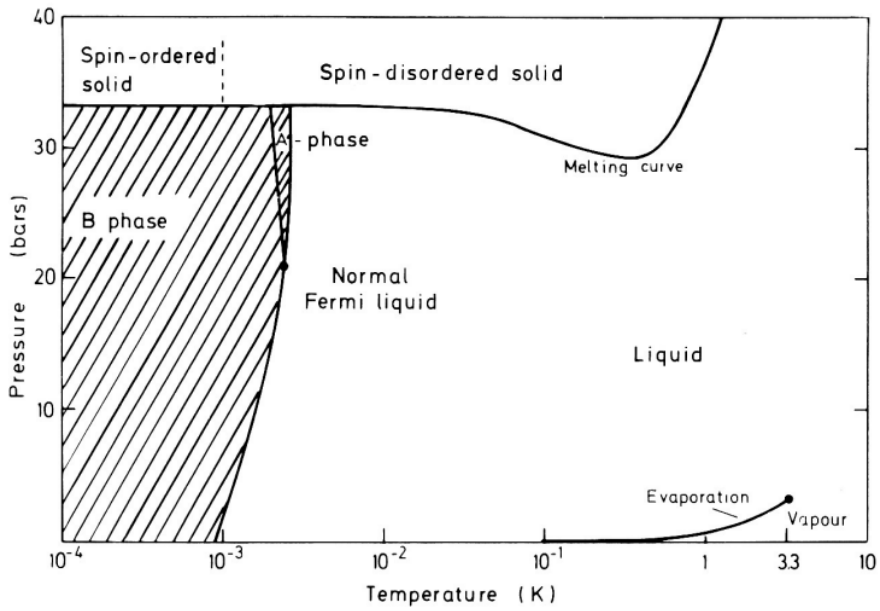

Fig 2.18: Phase diagram of ^{3}He drawn in logarithmic temperature scale and zero magnetic field (Vollhardt & Wolfle, 1990).

2.11.4: Fermions

Figure 2.19 shows the electron–electron pair-correlation function computed for 36 electrons with angular momentum L = 708. It should be emphasized that the angular momentum L = 708, although a large number, is relatively small. In fact, it corresponds to L = 24 for seven particles, where according to figure 2.24 no localization of particles is expected.

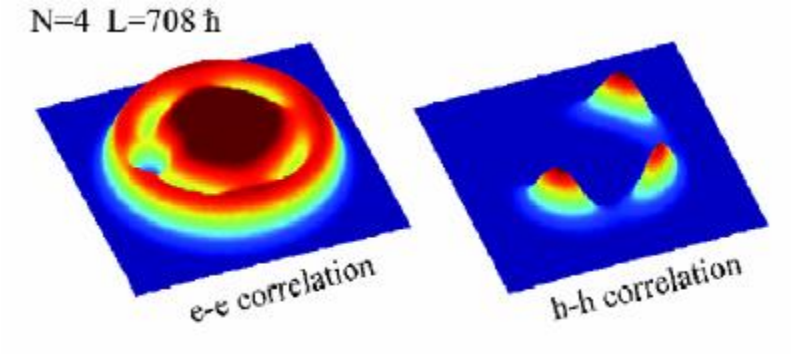

Figure 2.19: Pair correlation function of 36 electrons in a harmonic trap with angular momentum L = 708 showing the exchange-correlation hole and four vortices (left) and the vortex–vortex correlation function showing that the vortices are well localized(right)

Finally, it is noted that localization by rotation can also happen in the case of quasi-particles, even when they are collective excitations. An example here are the vortex patterns emerging in rotating clouds of bosons or fermions at smaller angular momenta (Saarikoski, et.al., 2004). For clear vortex states, naturally, the number of particles should be much larger than that of the vortex quasi-particles. It is thus limited to study polarized fermions (or spinless bosons).

In addition to the exchange-correlation hole around the reference electron, four minima in the otherwise smooth density distribution are observed.

It is shown that quantum mechanical particles, when set rotating in a two-dimensional harmonic trap, tend to localize to Wigner molecules. The localization is seen clearly in the periodic oscillations in energy spectrum as a function of the angular momentum. The many-particle spectrum can be explained in detail by rigid rotation and vibrational modes calculated using classical mechanics. These results seem universal. They are independent of the shape or range of the inter-particle interaction, and fermions and bosons show similar localization. Considering also that the spin degree of freedom does not change the

tendency for localization. With spin, the many-body states form a very narrow band, clearly separated from high-lying collective excitations. When the particle number is sufficiently large, the rotational spectrum shows localization of quasi-particles which can be identified as vortices.

2.12: Exchange-induced crystallization of soft-core bosons

The phase diagram of a two-dimensional assembly of bosons interacting via a soft-core repulsive pair potential of varying strength can be studied, and compare it to that of the equivalent system in which particles are regarded as distinguishable. In this quantum-mechanical exchanges stabilize a 'cluster crystal' phase in a wider region of parameter space than predicted by calculations in which exchanges are neglected. This physical effect is diametrically opposite to that which takes place in hard-core Bose systems such as ^{4}He, wherein exchanges strengthen the fluid phase. This is underlined in the cluster crystal phase of soft-core bosons by the free energy gain associated with the formation of local Bose–Einstein condensates.

The role played by quantum-mechanical exchanges of indistinguishable particles in determining the fluid–solid phase boundary is a subject of fundamental interest in Condensed Matter and quantum many-body Physics. It has long been the conventional wisdom that exchanges should have little or no influence over the freezing–melting phase transition. On its face, this assumption would seem reasonable; after all, in naturally occurring crystals quantum exchanges are strongly suppressed, both by particle localization at lattice sites as well as by the strongly repulsive core at the short distance of any known inter-atomic or intermolecular potential. Furthermore, the melting of most solids occurs at temperatures at which the average rms excursion of particles away from their lattice sites is dominated by thermal effects, with quantum-mechanical corrections being generally negligible (Boninsegui, *et. al.,* 2012). For this reason, it has been customary to neglect quantum statistics altogether in theoretical studies of quantum crystals also near the melting line.

Recent work (Boninsegui, *et.al.,* 2012) has challenged this assumption, however, by showing that in Bose systems with hard-core type interactions (such as Condensed ^{4}He),

quantum exchanges have the effect of greatly expanding the region of stability of the fluid phase, with respect to what it would be if exchanges were not present, i.e. if particles were distinguishable (henceforth distinguishable quantum particles shall be referred to as 'boltzmannons'). To phrase this more quantitatively, the free energy gain associated with the occurrence of long cycles of permutation of identical particles has the effect of moving the freezing line to a considerably higher density than one would predict based on calculations only including the zero-point motion. For this reason, theoretical studies of the phase diagram of a Bose system neglecting exchanges are likely to incur significant quantitative error in the determination of the solid–fluid phase boundaries, and predict unphysical thermo crystallization (i.e. re-entrance of the solid phase) at finite temperatures (Boninsegui, *et.al.*, 2012). Furthermore, long bosonic exchanges (i.e. comprising a macroscopic fraction of all particles in the system) can underlie and impart significant resilience (i.e. long lifetime) to metastable, glassy superfluid phases. Microscopically, this can be phrased in the language of path integrals, in terms of 'frozen' exchange cycles, in which the paths of many particles become entangled. Because a macroscopic number of single-particle (or, rare multi-particle) tunneling events are required, in order to disentangle all particles, the system may remain 'stuck' in a metastable disordered, glassy superfluid phase.

It can be understood that the findings of crucially rely on the presence of a 'hard' repulsive core at short distances in the pair-wise interaction $v_{(r)}$. Indeed, if $v_{(r)}$instead features a 'soft' core (i.e. ,$v(r \to 0) \sim \hbar^2/2md^2$ where *m* is the particle mass and *d* the mean inter-particle distance), the effect of the Bose statistics is in fact the opposite. Specifically, a high-density 'droplet' (or 'cluster') crystal phase, featuring a multiply occupied unit cell (Cinti, et.al., 2010), is strengthened over the fluid one, again with respect to the Physics of a system of boltzmannons (or classical systems featuring the same kind of interaction, e.g. macromolecules (Lenz, *et.al.*, 2012). Phrased differently, since the energy cost associated with particles laying at a close distance is relatively small, a phase in which each unit cell acts in a sense as a mesoscopic Bose condensate has a lower free energy than the uniform fluid phase 6 . This conclusion can be reached by studying a two-dimensional system of soft-core bosons by means of quantum Monte

Carlo simulations. Although the results presented here are for a specific kind of soft-core interaction (Henkel, *et.al.*, 2010), experimentally realizable in an assembly of cold atoms, the Physics described here are independent of the detailed form of the potential utilized in our study, but only with the presence of a soft core at short inter-particle separation.

2.12.1: Model for crystallization

Consider an ensemble of *N* spin-zero Bose particles of mass *m*, whose motion is confined to two physical dimensions (a choice made for convenience only, the main physical conclusions being independent of the dimensionality). The system is enclosed in a square cell of area *A*, with periodic boundary conditions, and is described by the following many-body Hamiltonian:

$$\widehat{H} = -\frac{\hbar^2}{2m}\sum_i \nabla_i^2 + \sum_{i<j} v\left(\left|r_i - r_j\right|\right) \tag{2.19}$$

The specific form of the potential could be

$$v(r) = \frac{v_0}{r_c^6 + r^6} \tag{2.20}$$

with $v_0 > 0$ Such a potential describes the interaction between two Rydberg atoms (Gallagher, 1994) in the so-called Rydberg blockaded regime (Henkel,et.al., 2010). The above choice of interaction is motivated by the fact that a quasi-2D Bose assembly with such pair-wise potential can be experimentally realized in an assembly of cold Rydberg atoms (Schausz, et.al., 2012), which feature strong van der Waals interactions (Beguin, et.al., 2013). These are currently utilized in numerous experiments to study long-range interacting effective spin systems (Schausz, et.al., 2012), as well as for applications in quantum optics (Dudin, et.al., 2012) and *quantum information science.*

The most important feature of the potential (2.20) is the soft repulsive core of radius r_c, which is the main consequence of the 'Rydberg blockade' mechanism, causing a flattening off of the repulsive part at short inter-particle separation . The rapidly decaying tail, also repulsive, does not play an important role in the context of this work; indeed, as mentioned in the introduction, the same qualitative behavior shown here can be observed

with a broad class of physical potentials displaying a repulsive soft core at a short distance, with the only requirement being the presence of a negative Fourier component (Modugno,et.al., 2002). Another important feature is that the strength of the repulsive core of the pair-wise interaction can be 'tuned', allowing one to go from the soft to the hard core regime, in which qualitatively different Physics arise.

The equation

$$\epsilon_0 = \hbar^2/mr_c^2 \tag{2.21}$$

could be taken as the unit of energy (and temperature, i.e. the Boltzmann constant k_B is set to one), and $r_c$that of the length. Thus, the density of particles $\rho \equiv N/A$ is expressed in units of r_c^{-2}. The dimensionless parameter

$$v_0 = mv_0/\hbar r_c^4 \tag{2.22}$$

measures the relative strength of the interaction compared with the characteristic kinetic energy ϵ_0.

The phase diagram of this system is similar to that of other soft-core Bose systems. If $V_0 \to \infty$, the Physics approaches that of an ensemble of hard disks, whose phase diagram features a low-density fluid (gas), turning superfluid at low temperature, and transitioning at sufficiently high density into a crystalline phase with one particle per unit cell (the presence of a weak repulsive tail stabilizes such a crystalline phase at $t = 0$, even at low density). Multiple occupation crystals occur at density $\rho \gtrsim 1$; in this regime, in which no supersolid phase is observed, the Physics of the system in the solid phase mimic those of the Bose Hubbard model. On the other hand, in a range of values of V_0(roughly)$1 \lesssim V_0 \lesssim 20$, at low temperature the system transitions from the fluid phase directly into a crystalline one featuring multiply occupied sites (unit cells) (Macri, et.al., 2013). This is the physical regime of interest here.

The low-temperature phase diagram of the system was studied by the Hamiltonian in eq.(2.19) by means of first-principle computer simulations based on the worm algorithm in the continuous-space path integral representation. This is a fairly well-established

computational methodology, allowing one to essentially obtain the exact thermodynamics properties of Bose systems at finite temperature, using only the microscopic Hamiltonian as the input. Because the continuous-space worm algorithm is thoroughly illustrated elsewhere, its implementation here has not been reviewed. It suffices to mention that the details of the calculations are standard, as the use of the potential in eq.(2.20) entails no particular difficulty. The usual fourth-order approximation is utilized for the high-temperature density matrix. All of the results reported here can be extrapolated to the limit of the zero time step.

The main quantity of interest here is the superfluid density, which is computed by means of the well-known 'winding number' estimator. Most of the calculations were carried out with a number of particles, of the order of a few hundred, with $N = 800$ being the largest system size considered. Parallel simulations can be carried out, at the same thermodynamic conditions, of a system of boltzmannons described by the same Hamiltonian, in order to assess the effect of Bose statistics on the phase diagram. It is worth remembering that the two systems have the same ground state; this is a straightforward consequence of the fact that the ground state wave function of a many-boson system is nodeless (Feynman, 1972).

As mentioned above, the regime of interest here is to understand that the repulsive core of potential in eq.(2.20) is soft, i.e. $V_0 \lesssim 20$. In this range of repulsive interaction, at a density $\rho \lesssim 1$, the system transitions from a fluid to a droplet crystal phase with a site occupation of the order of a few. In particular, considering a density $\rho \approx 1$ and with an incommensurate occupation number per site, it was recently shown that zero-point vacancies cause a superfluid flow of particles through the crystal (Cinti,et.al., 2014), accordingly with the seminal works of Andreev–Lifshitz–Chester on supersolidity. However, in this study number of particles considered was 10 or above.

The occurrence of a specific phase, and in particular one that has crystalline long-range order, can be established in a computer simulation by calculating structural quantities like the pair correlation function, which displays marked oscillations in the crystalline phase. Equivalently, its Fourier transform, related to an experimentally measurable quantity

known as the static structure factor, features a peak in the correspondence of the wave vector $k = 2\pi/a$, with a being the lattice constant (typically $a \sim r_c$). However, the presence of crystalline order can also easily be assessed by visual inspection of particle world lines, an example of which is offered in figure 2.20, which clearly shows the formation of a droplet crystal for a system of Bose particles.

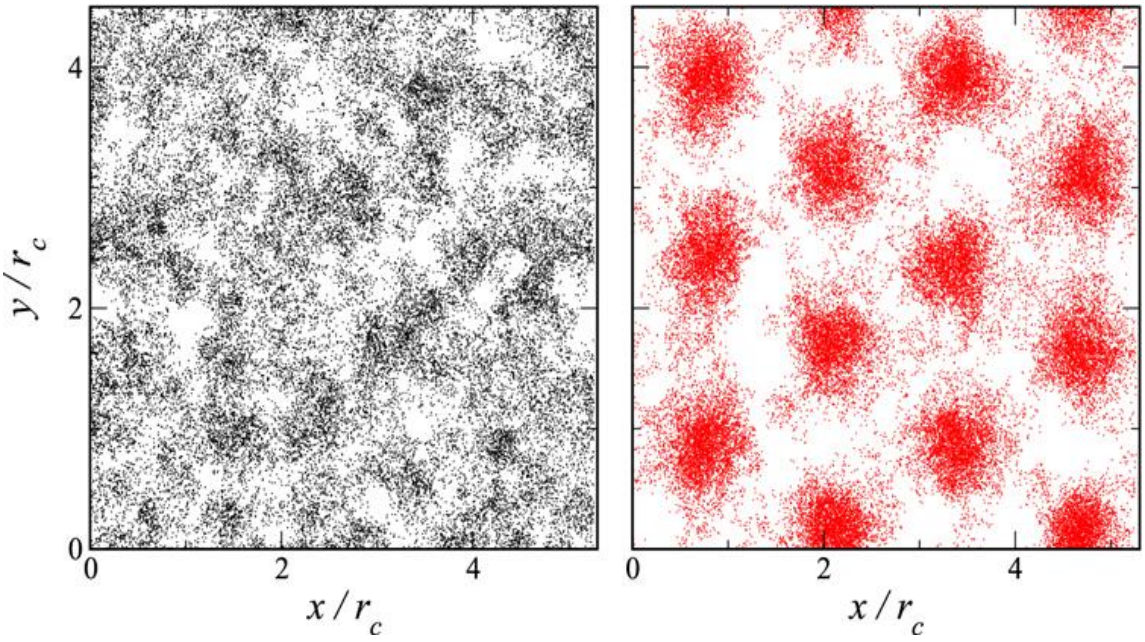

Figure 2.20: Configuration snapshots (particle world lines) for a system with N = 600 particles and α=30 at a temperature of t=T⁄ρ=0.3. The left panel refers to a system of distinguishable particles (boltzmannons), and the right to one of Bose particles.

A mean-field treatment (Macri, *et.al.*, 2013) shows that the Physics of the system in the ground state are governed by the single dimensionless parameter $\alpha \equiv V_0$. This can be verified, by direct numerical simulation, that this assertion holds quantitatively for both Bose and Boltzmann statistics at low temperature. To illustrate this point, in figure 2.21, the result is shown for the superfluid fraction f_s computed for the Bose system in the ground state limit (i.e. temperature$T \to 0$) for three different densities, namely 4.53, 6.78 and 11.33 (roughly corresponding to 10, 15 and 25 particles per unit cell, respectively). The results are shown as a function of the renormalized interaction parameter α, in a

range corresponding to the values of the interaction strength $3 \lesssim V_0 \lesssim 8$. Within the statistical errors of the calculations, the values of the superfluid density all fall on the same curve, with three different regimes clearly identifiable. Specifically, at low α the superfluid fraction is ~ 1, as the system is in the fluid phase; as α is increased to a value close to 28, f_s abruptly drops to a lower (but finite) value, as expected for a superfluid system breaking transational invarianc. Finally, as α is increased even further (close to 37), the system transitions into an insulating droplet crystal phase, with negligible particle tunneling across adjacent unit cells.

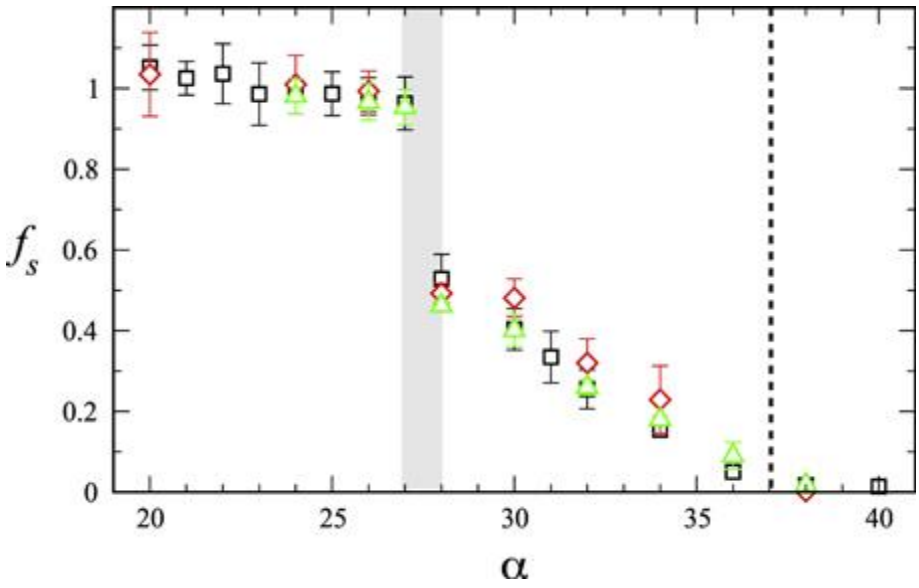

Figure 2.21: A superfluid fraction in the limit of T→0 , computed by simulation as a function of the renormalized interaction parameter ∝=ρV_0 (see text) for the three densities ρ=4.53 (triangles), 6.78 (diamonds) and 11.33 (squares).

Figure 2.22 shows the superfluid fraction f_s for the Bose system at finite temperature, computed for $\alpha = 28$, at which value the system displays a supersolid phase at low temperature. Here two values of the density are considered, namely $\rho = 9.02$ and 11.33;the simulated system comprises N = 800 particles. The values of f_s as a function of the reduced temperature $t \equiv T/\rho$ are plotted, and observe the collapse of the data. As one can see, f_s starts off at a value slightly less than 0.6 at t = 0, as the system is in the supersolid phase, and jumps up to a higher value at $t \approx 0$, in correspondence with the

melting of the crystal into a uniform superfluid. The numerical data for f_s in the superfluid regime are fitted in the usual way, based on Berezinskii–Kosterlitz–Thouless theory, to obtain an estimate of the superfluid transition temperature.

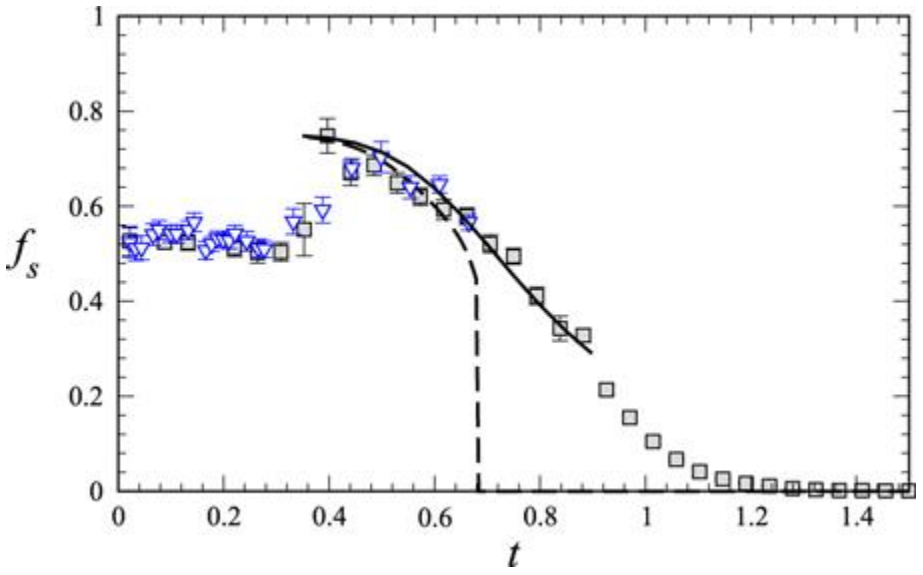

Figure 2.22: Superfluid fraction versus reduced temperature t≡T/ρ for a system with α=28, ρ=11.33 (boxes) and ρ=9.02 (triangles). The simulated system comprises N = 800 particles. The line through the data point is a fit based on the Berezinskii–Kosterlitz–Thouless theory, whereas the line falling steeply to zero at $t \sim 0.68$ is the prediction for the thermodynamic limit.

A schematic phase diagram is obtained of both the Bose and the distinguishable particle systems in the (a, t) plane through a number of vertical 'cuts' at different values of α. The resulting phase diagrams are shown in figure 2.23. The first obvious observation, aside from the fact that no superfluid phase can exist in a system of boltzmannons at any finite temperature, and that at exactly $t = 0$ the phase diagram is of course the same, is the much greater region of stability of the droplet crystal phase in the Bose system. This is the most remarkable outcome of this study, as it runs counter to the notion that quantum-mechanical exchanges should in principle favor a uniform phase in Bose systems. This is indeed what is observed in numerical studies of hard-core Bose systems (Boninsegui,et.al., 2012), and it is what takes place in the system studied here as well, in the $V_0 \gg 1$ (hard core) limit. However, if the repulsive core of the interaction is soft

enough that a droplet crystal is present in the phase diagram, then quantum-mechanical exchanges of Bose particles actually strengthen the crystalline phase. Thus, Bose statistics stabilize the crystal phase at a higher temperature than in the system of distinguishable particles.

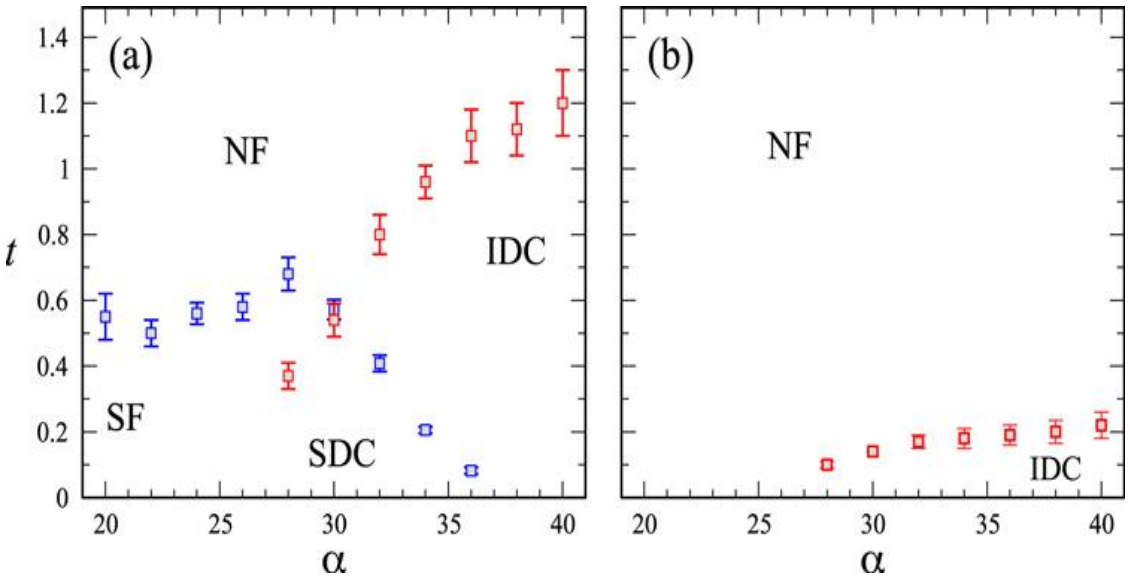

Figure 2.23: Phase diagrams in the∝-t (see text) plane. (a) Bose statistics with normal fluid (NF), a superfluid (SF), a superfluid droplet crystal (SDC), and an insulating droplet crystal (IDC). (b) A system of distinguishable particles with NF and IDC phases. The symbols represent the numerical determination of the appropriate transition temperatures.

Thus the greater stability of the crystal in the Bose system can be understood in entropic terms. In a system of distinguishable particles, the crystal melts into a fluid due to the greater entropy of the phase with higher symmetry. On the other hand, in the Bose system at low temperature, the entropy of a normal fluid phase in which exchanges are only local in character is comparable to that of a crystal in which exchanges occur among particles confined to within the same unit cell (droplet). Thus, the thermodynamically preferred phase is that of lower energy, i.e. the crystal. As the strength of the repulsion increases,

the number of particles in a droplet decreases and the crystalline phase becomes entropically less competitive with the fluid.

Thus one can say that in a Bose system characterized by pair-wise interactions with a repulsive core at short distances, quantum-mechanical exchanges can act to stabilize either the fluid or solid phase, depending on the strength of the repulsive interaction. While in the hard-core limit, exchanges strengthen the fluid phase, the opposite is true in a system in which the core is soft enough to allow the formation of a cluster (droplet) crystal phase at low temperature. It is shown that this effect is true for a two-dimensional system of Rydberg atoms, but the result is quite general, and in particular is independent of the long-range part of the potential.

In these cases, the occurrence of cluster crystal phases can be understood in terms of potential energy alone.

Quantum-mechanical exchanges may be restricted to particles in the same cell, in which case the crystal is insulating, or particles may hop to adjacent cells and a supersolid phase may ensue, but this aspect is not crucial to the Physics of interest here.

Obviously, at a sufficiently short distance the repulsion will start increasing rapidly again as the Pauli exclusion-principle prevents electronic clouds of different atoms or molecules from spatially overlapping. The assumption made here is that r_c is much greater than the radius of such an inner hard core.

2.13: Crystallization of Fully-Polarized Dipolar Fermions

Consider a two dimensional model of non-interacting chains of spinless fermions weakly coupled via a small inter-chain hopping and a repulsive inter-chain interaction. The phase diagram of this model has a surprising feature: an abrupt change in the Fermi surface as the interaction is increased. The study of this meta-nematic transition, shows the well-known 2 1 2−order Lifshitz transition is the critical endpoint of this first order quantum phase transition. Furthermore, in the vicinity of the endpoint, the order parameter has a non-perturbative BCS-like form. The competing crystallization transition in this model was studied, and the full phase diagram was derived. This Physics can be demonstrated

experimentally in dipolar ultra-cold atomic or molecular gases. In the presence of a harmonic trap, it manifests itself as a sharp jump in the density profile.

The study of phenomena which deform the Fermi surface in both electron and cold atom systems has gained much popularity recently. For example, it has been suggested that the Fermi surface shape-changing Pomeranchuk instability (Pomeranchuk,et.al., 1958) may describe experiments in heavy fermions, quantum hall devices, and ruthenates, (Grigera, *et.al.,* 2009) leading to a plethora of theoretical papers on the subject. The Pomeranchuk instability, which breaks rotational symmetry but no translational symmetries, is essentially a transition to an electronic nematic phase. An analogue in spin systems has also been studied. Incorporating other electronic analogues of liquid crystal phases into this picture has been put forward as a general picture of strong correlations (Kivelson & Fradkin, 2007) with evidence for smectic phases being observed experimentally in manganites and cuprates. These electronic liquid crystal phases also have a strong relation to dimensional crossover phenomena, where one can ask the question whether an array of one-dimensional chains (Luttinger liquids) coupled by a weak inter-chain hopping $t_\perp$ remains strictly one dimensional (confinement), or becomes a quasi-one dimensional Fermi liquid (deconfinement). Indeed, calculation methods such as self-consistent perturbation theory and functional renormalization (Ledowski, 2007) support the idea that the warped Fermi-surface is unstable for sufficiently small $t_\perp$, in principle therefore leading to a Fermisurface modifying transition at some finite value of interchain hopping.

While the issue of the Luttinger liquid to Fermi liquid crossover/transition is not yet fully resolved, it is possible to ask a much simpler question: what happens if an array of one-dimensional Fermi liquids are coupled together? A rather specific example in this direction was the study of coupled edge states (chiral one-dimensional Fermi liquids) in superlattices which exhibit integer quantum Hall effect (Betouras & Chalker, 2000). While such a toy model may not be realistic for any real materials, advances in laser trapping and cooling technology have led to the rapidly expanding field of trapped ultra-cold atoms, which in the context of Condensed Matter Physics can be thought of as a sort of quantum analogue simulation of a bulk system, (Campo & Ho, 2010) with

unprecedented control over disorder and interactions. It was suggested a few years ago (Baranov, *et.al.,* 2004) that exploiting the dipole interaction between cold polar molecules or highly dipolar atoms allows further control over effective interactions, in order to build exotic strongly correlated phases. Of particular interest in the present context is the case when the atoms or molecules are fermions. On the experimental front, there has been much recent experimental progress towards this goal using highly polar ^{40}K and ^{87}Rb molecules (Ni, 2008) and a fermionic isotope of the highly magnetic atom ^{163}Dy (Lu, 2010). On the theoretical front there has been a flurry of activity (Miyakawa,et.al., 2008). Unlike the long-wavelength scattering induced by Feshbach resonances, dipolar interactions have a power-law dependence on the distance between the interacting particles and a non-trivial dependence on the relative position of the two particles and orientation of the magnetic dipoles. In the presence of a strong polarization field the latter translates into a strongly anisotropic interaction which leads to a spontaneous (though not symmetry breaking) deformation of the Fermi surface (Miyakawa, 2008) Indeed depending on the strength of the dipolar interaction additional, symmetry-breaking (Pomeranchuk) Fermi surface deformations may also occur (Carr, *et.al.,* 2009). Even more interestingly, such polarization dipolar gases can in theory be combined with optical lattices to generate non-trivial tailor-made effective Hamiltonians. It was shown that (Quintanilla, *et.al.,* 2009) a quasi-one dimensional (quasi-1D) optical lattice could be used to create a system whose phase diagram features Fermi liquid, stripe and checkerboard ground states, as well as a meta-nematic quantum phase transition into a state with distorted Fermi surface.

The model (Quintanilla, *et. al.,* 2009), features chains within which there are no interactions, achieved by the alignment of the polarization field at the ‘magic angle’ to the tube direction. For this particular orientation of the field, the interactions between particles on different chains are purely repulsive. An experimental polarization of this model would thus furnish an example of the coupled one-dimensional Fermi liquids mentioned above. Interestingly, the spontaneous Fermi surface distortion encountered in this model corresponds also to an interaction-induced change of dimensionality, from quasi- 1D (open Fermi surface) to fully 2D (closed Fermi surface) behavior. An

important property of this model is that these various transitions can all happen in different, well separated, regions of phase space. Thus, each of the phase transitions can be studied independently without its properties being masked by the other ones. More recently other scientists have studied a closely related model, featuring continuum tubes rather than discrete chains (Huang & Wang, 2009). In this case only the strictly 1D limit was considered but on the other hand the polarization field was allowed to point in any direction. This leads to a rich variety of effective interactions and a correspondingly rich phase diagram: in addition to density wave and meta-nematic phases, different superfluid ground states are expected. The present work extends the theories (Quintanilla & Carr, 2009) by considering finite temperature phase transitions in addition to the quantum phase transitions discussed to date. A fully analytic theory of the metanematic transition in the neighborhood of its critical end point was developed. The Hamiltonian of the model that was analyzed in detail consists of spinless fermions hopping along parallel chains (labelled by n), with a weak hopping and an interaction between nearest neighbor chains:

$$H = \sum_{i,n}\{-t||(c_{i,n}^{\dagger}c_{i+1,n} + c_{i+1,n}^{\dagger}c_{i,n} - t_{\perp})(c_{i,n}^{\dagger}c_{i,n+1} + c_{i,n+1}^{\dagger}c_{i,n}) + V\rho_{i,n}\rho_{i,n+1}\} \quad (2.23)$$

Where the density

$$\rho_{i,n} = c_{i,n}^{\dagger}c_{i,n} \quad (2.24)$$

The calculation was done as follows: The meta-nematic transition was studied in full detail, explaining its origins and its link to the Lifshitz transition and the other competing instability of the model to a crystalline phase. It also considered both the specific properties of this model, and how these may be generalized to a more realistic microscopic model in Condensed Matter systems.

2.14: Physics of Neutron Rich Nuclei, Neutron Matter and Neutron Stars

The Physics of neutron rich nuclei requires accurate treatment of many-body correlations, proper inclusion of coupling with continuum degrees of freedom and open channels (Gaute & Elena, 2016), and even many-body interactions. The first basic approach is to

study the elementary particles, their properties and mutual interaction. Thus one hopes to obtain the knowledge of the nuclear forces. If the forces are known, one should, in principle, be able to calculate deductively the properties of individual nuclei. Upon accomplishing this, one completely understands nuclear structure. The other approach is that of the experimentalist and consists in obtaining by direct experimentation as many data as possible for individual nuclei. One hopes in this way to find regularities and correlations which give a clue to the structure of nuclei. The shell model, although proposed by theoreticians, really corresponds to experimentalist's approach (Goeppert & Mayer, 1963). Now to study the properties of neutron rich nuclei (heavy nuclei), neutron matter and neutron stars, it is necessary to have as accurate a knowledge of nucleon-nucleon interaction, a Repulsive Core lear forc Yukaw ld be understood that the nucleons in the interior of a nuclear medium do not a the same bare force, say V. They 0 experience an effective force, say G, which is calculated from V in abinitio methods. Since the nucleons are fermions, the Pauli principle prohibits the scattering into states, which are already occupied in the medium. Therefore the effective force is density d V(Mev and is written as G(ρ). The force G is much weaker than the bare force V. Nucleons move nearly freely in the medium and feel only a strong attraction at the -150 e (shell model). The nucleon-nucleon interaction is shown in Fig. 2.24.

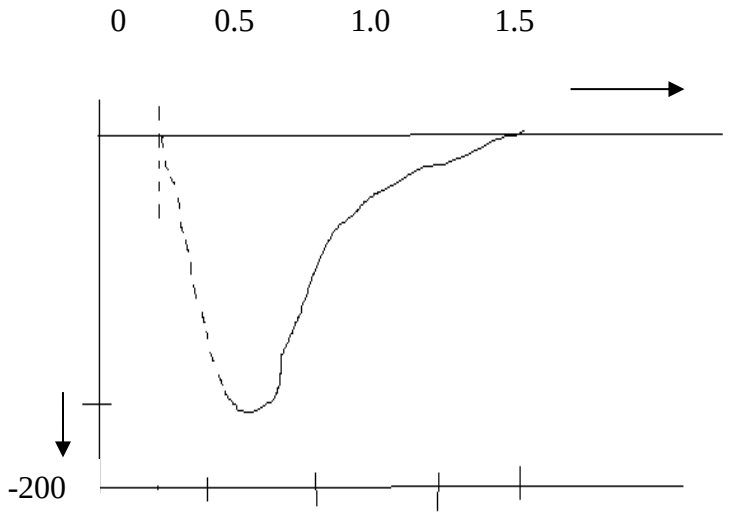

Fig. 2.24: Nucleon-nucleon interaction

In heavy nuclei the number of neutrons (N) is quite large compared to the number of protons (Z), the surface region of heavy nuclei is said to be neutron skin where the excess neutron may exist resulting in strong attractions at the surface since the neutron-neutron interaction is attractive. Now the simplest method to study the nuclear many-body problem is to know the bare NN force, the effective interaction, self-consistence via Hartree-Fock and Hartree-Fock-Bogoliubov (HF and HFB) theory. Assuming two-body interaction, the Hamiltonian H is written as,

$$H=\sum_{ij} t_{ij}c_i^+ c_j^+ + \frac{1}{4}\sum_{ijkl} v_{ijkl}c_i^+ c_j^+ c_l c_k \qquad (2.25)$$

This Hamiltonian is diagonalized by using the Bogoliubov canonical transformation to obtain the quasi-particle energy dispersion relation. This method has been extended by several authors to study the problem of infinite nuclear and neutron matter.

2.15: Neutron matter

It has been understood that the properties of neutron matter are very critical to the understanding of the properties of neutron-rich nuclei and neutron stars. Low-density neutron matter has direct impact on our understanding of neutron-rich nuclei. Correspondingly the equation of state of high-density low-temperature neutron matter is important in understanding the properties of neutron stars, particularly the mass-radius relation of the neutron star and also the mass of the neutron star.

Due to various reasons, in the past few years interest in the properties of neutron matter has acquired great importance. At very low densities, the neutron matter is quiet similar to the cold atoms, rather Fermi atoms, near unitarity (when the scattering length, a, is infinite), since two free neutrons are very nearly bound. This allows stringent tests of theories of fermions in this strongly interacting regime (Giorgin, Pitaevskii & Stringari, 2008). The equation of state (Ku, *et. al.*, 2012) and pairing gap of unitary fermions (Schirotzek, *et. al.*, 2008) have been calculated precisely. Accurate experimental measurements have provided severe tests of the theories, of course, some of the calculations gave excellent predictions, while others were less successful.

2.15.1: Neutron Star

Neutron stars, discovered in 1967, are created when giant stars die in supernovas and their cores collapse, with the protons and electrons essentially melting into each other to form neutrons. Neutron stars are city size stellar objects with a mass of about 1.4 times that of the sun. A neutron star is the densest object astronomers can observe directly. Neutron stars comprise one of the possible evolutionary end-points of high mass stars. Neutron star material is some of the most dense matter in the universe.

(Stuart, 2016) stated that for a start, a neutron star could never hit the Earth, the Earth would be drawn to it before it got anywhere near. For a finish, the nearest neutron star is between 250 and 1000 light years away in the direction of ursa minor star (ursa minor also known as little bear, is a constellation in the Northern sky.) So it won't be anywhere close to Earth in 75 years or 75 thousand, or 75 million years.

The equation of state for cold neutron matter at high density can be studied in the t-matrix formalism, and it can be shown that energetically it is convenient to have neutrons in a crystalline configuration rather than in a liquid state for values of the density exceeding 1600Tg/cm^3. Using t-matrix formalism means all the many-body interactions are taken into account to obtain the energy and the equation of state of the assembly. The other method is to use the hard-sphere interaction between the neutrons, and obtain the energy and the equation of state.

However, in this thesis, I have studied the properties of crystalline neutron matter, a state that exists in neutron stars. It should be understood that neutron stars are very high density systems with density $\rho_{n\cong 10\rho_s}$ (ρ_s is the saturation density of heavy nuclei).The properties of neutron stars are studied using the theory of crystallization of fermions.

The mass number (A) of the nuclei is equal to the number of protons (Z) and the number of neutrons (N) in a nucleus. In low mass nuclei Z=N, and as I progress towards medium and heavy nuclei, the neutron number (N) increases faster than the proton number (Z). For a nucleus to remain a bound system, attractive force must be greater than the repulsive force, and as the proton number (Z) increases, Coulomb repulsion increases,

and to balance this the neutron number (N) must increase faster than the proton number since the nuclear force between the neutrons is attractive. In very heavy nuclei when Z≥90, natural disintegration takes place by the emission of alpha (α), beta (β) and gamma (γ) radiations. Some of these nuclei have been found to have a surface region of the nucleus composed of neutrons only. This is called the neutron skin of the nucleus. These days both low mass and heavy mass designer nuclei have been produced experimentally. In such nuclei, the number of neutrons (N) is abnormally large compared to the number of protons (Z). The well-known such a nucleus is ${}^{11}_{3}Li$. When compared with the real nuclei ${}^{6}_{3}Li$ or ${}^{7}_{3}Li$, the number of neutrons is quite large. For such nuclei, the neutrons excess parameter $\eta = \frac{N-Z}{A}$ or the asymmetry coefficient becomes very large. In such nuclei, the excess neutrons are supposed to be in the surface region of the nucleus forming what is called the neutron skin of the nucleus.

From time to time, many nuclear models have been proposed (Kate, Jones & Witold, 2010), but no model is able to explain the properties of a given nucleus. Recently properties of medium-heavy and heavy nuclei with many active valence nucleons have been described in the framework of self-consistent mean-field methods. The self-consistent mean-field approach enables a description of the nuclear many-body problem in terms of a universal energy density functional. The exact energy functional which includes all kinds of correlations is approximated with powers and gradient of ground-state nucleon densities. Although it models the effective interaction between nucleons, a general density functional is not necessarily related to any given nucleon-nucleon (NN) potential. By using global effective interactions, adjusted to empirical properties of symmetric and asymmetric nuclear matter, and to bulk properties of few spherical nuclei, self-consistent mean-field models have achieved a high degree of accuracy in the description of ground states and properties of excited states in arbitrary heavy nuclei. One of the major aims of modern nuclear theory is to build a universal energy-density functional theory. The theory has to be universal in the sense that the same functional is used for all the nuclei with the same set of parameters. Such a frame work could provide a basis for a consistent microscopic treatment of the nuclear many-body problem, including infinite nuclear matter and neutron matter, ground state properties of all bound

nuclei, low-energy excited states, small-amplitude vibrations, large-amplitude adiabatic properties, and reliable extrapolations towards the drip line.

Using density-dependent effective interactions, nuclear matter properties at saturation have been calculated, and the values are (Lalazissis, Niksik, Vretener & Ring,2005), density at the saturation $\rho_s(fm^{-3}) = 0.152, \frac{E}{A}(Mev) = -16.14,$ compressibility $K_o(Mev) = 250.89$ and the effective mass $m^* = 0.572$. Same interactions have been used to obtain equations of state for symmetric nuclear matter and neutron matter (Niksik, Vretenar, Finelli & Ring, 2002). These calculations refer to nuclear systems which are, of course, degenerate, and superfluid, and whose densities are at best the saturation density of say heavy nuclei. A quantum solid is intrinsically restless, that the atoms continuously vibrate around their position and exchange places even at obsolete zero of temperature. Hence, quantum solid is different from classical solid. The properties of quantum solid are dominated by the zero-point motion, and this means Heisenberg's uncertainty principle. Part of the energy of the neutron stars has been calculated using the uncertainty principle. Since in the crystalline state, the constituents are closest to each other, and they cannot approach closer than that distance (the distance of the nearest approach), there could exist strong repulsive force between the particles, and I have assumed this force to be hard-sphere repulsion of infinitely repulsive force. In the crystalline state, the kinetic energy can be neglected, and hence the total energy or equation of state will be the sum of the energy due to zero-point motion and the hard-sphere interaction. This could be an oversimplification of the actual system, but to obtain some acceptable results, Physics eliminates complexity to expose the underlying simplicity. After all, it is not possible to conduct actual observations on neutron stars; their properties can be calculated by assuming some sort of possible interactions; and this is what poses the gap!

It should be mentioned that calculations have been assuming phenomenological density dependence of nucleon-meson couplings to reproduce the properties of finite nuclei, symmetric and asymmetric nuclear matter, and such calculations can be used for neutron

matter also (Antoniadis, *et.al.*, 2013), but I have not tried to attempt such calculations as of today.

The study of neutron stars has become very important in recent years. The discovery of the first two-solar-mass neutron stars (Demorest, & Antoniadis, 2013) has provided critical constraints on the dense matter equation of state. These observations have eliminated whole classes of models that predicted that the critical mass of a neutron star is $\simeq 1.4M_{\oplus}$, where $M_{\oplus}$ is the mass of the sun, combined with the recent observation of massive neutron stars, the attractive nature of neutron-neutron interaction at low momentum means the equation of state must be soft at low density with a rapid transition to high-pressure when the higher-momentum neutron-neutron and many-body interactions may become important, particularly three-neutron and higher interactions. It is important to know that the inner crust of neutron star is inhomogeneous neutron matter, and may be composed of lattice of heavy neutron-rich matter. Understanding the properties of neutron-rich matter could assist in obtaining heavy-element synthesis.

Some of the high-lights of the neutron-star masses, radii, and the EOS (Equation of State) are given below (Gandolfi, Giezerlis & Carlson, 2012). However, it should be mentioned that the most modern EOS for neutron matter implies that the maximum neutron star is of the order of 13.5 Km, whereas earlier value was 10.0 Km.

The Tolman-Openheimer-Volkov (TOV) equations are

$$\frac{dp}{dr} = -\frac{G\left[m(r)+\frac{4\pi r^3 p}{c^2}\right]\left[\varepsilon+\frac{p}{c^2}\right]}{r\left[r-\frac{2Gm(r)}{c^2}\right]} \tag{2.26}$$

$$\frac{dm(r)}{dr} = 4\pi\varepsilon r^2 \tag{2.27}$$

where $p = \rho^2\left(\frac{\partial E}{\partial \rho}\right)$ =Pressure in the star (2.28)

$\varepsilon = \rho(\varepsilon + m_N) =$ energy density (2.29)

$m_N =$ Mass of the neutron

$m(r)$ = Gravitational mass enclosed within radii r

G = Gravitational constant

E = Energy per neutron

The solution of the TOV equations for a given central density gives the profiles of ρ.ϵ and P as functions of radius r, and also the total radius R and mass M=m(R). The total radius R is given by the condition P(R)=0, i.e., The pressure P is zero at the edge of r. The speed of sound in the interior of the star is given by $C_s^2 = \frac{dp}{d\varepsilon}$, and this should be less than the speed of light. These are some of the equations which are used to study the properties of neutron stars and neutron matter.

Another important physical quantity which is critical in the study of the properties of neutron matter and neutron stars is, E (ρ_n), which is the energy per neutron as a function of the neutron density ρ_n. For this purpose the equation of state (EOS) given by E(ρ_n) was parameterized. However, our approach described in chapter four studies the variation of E(ρ_n) with ρ_n only.

CHAPTER THREE

METHODOLOGY

3.1: Introduction

There are two types of particles in nature. One type is known as fermions and the other type is called bosons. The concept of bosons was put forward first. In 1924, the Indian physicist Satyendra Nath Bose working on the question of distinguishability of particles started a revolution in statistical mechanics (Bose, *et.al.*, 1924). At that time Bose was working on a derivation of Planck`s formula for black-body radiation by treating the photons as a gas. Bose`s approach to the problem meant asking a question as to how many particles/ photons occupy a certain energy state of the system, instead of which particle occupies which energy level. The latter concept gives rise to the classical Maxwell- Boltzmann gas of distinguishable particles, whereas the former leads to either Bose-Einstein or Fermi-Dirac statistics depending upon the physical properties of the system such as spin.

In Bose-Einstein statistics, each single particle state can be occupied by an arbitrary number of particles. But in Fermi-Dirac statistics, due to Pauli Exclusion Principle, a single particle state can be occupied by only a single particle. Particles obeying Fermi-Dirac statistics are called fermions. However, it was in 1939 that the connection between the spin of a particle and its quantum statistics was fully discovered. Particles with half-integer spin such as the electron obey Fermi-Dirac statistics. Composite particles also fall into one of these categories, depending on the total spin. As such, the basic building blocks of an atom (electron, neutron, proton) are all fermions. Thus, the atom as a whole can be either a boson or a fermion, depending on the total number of electrons and nucleons.

Although the concept of Bose-Einstein Condensation (BEC) was introduced theoretically by Einstein in 1925, it was experimentally realized for ^{87}Rb and ^{23}Na in 1995 only (Anderson, *et.al.*, 1995). Since then the field of atomic BEC has exploded, and to-day many groups worldwide study the properties of these BEC`s.

Parallel to the work of bosonic atoms, there was great interest in fermionic gaseous ensembles encouraged by the perspective of observing Cooper pairing between atoms in the system. Compared to bosonic systems, fermionic experiments were subject to delays. Partly, this was due to technical difficulty in applying techniques of evaporative cooling to fermionic systems, and partly due to the popular misconception that fermions do not interact. There is some truth to the above statement since s-wave scattering between identical fermions is forbidden due to the Pauli Exclusion Principle, and at very low temperatures, higher order scattering processes are generally energetically forbidden. The final experimental steps that are very successful in producing atomic BEC become highly inefficient when applied to a spin-polarized Fermi gas. However, fermions in different spin states (distinguishable fermions) do interact, and a quantum Fermi gas of atoms (generally called degenerate Fermi gas) can be observed as a result of evaporative cooling of an interacting spin mixture (Demarco & Jin, 1999). A large number of experimental observations (Modugno, et.al., 2002) confirmed that fermions do interact, even strongly.

Thus, fermionic superfluidity has been realized using the attractive interaction required for Cooper pairing, and the attractive interaction is provided by direct scattering between fermions in different spin states. This is similar to the attractive interaction between electrons in superconductivity and this interaction is provided by phonons in the BCS (Bardeen, Cooper, Shrieffer) theory. Thus, a Fermi gas is a spin mixture of ultracold fermionic atoms in different spin states and can interact via S-wave scattering. Spin mixtures are usually composed of two clouds in different magnetic hyper fine states with equal atomic number. Generally, interactive fermions in the normal state are described by Landau's Theory of Fermi liquids (Landau & Lifshitz, 1980). According to this, when the interaction is turned on, a fermion disturbs the surrounding ones locally, forming together with disturbance a quasi-particle. The (interacting) quasi-particles have the same spin and

momentum as the initially non-interacting fermions, and their number is equal. They therefore behave similarly to non-interacting fermions, and their number is equal. Thus, like the superfluidity of bosons, superfluidity of fermion atoms as well as weakly bound diatomic molecules can be studied. This has been done experimentally in potassium.

Once the superfluid state was experimentally observed for bosons (liquid ^{4}He) and fermions (liquid ^{3}He), the next step was to study the conditions that can lead to the solidification or crystallization of the system involved. The first to be studied was the solidification of ^{4}He. It becomes solid at very low temperature close to zero Kelvin, and under an external pressure of 25 Atm. (25 bar) or more. In the solid state, ^{4}He has Hexagonal Crystal Structure, and it is highly compressible.

For any physical system, whether a boson system or a fermion system, the most important physical parameters that will be required to realize that crystalline state of the system are, temperature, the density and the inter-particle interaction. In general reduction of temperature followed by the application of large external pressure can lead to freezing and or crystallization.

However, recently, scientists led by Professor Raymond Ashoori (Raymond & Ashoori, 2016) at MIT-USA, believed that they had finally captured the process of quantum melting; a phase transition in quantum mechanics in which electrons that have formed a crystal structure purely through their quantum interactions melt into a more disordered fluid, in response to quantum fluctuations to their density. Thus, for the first time, MIT Physicists have observed a highly ordered crystal of electrons in a semiconducting material and documented its melting, much like ice thawing into water. Electrons in a (semiconductor) semiconducting material were cooled to extremely low temperature, just above absolute zero (Scientists Detect a Quantum Crystal of electrons at MIT, USA, 20th December, 2016). Thus, crystallization of fermions is a realistic physical phenomenon, and this is what has been focused on in this thesis.

3.1.1: Hamiltonian for interacting particles and Bogoliubov-Valatin transformation

In 1947, (Bogoliubov, 1947) introduced a novel linear transformation to diagonalize the quantum quadratic Hamiltonian present in superfluidity. This method was later extended by Bogoliuv himself (Bogoliubov, et.al., 1958) and also by (Valatin & Nuovo, 1958) to the Fermi case in the theory of *superconductivity*. It has ever since got widely used in different fields, and known as Bogoliubov-Valatin (BV) transformation, including both the bosonic and fermionic versions.

To show the underlying idea of the method due to Bogoliubov and Valatin, consider the quadratic Hamiltonian H,

$$H = \sum_{i,j=1}^{n} (\alpha_{ij} c_i^{\dagger} c_j + \frac{1}{2}\gamma_{ji} c_i^{\dagger} c_j^{\dagger} + \frac{1}{2}\gamma_{ji}^{*} C_i C_j \tag{3.1}$$

where n≥1 is a natural number, and c_i and $c_i^{\dagger}$ are, respectively, the annihilation and creation operators for bosons or fermions. They satisfy the standard commutation relations

$$\left[c_i, c_j^{\dagger}\right] = c_i c_j^{\dagger} \pm c_j^{\dagger} c_i = \delta_{ij}\,, \tag{3.2}$$

$$\left[c_i, c_j\right] = c_i c_j \pm c_j c_i = 0, \tag{3.3}$$

$$\left[c_i^{\dagger}, c_j^{\dagger}\right] = c_i^{\dagger} c_j^{\dagger} \pm c_j^{\dagger} c_i^{\dagger} = 0, \tag{3.4}$$

where $\delta_{ij}$is the Kronecker delta function, and +ve sign denotes fermions while –ve denotes bosons. The coefficients $\alpha_{ij} \in \mathbb{C}$ and $\gamma_{ij} \in \mathbb{C}$ have the following symmetries,

$$\alpha_{ij} = \alpha_{ji}^{*}\,,\ \gamma_{ij} = \mp Y_{ij} \tag{3.5}$$

Where α^{*}denotes the complex conjugate of α. Throughout this thesis, the complex field $\mathbb{C}$ will be used as the base field of the Hamiltonian H.

Using the form of matrix, Eq.(3.1) can be written as

$$H = \frac{1}{2}\psi^{\dagger}M\psi \pm \frac{1}{2}tr(\alpha), \tag{3.6}$$

Where tr(α) denotes the trace of the matrix A. The ψ is a column vector and $\psi^{\dagger}$ its Hermitian conjugate, M is coefficient matrix,

$$\psi = \begin{bmatrix} c \\ \tilde{c^{\dagger}} \end{bmatrix}, \psi^{\dagger} = [c^{\dagger}, \check{c}], \tag{3.7}$$

where c and $c^{\dagger}$ are the subvectors of size n,

$$c = \begin{bmatrix} c_1 \\ c_2 \\ \vdots \\ c_n \end{bmatrix}, c^{\dagger} = (c_1^{\dagger}, c_2^{\dagger}, \ldots\ldots, c_n^{\dagger}. \tag{3.8}$$

Here $\tilde{A}$ denotes the transpose of the matrix A. The coefficient matrix M has the form

$$M = \begin{bmatrix} \alpha & \gamma \\ \gamma^{\dagger} & \mp\check{\alpha} \end{bmatrix} \tag{3.9}$$

here $\propto$ and γ are the submatrices with $\propto_{ij}$ and γ_{ij} as their entries, respectively,

$$\propto^{\dagger}=\propto, \check{\gamma} = \mp\gamma, M^{\dagger} = M \tag{3.10}$$

That is to say, $\propto$ and M are both Hermitian matrices whereas γ is a symmetric matrix, which is determined by whether the system is bosonic or fermionic. Besides, the matrices $\propto$ and γ will not vanish simultaneously; otherwise, the Hamiltonian *H* is zero.

Defining a new product between the two operators $c_i(or\ c_i^{\dagger})$ and $c_j(or\ c_j^{\dagger})$ as

$$c_i.c_j = [c_i, c_j], \tag{3.11}$$

then Eqs. (3.2) - (3.4) can be expressed compactly as

$$\psi.\psi^{\dagger} = I \pm, \tag{3.12}$$

where

$$I\pm = \begin{bmatrix} I & 0 \\ 0 & \pm I \end{bmatrix} \tag{3.13}$$

With *I* being the identity matrix of size *n*.

To diagonalize the Hamiltonian of Eqn.(3.6), Bogoliubov and Valatin introduced a linear transformation,

$$c = Ad + B\widetilde{d^{\dagger}}, \tag{3.14}$$

where *A* and *B* are two square matrices of size *n*, and *d* and $d^{\dagger}$ are the vector as follows,

$$d = \begin{bmatrix} d_1 \\ d_2 \\ \vdots \\ d_n \end{bmatrix}, d^{\dagger} = \left[d_1^{\dagger}, d_2^{\dagger}, \dots \dots \dots d_n^{\dagger}\right]. \tag{3.15}$$

Here d_i and $d_j^{\dagger}$ are the new annihilation and creation operators respectively, they satisfy the standard commutation or anti-commutation relations as in Eqs. (3.2) - (3.4), which means,

$$\varphi.\varphi^{\dagger} = I \pm \tag{3.16}$$

where

$$\varphi = \begin{bmatrix} d \\ \widetilde{d^{\dagger}} \end{bmatrix}, \varphi^{\dagger} = (d^{\dagger}, \tilde{d}) \tag{3.17}$$

From Eqs. (3.7), (3.16) and (3.17), it follows that

$$\psi = \mathrm{T}\varphi \tag{3.18}$$

where

$$T = \begin{bmatrix} A & B \\ B^* & A^* \end{bmatrix}. \tag{3.19}$$

Here A^*denotes the complex conjugate of the matrix A. By the way, it is noted that such a form of T originates from the requirement that c and $c^\dagger$ must be Hermitian conjugates of each other. For convenience, the operator vector such as ψ and φ shall be called the field operator.

Using the transformation of Eqs. (3.18), the Hamiltonian of Eq.(3.6) becomes

$$H = \frac{1}{2}\varphi^\dagger T^\dagger M T \varphi \pm \frac{1}{2} tr(\alpha) \tag{3.20}$$

where $T^\dagger MT$ is the new coefficient matrix. Meanwhile, Eq.(3.12) turns into

$$TI \pm T^\dagger = I \pm \tag{3.21}$$

where Eqn.(3.16) has been used. Obviously, this is a condition for the transformation of Eqn.(3.18).

For the Hamiltonian H to be diagonalized with respect to the new annihilation and creation operators, it is necessary that the new coefficient matrix T^+MT is diagonal, i.e.,

$$T^\dagger MT = \begin{bmatrix} \omega_1 & 0 \\ 0 & \ddots\ \omega_{2n} \end{bmatrix} \tag{3.22}$$

Where ω_i for i = 1, 2, …….2n are the diagonal entries, they are real: $\omega_i \in R$ Equation (3.22) means that all the off-diagonal entries of the matrix $T^\dagger MT$ must vanish identically. Under this condition, Hamiltonian H becomes

$$H = \frac{1}{2}\sum_{i=1}^{n}(\omega_i \mp \omega_{n+1}) d_i^\dagger d_i + \frac{1}{2}\sum_{i=1}^{n}\omega_{n+i} \pm \frac{1}{2} tr(\alpha)\,. \tag{3.23}$$

This is the so-called diagonalized form for the Hamiltonian H.

To sum up, Eqs. (3.21) and (3.22) are two conditions that must be fulfilled by the transformation matrix T. The former ensures the statistics of the system, i.e, the system will remain bosonic or fermionic after the transformation if it is bosonic or fermionic before the transformation, that is a physical requirement. The latter ensures the diagonalization of the Hamiltonian, it is just a mathematical requirement. According to Bogoliubov and Valatin, the transformation matrix *T* can be determined from Eqs. (3.21) and (3.22). After the determination of *T*, the diagonal entries $\omega_i$for $i = 1,2, \dots \dots 2n$ will be obtained, which accomplishes the diagonalization procedure. That is the main idea of the Bogoliubov-Valatin transformation.

As indicated by Eqn.(3.10), the matrix *M* is Hamiltonian. So it can always be diagonalized by a unitary transformation. At first glance, it seems as if the Hamiltonian of Eqn.(3.20) could be brought into diagonalization by the same unitary transformation. However, a close observation shows that such a unitary transformation can, in general, neither take the form of Eqn.(3.19) nor meet the requirement of Eqn.(3.21) although it always satisfies the condition of Eqn.(3.22). Therefore the unitary transformation for the diagonalization of the coefficient matrix *M* cannot generally diagonalize the Hamiltonian of Eqn.(3.20). That is because both field ψ and the field φ are now the vectors of operators (quantum numbers) rather than the usual simple vectors of complex variables (classic numbers). For the latter, it is well known that a Hermitian quadratic form can always be diagonalized by the unitary transformation for the diagonalization of its coefficient matrix. In short, the BV diagonalization for a quantum quadratic Hamiltonian is much more complicated than the unitary diagonalization for the usual Hermitian quadratic form of complex variables.

Finally analyzing the BV method in more detail, it can easily be seen from Eqn.(3.19) that the transformation matrix *T* has $4n^2$ independent unknown entries. However, Eqs. (3.21) and (3.22) contain $4n^2$and $4n^2 - 2$ constraints only *T*, respectively. That is to say, the constraints are much more than the total number of the free unknown entries of *T*. Therefore, there are two possibilities: (1) Those constraints are consistent with the requirement of *T*, and thus *T* has solutions. (2) The constraints are inconsistent with the requirement of *T* has no solution. Theoretically, it is very difficult to judge which case

will happen because, as indicated by Eqs. (3.21) and (3.22), the constraints constitute $8n^2 - 2$ coupled quadratic equations for $4n^2$ free unknowns. Furthermore, it will still be hard to solve for the multiple unknowns from the multiple equations of second degree even if there exist solutions for the matrix *T*. Mathematically, these difficulties arise from the well-known fact that there is no much knowledge about the multiple equations of second degree with multiple unknowns at present. In practice, one often has to rely on experience and tricks when one uses the BV method to resolve practical problems.

To overcome those difficulties, developing a new theory for BV transformation. It is expected that this theory can not only judge straightforwardly whether a quantum quadratic Hamiltonian is BV diagonalizable but also yield the required transformation by a simple procedure if the Hamiltonian is BV diagonalizable.

3.1.2: Equation of motion

As shown in the preceding subsection, the diagonalization scheme adopted by Bogoliubov and Valatin is merely algebraic. That is to say, the scheme treats the diagonalization just as a pure algebraic problem, it does not consider the physics in diagonalization at all. It could be complemented with physical contents so as to find the necessary and sufficient conditions for the diagonalization of a quantum quadratic Hamiltonian. Simply speaking, it is taken into account the equation of motion of the system. i.e., the Heisenberg equation.

To make the idea more explicit, consider the classical system of harmonic oscillators-the counterpart of the Bose system with quadratic Hamiltonian (Goldstein, 1980),

$$H = \frac{1}{2}\sum_{i,j=1}^{n} K_{ij}p_i p_j + \frac{1}{2}\sum_{i,j=1}^{n} V_{ij}q_i q_j\,, = \frac{1}{2}\tilde{p}Kp + \frac{1}{2}\tilde{q}Vq \qquad (3.24)$$

Where q_i and $p_i(i = 1, 2, \ldots\ldots\ldots\ldots, n))$ are, respectively, the generalized coordinates and conjugate momenta, with *q* and *p* being the corresponding column vectors,

$$q = \begin{bmatrix} q_1 \\ q_2 \\ \vdots \\ q_n \end{bmatrix}, p = \begin{bmatrix} p_1 \\ p_2 \\ \vdots \\ p_n \end{bmatrix}. \quad (3.25)$$

The K and V are the kinetic and potential energy matrices with K_{ij} and V_{ij} as their entries, respectively. They are both real and symmetric,

$$\widetilde{K} = K > 0, \quad (3.26)$$

$$\widetilde{V} = V \geq 0. \quad (3.27)$$

It is worthy to emphasize that K is a positive definite matrix, that is because the kinetic energy is always positive definite. In addition the matrix V is only positive semi definite, the bottom of potential being chosen as zero.

As is well known, q_i and p_i (i=1,2,…,n) satisfy the following canonical relations,

$$\{q_i, q_j\} = 0, \quad (3.28)$$

$$\{p_i, p_j\} = 0 \quad (3.29)$$

$$\{q_i, p_j\} = \delta_{ij}, \quad (3.30)$$

Or equivalently,

$$q.\tilde{q} = 0, \quad (3.31)$$

$$p.\tilde{p} = 0, \quad (3.32)$$

$$q.\tilde{p} = I \quad (3.33)$$

Where $\{a,b\}$ denotes the Poisson bracket of a and b, and $a.b$=$\{a,b\}$.

Of course, the Bogoliubov-Valatin scheme can be transplanted directly to diagonalize the classical quadratic Hamiltonian of Eqn.(3.24) with respect to the new generalized

coordinates and momentum .However, it would be more convenient here to turn to another way-the canonical equation of motion.

The canonical equation of motion can be deduced from the Hamiltonian of Eq.(3.24) and the Poisson brackets of Eqs.(3.28)-(3.30) as follows,

$$\frac{d}{dt}q = \{q, H\} = Kp,$$

(3.34)

$$\frac{d}{dt}q = \{p, H\} = -Vp. \quad (3.35)$$

Where t denotes the time. As a result,

$$\frac{d^2}{dt^2}\mathrm{q} = -\mathrm{KVq} \quad (3.36)$$

That is a homogeneous system of linear ordinary differential equations with constant coefficients.

From the theory of ordinary differential equations (Walter, 1998), it is known that the solution of homogeneous linear system depends on the eigen value problem,

$$\omega^2\mathrm{q} = \mathrm{KVq}. \quad (3.37)$$

This eigen value problem can be solved rigorously with the help of the Cholesky decomposition of K,

$$\mathrm{K} = Q\tilde{Q} \quad (3.38)$$

Where Q is an invertible matrix. The existence of such a decomposition stems mathematically from the positivity of K (Strang, 2005). By introducing a temporal variable ξ,

$$\xi = Q^{-1}q \quad (3.39)$$

Eqn.(3.37) can be transformed into

$\omega^2\xi = \wedge\,\xi,$ (3.40)

where

$\wedge = \tilde{Q}VQ = \tilde{\wedge} \geq 0.$
(3.41)

Just as *V*, the matrix $\wedge$ is still real, symmetric, and non –negative definite. So it can be orthogonally diagonalized,

$\tilde{S}\,\wedge S = \Gamma,$ (3.42)

where

$\tilde{S}S = S\tilde{S} = I$ (3.43)

$\Gamma = \begin{bmatrix} \omega_1 & 0 \\ 0 & \ddots\ \omega_n^2 \end{bmatrix}$ (3.44)

Here $\omega_i^2 \geq 0$ (i=1, 2 . . . n) are the eigen values of Λ, and S the orthogonal matrix with the eigenvectors of Λ as its column vectors.

From Eqs. (3.38), (3.41), (3.42), and (3.43), it follows that

$T^{-1}KVT = \Gamma,$ (3.45)

where

T=QS. (3.46)

If I put

$T = [v_1, v_2, \ldots.\ , v_n],$ (3.47)

where v_i (i= 1, 2,. . . ,n) denotes the column vectors of *T*. Equation (3.45) shows that v_i are the eigenvectors of the matrix *KV* ,

$\omega_i^2 v_i = KV v_i,$

(3.48)

belonging to the eigen values ω_i^2, respectively. In other words, they are the solutions of the eigen value problem of Eqn.(3.37). Evidently, they are orthonormal and complete,

$$\tilde{T}GT = I, \tag{3.49}$$

$$T\tilde{T}G = I, \tag{3.50}$$

where $G = K^{-1}$. Namely, they constitute a *n*-dimensional Hilbert space with *G* as its metric tensor.

Just as usual, the general solution of Eqn.(3.36) can be expanded in this Hilbert space as

$$q(t) = \sum_{i=1}^{n} \psi_i(t) v_i \tag{3.51}$$

where ψ_i(t) (*i= 1, 2, ...,n)* are the expanding coefficients. But, not as usual, it does not matter here how to determine those coefficients from the initial conditions. Instead, it is preferable to view this expansion as a linear transformation,

$$q(t)=T\,\psi(t) \tag{3.52}$$

where ψ(t) is the column vector,

$$\psi(t)=\begin{bmatrix} \psi_1(t) \\ \psi_2(t) \\ \vdots \\ \psi_n(t) \end{bmatrix}. \tag{3.53}$$

As will be seen later, this view is crucial for the diagonalization of the Hamiltonian. Since *T* has full rank, the transformation is inevitable. The inverse is

$$\psi(t) = T^{-1} q(t).$$

(3.54)

Physically, $\psi(t)$ represents the new generalized coordinates, and q(t) the old ones.

The corresponding transformation for the generalized momenta can be deduced from Eqn.(3.33). As is well known, a Poisson bracket is a bilinear function of its two arguments. This together with Eqn.(3.33) indicates that there exists a duality relationship between *p*(t) and *q*(t) (Roman, 1998). This duality implies that *p(t)* will transform contravariantly with *q*(t), i.e.,

$$\pi(t)=\tilde{T}p(t) \tag{3.55}$$

where π(t) represents the new generalized momenta.

Under the transformation of Eqs. (3.54) and (3.55), the Hamiltonian of the system becomes as follows,

$$H=\frac{1}{2}\tilde{\pi}\pi+\frac{1}{2}\tilde{\psi}\Gamma\psi=\frac{1}{2}\sum_{i=1}^{n}(\pi_i^2+\omega_i^2\psi_i^2), \tag{3.56}$$

where

$$\psi.\tilde{\psi}=0, \tag{3.57}$$

$$\pi.\tilde{\pi}=0, \tag{3.58}$$

$$\psi.\tilde{\pi}=I. \tag{3.59}$$

They are identical to the system of Eqn.(3.24) and Eqs. (3.31)-(3.33), with the Hamiltonian being diagonalized with respect to the new generalized coordinates and momenta

3.1.3: Bogoliubov-Valatin Transformations

After Schrieffer conceived of the BCS wave function on a New York subway, upon getting back to the University of Illinois at Urban-Champaign (where he was a graduate student with John Bardeen), the three BCS principals –Schrieffer, Cooper, and Bardeen – worked out the thermodynamic properties of their model shortly (11 days!) and saw that their theory agreed reasonable well with experiments (Dirac, 1958). It turns out however that the variational treatment that was introduced in (the approach used by BCS

(Bogoliubov, 1947)) is not very convenient for doing calculations. A much powerful technique, readily extensible to nonzero temperature for instance, was developed independently by (Bogoliubov & Valatin, 1958). Central to this scheme are the Bogoliubov-valatin transformations that is discussed below.

The essential idea underlying the Bogoliubov-Valatin approach is to approximate the BCS Hamiltonian

$$\kappa = H - \mu N = \sum_{k\sigma} \xi_k \hat{a}^{\dagger}_{k\sigma} \hat{a}_{k\sigma} + \sum_{k,k'} V_{k,k'} \hat{a}^{\dagger}_{k\uparrow} \hat{a}^{\dagger}_{-k\downarrow} \hat{a}_{-k\downarrow} \hat{a}_{k'\uparrow} \qquad (3.60)$$

discussed by some quadratic form (the above Hamiltonian is quadratic in Fermi operators) and diagonalize the resulting expression. This of course is a very standard scheme in modern CMP. The usefulness of this approach is that a quadratic Hamiltonian can always be solved exactly, describing a non interacting gas of quasiparticles. The quasiparticles are the particles which arise after the Bogoliubov-Valatin transformation is applied to the approximate quadratic Hamiltonian.

In general it's not possible to approximate a Hamiltonian with interactions (quadratic in Fermi operators) by some quadratic expression. Fortunately, one time when it is usually possible to make such an approximation is when the system under consideration is in an ordered phase such as a superconductor. In this case, the expectation value of some combination of operators represents the order parameter. Assuming that there is a significant occupation of the ordered state (of the order of the total particle number), one can replace some of the operators appearing in the Hamiltonian by their expectation value (i.e., the order parameter).

To see how this works, recall that the operator$(\mathrm{u(k)/v(k)}\hat{a}^{\dagger}_{k\uparrow}\hat{a}^{\dagger}_{-k\downarrow}$creates a Cooper pair. Since there are a macroscopic number of Cooper pairs, the expectation value b_k (it is assumed for simplicity that the order parameter is real)

$$\langle \hat{a}^{\dagger}_{k\uparrow} \hat{a}^{\dagger}_{-k\downarrow} \rangle = \langle \hat{a}_{-k\downarrow} \hat{a}_{k\uparrow} \rangle \equiv b_k \qquad (3.61)$$

is nonzero. You can check this by evaluating this expectation value using the BCS wave function; you will find $b_k = u_k v_k$. Making a mean-field approximation by assuming that the fluctuations past this value are small, which is done by substituting

$$\hat{a}_{-k\downarrow}\hat{a}_{k\uparrow} = b_k + \delta\hat{b}_k; where\ \delta\hat{b}_k \equiv \hat{a}_{-k\downarrow}\hat{a}_{k\uparrow} - b_k$$
(3.62)

into the Hamiltonian (3.60) and retain only terms linear in the fluctuation $\delta\hat{b}$. This gives

$$\kappa = \sum_{k\sigma} \xi_k \hat{a}^\dagger_{k\sigma}\hat{a}_{k\sigma} + \sum_{k,k'} V_{k,k'}\left[b_k \hat{a}_{-k'\downarrow}\hat{a}_{k'\uparrow} + b_{k'}\hat{a}^\dagger_{k\uparrow}\hat{a}^\dagger_{-k\downarrow} - b_k b_{k'}\right] + \sigma(\delta b^2) \qquad (3.63)$$

Equation (3.63) confirms that neglecting fluctuation contributions past first order, yields a Hamiltonian which is quadratic in Fermi operators and hence which can be diagonalized by some judicious choice of transformation. This is not just a mathematical trick however! The transformation will reveal the physical excitation of a superconductor and allow me to calculate thermodynamic properties in terms of this excitation. First, "defining" the quantity

$$\Delta_k \equiv -\sum_{k'} V_{k,k'} b_{k'} \qquad (3.64)$$

Indeed, using $b_k = u_k v_k$ these equations are in fact the same. Using eq.(3.64) in eq.(3.63), the latter becomes

$$\kappa = \sum_{k\sigma} \xi_k \hat{a}^\dagger_{k\sigma}\hat{a}_{k\sigma} - \sum_{k}\left[\Delta_k \hat{a}_{-k'\downarrow}\hat{a}_{k'\uparrow} + \Delta_k \hat{a}^\dagger_{k\uparrow}\hat{a}^\dagger_{-k\downarrow} - \Delta_k b_{k'}\right] \qquad (3.65)$$

Equation (3.65) is diagonalized by

$$\hat{a}_{k\uparrow} = u_k \hat{\gamma}_{k0} + v_k \hat{\gamma}^\dagger_{k1}$$

$$\hat{a}^\dagger_{-k\downarrow} = -v_k \hat{\gamma}_{k0} + u_k \hat{\gamma}^\dagger_{k1} \qquad (3.66)$$

Here, u_k and v_k are the same Bogoliubov-coherence factors that arose in the minimization of the BCS free energy, although for the moment, assuming that it is not known and instead derive their form by the requirement that they diagonalize eq.(3.65). To show this, one first derives the appropriate anti-commutation relations for the new operators $\hat{\gamma}_0$ and $\hat{\gamma}_1$. Assuming the normalization condition $u_k^2 + v_k^2 = 1$, the Bogoliubov-Valatin transformation eq.(3.66) can be inverted:

$$\hat{\gamma}_{k0} = u_k \hat{a}_{k\uparrow} - v_k \hat{a}^{\dagger}_{-k\downarrow}$$

$$\hat{\gamma}^{\dagger}_{k'} = +v_k \hat{a}_{k\uparrow} + u_k \hat{a}^{\dagger}_{-k\downarrow} \qquad (3.67)$$

Using this in conjunction with the usual Fermi anti-commutation relations $\{\hat{a}^{\dagger}_{k\sigma,}\hat{a}^{\dagger}_{k'\sigma'}\} = \delta_{k,k'}\delta_{\sigma,\sigma'}$ and $\{\hat{a}^{\dagger}_{k\sigma}, \hat{a}^{\dagger}_{k'\sigma'}\} = \{\hat{a}_{k\sigma}, \hat{a}_{k'\sigma'}\} = 0$, one finds that the $\hat{\gamma}_0$ and $\hat{\gamma}_1$ operators also obey Fermi anti-communication relations

$$\{\hat{\gamma}_{ki}, \hat{\gamma}^{\dagger}_{k'j}\} = \delta_{k,k'}\delta_{i,j};\ \{\hat{\gamma}^{\dagger}_{ki}, \hat{\gamma}^{\dagger}_{k'j}\} = 0 \qquad (3.68)$$

Inserting eq.(3.66) into eq.(3.65) and making use of the commutation relations eq.(3.68), the BCS Hamiltonian becomes

$$\mathrm{K} = \sum_k \xi_k \left[(u_k^2 - v_k^2)(\hat{\gamma}^{\dagger}_{k0}\hat{\gamma}_{k0} + \hat{\gamma}^{\dagger}_{k0}\hat{\gamma}_{k1}) + 2v_k^2 + 2u_k v_k(\hat{\gamma}_{k1}\hat{\gamma}_{k0} + \hat{\gamma}^{\dagger}_{k0}\hat{\gamma}^{\dagger}_{k1}\right]$$
$$+ \sum_k \left[2\Delta_k u_k v_k\left(\hat{\gamma}^{\dagger}_{k0}\hat{\gamma}_{k0} + \hat{\gamma}^{\dagger}_{k1}\hat{\gamma}_{k1} - 1\right) + \Delta_k((v_k^2 - u_k^2)\left(\hat{\gamma}_{k1}\hat{\gamma}_{k0} + \hat{\gamma}^{\dagger}_{k0}\hat{\gamma}^{\dagger}_{k1}\right) + \Delta_k b_k\right] \qquad (3.69)$$

To be useful, the Bogoliubov-Valatin transformation has to diagonalize this expression, by which it is meant that there are no cross terms of the form e.g.$\hat{\gamma}_{k1}\hat{\gamma}_{k0}$. By inspection, one sees that such terms will vanish from eq.(3.69) if

$$2\xi_k u_k v_k + \Delta_k((v_k^2 - u_k^2) = 0 \qquad (3.70)$$

This expression is indeed solved if u_k and v_k are the Bogoliubov coherence factors:

$$u_k^2 = \frac{1}{2}\left(1 + \frac{\xi_k}{E_k}\right), v_k^2 = \frac{1}{2}\left(1 - \frac{\xi_k}{E_k}\right) \qquad (3.71)$$

The remaining diagonal terms in the BCS Hamiltonian become

$$\mathrm{K} = \sum_k \mathrm{E}_k\left(\hat{\gamma}_{k0}^{\dagger}\hat{\gamma}_{k0} + \hat{\gamma}_{k1}^{\dagger}\hat{\gamma}_{k1}\right) + \sum_k (\xi_k - \mathrm{E}_k + \Delta_k b_k) \tag{3.72}$$

Now, there is a very transparent expression with which to understand things! First off, $\hat{\gamma}_0^{\dagger}$ and $\hat{\gamma}_1^{\dagger}$ create excitations with energy

$$E_k = \sqrt{\xi_k^2 + \Delta_k^2} \tag{3.73}$$

i.e., the excitation spectrum is at least partially gapped as it was known to be the case from specific heat measurements. At the Fermi surface,$\xi_k = 0$, and the dispersion $E_{k=k_F} = \left|\Delta_{k=k_F}\right|$ no longer vanishes. The value of the gap can be determined self-consistently from eq.(3.61), (3.64), and (.372). Using the Bogoliubov-Valatin transformations eqn.(3.66), b_k can be written (as defined in eqn. (3.61) in terms of the new quasiparticle operators as (remember that off-diagonal terms such as $\langle\hat{\gamma}_0\hat{\gamma}_1\rangle$ are exactly zero)

$$b_k = \langle\hat{a}_{-k\downarrow}\hat{a}_{k\uparrow}\rangle = -u_k v_k\left[\langle\hat{\gamma}_{k0}^{\dagger}\hat{\gamma}_{k0}\rangle - \langle\hat{\gamma}_{k1}^{\dagger}\hat{\gamma}_{k1}\rangle\right] = -u_k v_k\left[\langle\hat{\gamma}_{k0}^{\dagger}\hat{\gamma}_{k0}\rangle + \langle\hat{\gamma}_{k1}^{\dagger}\hat{\gamma}_{k1}\rangle - 1\right] \tag{3.74}$$

Substituting this into (3.64), the "gap equation" (which is now finally understood as an equation for the gap) becomes

$$\Delta_k \equiv -\sum_k V_{k,k'} u_{k'}\, v_k[1 - f_{k'0} - f_{k'1}]. \tag{3.75}$$

Here, denoting the expectation values $\langle\hat{\gamma}_{ki}^{\dagger}\hat{\gamma}_{ki}\rangle$ by f_{ki}. Since both types of quasiparticle operators generate excitation of energy E_k and since the Hamiltonian eq.(3.72) describes an ideal gas of such quasiparticles, these expectation values will just be equal to the Fermi function

$$f_{k0} = f_{k1} = f(E_k) = \left(e^{\beta E_k} + 1\right)^{-1} \tag{3.76}$$

Using this in eq.(3.75) as well as the identity $u_k v_k = \Delta_k / 2E_k$, the gap equation reduces to

$$\Delta_k \equiv -\sum_{k'} V_{k,k'} \frac{\Delta_{k'}}{2E_{k'}} [1 - 2f(E_{k'})] \tag{3.77}$$

In principle, this equation can be solved for all types of interaction $V_{k,k'}$ and at all temperatures below T_c yielding temperature-dependent gaps $\Delta_k(T)$ with e.g., s- and d- wave symmetries (p-wave symmetry is disallowed for spin-singlet pairing which has been only considered so far). For our purposes and following BCS, it suffices to use the simple attractive interaction that is considered in the solution of the Cooper pairing problem:

$$V_{k,k'} = -V; \text{ for } |\xi_k| < \hbar\omega_D \; and |\xi_{k'}| < \hbar\omega_D \tag{3.78}$$

This is an isotropic interaction, independent of momentum, and hence the gap $\Delta_k = \Delta$

is well known. Using these in eq.(3.77) and making the approximations, the gap equation reduces at T= 0 to

$$\frac{1}{N(0)V} = \int_0^{\hbar\omega_D} d\xi \frac{1}{\sqrt{\xi^2 + \Delta^2}} = sinh^{-1}\left(\frac{\hbar\omega_D}{\Delta}\right) \tag{3.79}$$

Thus,

$$\Delta(T = 0) = \frac{\hbar\omega_D}{\sinh(1/N(0)V)} \simeq 2\hbar\omega_D e^{-\frac{1}{N(0)V}} \tag{3.80}$$

where in the final quasi-equality, it is again assumed weak-coupling :$N(0)V \ll 1$. Comparing with the binding energy found by Cooper, it is seen that the two quantities $-\Delta \; and \; E -$ are essentially equivalent, meaning that you think of Δ (at least for s-wave interactions) as being the energy of the Cooper pairs.

The gap equation is also used to solve for the critical temperature T_c at which the Cooper pairs form and Bose-condense. Given that Δ is essentially a binding energy, it won't

come as a surprise that $k_B T_c \sim \Delta$, meaning that the transition temperature is the temperature above which the Cooper pairs become disassociated, which is true for weak interactions. As interactions become stronger, the binding energy of the Cooper pairs becomes large and the temperature scale at which they de-pair can become larger than the temperature at which they undergo Bose-Einstein condensation. At any rate , T_c is more or less the lesser of the two temperatures.

3.1.4: Diagonalization Theory of Fermi Systems

Consider the existence and the uniqueness of the BV diagonalization for the Fermi system.

The Heisenberg equation for the fermionic field ψ can be derived from Eqn.(3.1),

$$i\frac{d}{dt}\psi = D\psi \tag{3.81}$$

Where *D* is the dynamic matrix for the Fermi system, given by $D = i\frac{d}{dt}$

$$D = \begin{bmatrix} \alpha & \gamma \\ -\gamma+ & -\tilde{\alpha} \end{bmatrix} \tag{3.82}$$

In contrast to the Bose system where the dynamic matrix is distinct from the coefficient matrix *D* is now identical to the coefficient matrix *M*,

$$M = \begin{pmatrix} \alpha & \gamma \\ \gamma^{\dagger} & -\tilde{\alpha} \end{pmatrix} \tag{3.83}$$

This demonstrates that the coefficient matrix *M* will control the dynamic behavior of the system, just as the dynamic matrix *D*. That is the radical difference between the Fermi and Bose systems. For the latter, as it is known, the coefficient matrix does not control the dynamic behavior of the system. Now that D=*M* is Hermitical, *D* is Hermitical, too. That is another feature of Fermi system, which will create much convenience.

From Eqn.(3.82) and (3.83), since the dynamic matrix D and coefficient matrix M have the relation D=I-M, the relation between dynamic matrix D and coefficient matrix M can be formally written as;

$$D = \mathrm{I} + M \tag{3.84}$$

This relation is useful in the diagonalization of the Fermi system.

As before, consider the eigen value problem,

$$\omega\psi = D\psi \tag{3.85}$$

For a quadratic Hamiltonian of fermions, its dynamic matrix is always BV diagonalizable.

As mentioned above, the dynamic matrix for a Fermi system is Hermitian matrix and it is diagonalizable, and all its Eigen values are real. Therefore, the dynamic matrix for a Fermi system is always BV diagonalizable. This property is basically different from the Bose system. Therefore, the dynamic matrix is not always diagnosable. Needless to say, it is not always BV diagnosable.

As $D = M$ and both are Hermitian, they can be diagonalized by an exactly identical unitary transformation. Mathematically, a unitary transformation is always a similar transformation; the diagonalization manner of D is not inharmonious with that of M any longer. The problem present in the Bose system disappears spontaneously in the Fermi system.

Analogous to the Bose system, one can easily show that the lemmas and the same laws are all valid for the Fermi system. Since the dynamic matrix is always BV diagnosable now, the necessary condition for the BV diagonalization will hold automatically for a Fermi system. That guarantees further that all those laws which stem from Hermiticity of the Hamiltonian also hold for the fermion system, irrespective of the statistics and metric of the system.

The eigenspace V_0 of zero eigen value is even dimensional, let the dimension of 2m ($m \in \mathbb{N}$), there always exists a basis for V_0 that satisfies the requirement of Eqn.(3.86), i.e.,

$$V_{m+l}(0) = \sum_x v_l^*(0), l = 1, 2, \dots, m, \quad (3.86)$$

When m = 1, dim(V_0)=2, there are two basis vectors, i.e., $v_1(0) and\ v_2(0)$, they are linearly independent. First of all, making $v_1(0)$ normalized,

$$v_I^\dagger(0) I_+ v_2(0) = 1 \quad (3.87)$$

And then consider $\boldsymbol{v_2(0)}$. In fact, it is also normalized,

$$v_2^\dagger(0) I_+ v_2(0) = 1 \quad (3.88)$$

that is because

$$v_2(0) = \sum_x v_1^*(0). \quad (3.89)$$

There are two possible cases for $v_2(0)$: (1) It is orthogonal to $v_1(0)$. (2) It is not orthogonal to $v_1(0)$.

If $v_2(0) \perp v_1(0)$, i.e.,

$$v_I^\dagger(0) I_+ v_2(0) = 0, \quad (3.90)$$

yields

$$v_I^\dagger(0) I_+ v_1(0) = 1, \quad (3.91)$$

$$v_2^\dagger(0) I_+ v_2(0) = 1, \quad (3.92)$$

$$v_I^\dagger(0) I_+ v_2(0) = 0. \quad (3.93)$$

and

$$v_2(0) = \sum_x v_1^*(0), \quad (3.94)$$

So the basis $\{v_1(0), v_2(0)\}$ is itself orthonormal and satisfies the requirement of Eqn.(3.86). In other words, the relation holds if $v_2(0) \perp v_1(0)$.

If $v_2(0)$ is not orthogonal to $v_1(0)$, i.e.,

$$v_1^{\dagger}(0) I_+ v_2(0) \neq 0, \tag{3.95}$$

Introducing two vectors $\omega_1(0) and\ \omega_2(0)$ as follows,

$$\omega_1(0) = a v_1(0) + b v_2(0) \tag{3.96}$$

$$\omega_2(0) = \sum\nolimits_x \omega_1^*(0). \tag{3.97}$$

Here $a \epsilon \mathbb{C}\ and\ b \epsilon \mathbb{C}$ are two coefficients, they will be determined by the orthonormal conditions,

$$\omega_1^{\dagger}(0) I_+ \omega_1(0) = 1, \tag{3.98}$$

$$\omega_1^{\dagger}(0) I_+ \omega_2(0) = 0 \tag{3.99}$$

Equations (3.96) and (3.97) show that both $\omega_1(0)$ and $\omega_2(0)$ are linier combinations of $v_1(0)$ and $v_2(0)$. Consequently, $\omega_1(0)$ and $\omega_2(0)$ are also the eigenvectors of zero eigenvalue of zero eigenvalue, i.e., $\omega_1(0) \in \mathrm{V}_0\ and\ \omega_2(0) \in V_0$.

Observe

$$v_1^{\dagger}(0) I_+ v_2(0) = \left[\tilde{v}_1(0) I_+ \sum\nolimits_x v_1(0)\right]^* \tag{3.100}$$

Adjusting the phase of $\boldsymbol{v_1(0)}$ anew so that

$$v_1^{\dagger}(0) I_+ v_2(0) > 0. \tag{3.101}$$

By use of Cauchy inequality, yields

$$v_1^{\dagger}(0)I_+v_2(0) < \sqrt{v_1^{\dagger}(0)I_+v_1(0)}\sqrt{v_2^{+}(0)I_+v_2(0)} \tag{3.102}$$

Where it has been used the fact that $\boldsymbol{v_1(0)}$ and $\boldsymbol{v_2(0)}$ are linearly independent. Since

$$\sqrt{v_1^{\dagger}(0)I_+v_1(0)}\sqrt{v_2^{\dagger}(0)I_+v_2(0)} = 1 \tag{3.103}$$

yields

$$v_1^{\dagger}(0)I_+v_2(0) < 1 \tag{3.104}.$$

In brief, it always yields

$$0<v_1^{\dagger}(0)I_+v_2(0) < 1, \tag{3.105}$$

when $v_2(0)$ is not orthogonal to $v_1(0)$

Under such choice, Eqns. (3.98) and (3.99) become

$$a^*a + b^*b + (a^*b + b^*a)v_1^{\dagger}(0)I_+v_2(0) = 1, \tag{3.106}$$

$$(a^*a^* + b^*b^*)v_1^{\dagger}(0)I_+v_2(0) + 2a^*b^* = 0, \tag{3.107}$$

It can be readily confirmed that there exists at least the following real solution for the coefficients a and b,

$$a = \frac{1}{2\sqrt{1 + v_1^{\dagger}(0)I_+v_2(0)}} + \frac{1}{2\sqrt{1 - v_1^{\dagger}(0)I_+v_2(0)}} \tag{3.108}$$

$$b = \frac{1}{2\sqrt{1 + v_1^{\dagger}(0)I_+v_2(0)}} + \frac{1}{2\sqrt{1 - v_1^{\dagger}(0)I_+v_2(0)}} \tag{3.109}$$

With this solution, yields

$$\omega_1^{\dagger}(0) I_{+} \omega_1(0) = 1, \tag{3.110}$$

$$\omega_2^{\dagger}(0) I_{+} \omega_2(0) = 1, \tag{3.111}$$

$$\omega_1^{\dagger}(0) I_{+} \omega_2(0) = 0, \tag{3.112}$$

$$\omega_2(0) = \sum_x \omega_1^{*}(0). \tag{3.113}$$

That is to say, the set $\{\omega_1(0), \omega_2(0)\}$ will form an orthonormal basis for V_0 , and satisfy the requirement of Eqn. (3.86). This implies that the same law also holds if $V_2(0)$ is not orthogonal to $V_1(0)$

To sum up, the law holds when $m = 1$

Suppose that the law holds when $m = l$ ($l \in \mathbb{N}$. Considering then the case where $m = l + 1$. Obviously, it has a proper subspace ω spanned by the linearly independent set $\{v_1(0), v_{l+2}(0)\}$, i.e.,

$$\omega = span(v_1(0), v_{l+2}(0)) \tag{3.114}$$

Taking notice of

$$v_{l+2}(0) = \sum_x v_1^{*}(0); \tag{3.115}$$

and following the same arguments as those for the case of m =1, it can yield an orthogonal basis for ω,

$$v_i^{\dagger}(0) I_{-v_j}(0) = -\lambda_i \delta_{ij}, \tag{3.116}$$

where $\lambda_i = \pm 1 \; and \; i, j = 1, l + 2$. It is evident that this basis satisfies the requirement of Eqn. (3.86).

The rest steps of mathematical induction are simply similar to those for the Bose case. The convention of Eqn. (3.86) can be kept by the modified Gram-Schmidt orthogonalization process

The law still holds for the Fermi system, with $\lambda_i = 1 \; for \; i = 1,2, \ldots\ldots,2n$

Since all the eigenvectors are normalized to +1 now, one cannot use the sign of the norm to stipulate an order within a mode pair. Here, resorting to the sign of the eigen value: the first eigen value in a pair of positive, and the second one negative; it is arbitrary if both the eigen values in a pair are equal to zero. Under such stipulation, the normal derivative BV transformation has the form,

$\Psi = T_n \varphi,$ (3.117)

$$T_n = [v(\omega_1), v(\omega_2), \ldots\ldots, v(\omega_n), v(-\omega_2), \ldots\ldots, v(-\omega_n)] \quad (3.118)$$

where

$$\omega_i \geq 0, i = 1, 2, \ldots\ldots, n. \quad (3.119)$$

That is to say, the left half of T_n is filled with the eigenvectors with non-negative eigenvalues; the right half of T_n is filled with the eigenvectors with non-positive eigenvalues.

With T_n ordered as above, the law holds for the Fermi case,

$$T_n^{\dagger} I_+ T_n = I_+, \quad (3.120)$$

i.e., T_n is a member of the U(2n) group (Chen,et.al., 2002). This law asserts that the new field is a standard fermionic field, which is modified as follows,

$$T_n^{+} M T_n = diag(\omega_1, \ldots\ldots \omega_n, -\omega_1, \ldots, -\omega_n). \quad (3.121)$$

$$T_n^{\dagger} M T_n = T_n^{\dagger} I_+ D T_n = T_n^{\dagger} I_+ T_n T_n^{-1} D T_n = T_n^{-1} D T_n, \quad (3.122)$$

where $T_n^{\dagger} I_+ T_n = I_+$ has been used.

Hence, the diagonalization theorem for the Fermi system,

which states that *any quadratic Hamiltonian of fermions is BV diagonizable.*

Apparently, the diagonalized form for the Hamiltonian is

$$H = \sum_{i=1}^{n} \omega_i d_i^{+} d_i - \frac{1}{2}\sum_{i=1}^{n} \omega_i + \frac{1}{2} tr(\alpha), \tag{3.123}$$

where all the eigen energies are non-negative

$$\omega_i \geq 0, i = 1,2, \dots, n \tag{3.124}$$

Here it is worth emphasizing that the BV diagonalization for a Fermi system is itself of unitary diagonalization, that is because T_n is, in fact, a unitary matrix, $T_n^{+} T_n = I_{+}$

All in all, the BV diagonalization for a quadratic Hamiltonian of fermions is much simpler than that for a quadratic of Hamiltonian of bosons.

The normal and pairing Hamiltonians have been considered, since they represent the problems which are encountered most frequently in practice.

3.1.5: The normal Hamiltonian

The normal Hamiltonian reads

$$H = \sum_{i,j=1}^{n} \propto_{ij} c_i^{\dagger} c_j \tag{3.125}$$

The normal Hamiltonian of Equation (3.125) can be BV diagonalized by the unitary transformation generated by the coefficient matrix $\propto$, or generally, a normal Hamiltonian of fermions can be BV diagonalized by the unitary transformation generated by its coefficient matrix.

That is also because the Heisenberg equation for the Hamiltonian of Eqn.(3.125) is reducible. It can be reduced as

$$i\frac{d}{dt}c = \propto c \tag{3.126}$$

Since $\propto$ is Hermitian, this equation of motion can generate a unitary transformation U for the field c,

$$c = Ud, \tag{3.127}$$

where

$$U^{\dagger}U = UU^{\dagger} = 1, \tag{3.128}$$

$$U^{\dagger} \propto U = diag(\omega_1, \omega_2, \dots\dots, \omega_n) \tag{3.129}$$

The d represents the new field, it is easy to show that d is a standard fermionic field,

$$d.d^{\dagger} = I, d.d = 0, d^{\dagger}.d^{\dagger} = 0 \tag{3.130}$$

Accordingly,

$$H = d^{\dagger}U^{\dagger} \propto Ud = \sum_{i=1}^{n} \omega_i d_i^{\dagger} d_j \tag{3.131}$$

Besides a particle-hole transformation will be needed if some eigen energies are negative.

To sum up, a normal Hamiltonian can be BV diagonalized by the unitary transformation generated by its coefficient matrix no matter whether the system is bosonic or fermionic as demonstrated below,

Consider

$$H = \varepsilon\left(c_1^{\dagger}c_1 + c_2^{\dagger}c_2\right) + \mu\left(c_1^{\dagger}c_2 + c_2^{\dagger}c_1\right), \tag{3.132}$$

where $\mu > 0$.

The coefficient matrix is

$$\propto = \begin{bmatrix} \varepsilon & \mu \\ \mu & \varepsilon \end{bmatrix}. \tag{3.133}$$

It has two eigen values,

$$\omega_1 = \varepsilon + \mu, \omega_2 = \varepsilon - \mu \tag{3.134}$$

The unitary matrix can be easily found,

$$U = [v(\omega_1), v(\omega_2)] = \frac{1}{\sqrt{2}} \begin{bmatrix} 1 & 1 \\ 1 & -1 \end{bmatrix}. \tag{3.135}$$

1. *If* $\varepsilon \geq \mu, \omega_1 > 0 \; and \; \omega_2 \geq 0$,

$$\begin{bmatrix} c_1 \\ c_2 \end{bmatrix} = \frac{1}{\sqrt{2}} \begin{bmatrix} 1 & 1 \\ 1 & -1 \end{bmatrix} \begin{bmatrix} d_1 \\ d_2 \end{bmatrix}, \tag{3.136}$$

$$H = \omega_1 d_1^\dagger d_1 + \omega_2 d_2^\dagger d_2 \tag{3.137}$$

2. *If* $-\mu \leq \varepsilon < \mu, \omega_1 \geq 0 \; and \; \omega_2 < 0$,

$$\begin{bmatrix} c_1 \\ c_2 \end{bmatrix} = \frac{1}{\sqrt{2}} \begin{bmatrix} 1 & 1 \\ 1 & -1 \end{bmatrix} \begin{bmatrix} d_1 \\ d_2^\dagger \end{bmatrix}, \tag{3.138}$$

$$H = \omega_1 d_1^\dagger d_1 - \omega_2 d_2^\dagger d_2 + \omega_2 \tag{3.139}$$

3. *If* $\varepsilon < -\mu, \omega < 0 \; and \; \omega_2 < 0$,

$$\begin{bmatrix} c_1 \\ c_2 \end{bmatrix} = \frac{1}{\sqrt{2}} \begin{bmatrix} 1 & 1 \\ 1 & -1 \end{bmatrix} \begin{bmatrix} d_1^\dagger \\ d_2^\dagger \end{bmatrix}, \tag{3.140}$$

$$H = -\omega_1 d_1^\dagger d_1 - \omega_2 d_2^\dagger d_2 + \omega_1 + \omega_2 \tag{3.141}$$

Here, a particle-hole transformation is performed to the d_2 −particles if $-\mu \leq \varepsilon < \mu$, and both the d_1 − and d_2 −particles if $\varepsilon < -\mu$.

3.1.6: The pairing Hamiltonian

The pairing Hamiltonian states

$$H = \sum_{i,j=1}^{n} \left(\propto_{ij} a_i^{\dagger} a_j + \varepsilon_{ij} b_i^{\dagger} b_j + \gamma_{ij} a_i \; b_j + \gamma_{ji}^{*} a_i^{\dagger} b_j^{\dagger} \right) \tag{3.142}$$

where

$$\propto^{\dagger} = \propto, \qquad \varepsilon^{\dagger} = \varepsilon, \qquad \tilde{\gamma} = -\gamma \tag{3.143}$$

Following the Bose case, introduces the new operators $c_i \; and \; c_i^{\dagger}$ as

$$c_i = b_i^{\dagger}, \qquad c_i^{\dagger} = b_i, \qquad i = 1,2, \dots, n. \tag{3.144}$$

The new anti-commutators will be

$$a.a^{\dagger} = I, \qquad a.a = 0, \qquad a^{\dagger}.a^{\dagger} = 0, \tag{3.145}$$

$$c.c^{\dagger} = I, \qquad c.c = 0, \qquad c^{\dagger}.c^{\dagger} = 0, \tag{3.146}$$

$$a.c = 0, \qquad a.c^{\dagger} = 0, \qquad a^{\dagger}.c = 0, \qquad a^{\dagger}.c^{\dagger} = 0. \tag{3.147}$$

Obviously, they are still standard, which is rather different from the Bose case. In terms of these new operators, Eqn.(3.142) can be expressed as

$$H = \psi^{\dagger} M \psi + tr(\varepsilon), \tag{3.148}$$

where M is the coefficient matrix,

$$M = \begin{bmatrix} \propto & \gamma \\ \gamma^{\dagger} & -\varepsilon \end{bmatrix}, \tag{3.149}$$

and ψ the field operator,

$$\psi = \begin{bmatrix} a \\ c \end{bmatrix}, \qquad \psi^{\dagger} = [a^{\dagger}, c^{\dagger}]. \tag{3.150}$$

It is evident that

$$M = M^{\dagger}, \tag{3.151}$$

$$\psi.\psi^{\dagger} = I_{+}, \tag{3.152}$$

Namely, M is Hermitian, and ψ is a standard fermionic field. This means that Eqn.(3.148) is, in fact, a normal Hamiltonian from which it is established that a pairing Hamiltonian of fermions can be first transformed into a normal Hamiltonian, and then BV diagonalized by the unitary transformation generated by the corresponding coefficient matrix.

As well known, Eqn.(3.144) represents a particle-hole transformation in Physics. So, and hence the pairing Hamiltonian of fermions can be transformed into a normal Hamiltonian by a particle-hole transformation. These diagonalization procedures can be used to get energy excitation spectrum of any system of particles, bosons or fermions, and in any phase, superfluid or crystalline.

3.2: Dilute Neutron Gas (low density)

The theoretical study of dilute quantum gases goes back to 1950's and 1960's (Pethick, *et.al*., 1995), but the experimental realization of such systems is a recent phenomenon. This has led to considerable insight into the properties of neutron matter.

At low energies, the effective interaction between two particles is determined by the S-wave scattering length, a. For two neutrons in the singlet spin state, the scattering length is -18.5 fm, which is large in magnitude compared with the range of nuclear interactions $\approx 1.0fm$. For densities much less than $\frac{1}{a^3} \approx 10^{-4}\ fm^{-3}$(particle number density) which in mass density $\approx 10^{-4}\ fm^{-3} \times 1.67\times 10^{-24}$g $\approx\ \rho_n'$ $=10^{-4} \times 10^{39} \times 1.67\times 10^{-24}$gcm^{-3} = 1.67×10^{11}gcm^{-3} which is much less than the range of values, ρ_n, of the density of neutron matter in neutron stars. For the neutron matter whose density is of the order of ρ_n', the leading interaction contribution to the properties of the system can be calculated, in momentum space, in terms of an effective interaction of the form (Gezerlis, *et.al.*, 2015),

$$U = \frac{4\pi\hbar^2 a}{m} \tag{3.153}$$

where m = mass of the neutron

This corresponds to a delta function in co-ordinate space (hard-sphere interaction).

It is well known that the condition for a gas to be dilute is that the inter-particle spacing,r_s, must be large compared with the magnitude of the scattering length, a, of the particles, or since the Fermi wave number, k_F is proportional to,$1/r_s$, this condition is equivalent to $k_F |a| \ll 1$.

For neutron matter at low density, where the interaction is mainly S-wave, the BCS Theory can be used to calculate the energy of the system, the energy gap, and the thermodynamic properties such as the specific heat C_v, the entropy, S, and the transition temperature T_c to the superfluid state.

3.2.1: High Density Neutron Matter

At higher densities, there are larger uncertainties because additional terms in the neutron-neutron interaction (three neutron interactions etc.) become increasingly important and the increased density complicates the calculations. However, it is also possible that in neutron matter, three-neutron interactions may be suppressed because configurations in which three-neutrons are close together may be unlikely, since at least two of the neutrons must be in the same spin state. Thus when neutrons are very close under high pressure and high density, neutron crystallization is certainly possible, and this is what has been studied. However, the theories developed are meant for superfluid neutron matter, whereas I am studying the properties of crystal neutron matter. Here again the Heisenberg's uncertainty principle and infinite repulsion between neutrons will be the basis for calculating the energy of the system which is a high density system.

Calculations have been done to get values of (E/N) and how it varies with the density, ρ_n, of the neutron star when it is in the crystalline state.

3.2.2: The Equation of state of nuclear systems in the t- matrix formalism

There are different types of nuclear systems, for instance, low mass nuclei ($A \leq 20$),medium mass nuclei($A \leq 100$),heavy mass nuclei($A \geq 120$),symmetric nuclear matter (N=Z, number of protons=number of neutrons),asymmetric nuclear matter($N \neq Z$,and this is the situation in heavy nuclei),neutron matter in which small percentage of protons and electrons also exist, and pure neutron matter (like neutron star)

From time to time, nuclear models were proposed to explain the properties of finite nuclei and larger nuclear systems. But no single model could explain the properties of all nuclear systems. In the last thirty years density-functional-theory(DFT),rather nuclear DFT which is an extension of the self-consistent -mean-field theory, has been used to study the ground state properties and low-lying excitation of medium mass and heavy nuclei. The procedure is to model the ground state properties of many-body systems by DFT, and the total energy E of the system becomes a function of the observable, say Q.

In each model, the ultimate objective is to calculate the total energy of the system. Just as in thermodynamics in which PV=RT is the equation of state, in nuclear physics also, the formula for the total energy will be called the equation of state. The total energy is composed of kinetic energy and the potential energy. In any system the general form of the kinetic energy is the sum of $\left(\frac{p^2}{2M}\right)$ or $\sum_k \epsilon_k a_k^\dagger a_k$ in terms of second quantization. However, the form of potential energy depends on type of interactions that may exist between the constituents of the nuclear system. Till a few years ago, pairing interaction between the nucleons of a nuclear system was considered to be most important and many nuclear theories were developed keeping this in mind. Recent discoveries and the properties of pure neutron matter and neutron stars emphatically point out the existence of the two-body and other many-body interactions. Such many-body interactions can be calculated using the many-body-theory via the t-matrix formalism. Once the total energy of the assembly can be calculated taking into account all kinds of nuclear and other interactions, I can obtain the equation of state which can be used to study the properties of the nuclear system under consideration.

3.3: Low Density Neutron Matter

Low-density neutron-matter can be described by a neutron-neutron potential that is central,V(r), i.e., the potential is a function of the inter-particle distance, r, only, and there is no angular variation that is, V(|r|) depends on the magnitude of |r|. In such a case, the essential feature of the interaction can be captured by the s-wave scattering length 'a' and the effective range r_e of the interaction. Thus the interaction is determined mainly by two terms 'a' and r_e.

As the density increases, different partial wave and spin states contribute to the interaction. This means that any theoretical formulation of the neutron-neutron or nucleon-nucleon potential has to take into account all of the allowed ways in which nucleons (neutrons) can interact with each other. Thus to derive the equation of state (that correlates energy with density via 'a' and maybe r_e) for pure neutron matter, quantum many-body method may be used keeping in mind the operator structure of standard nuclear forces.

CHAPTER FOUR

RESULTS AND DISCUSSIONS

4.1: Introduction

In this thesis, the properties of a crystalline Fermi system were studied with regard to transition temperature at which fermions crystallizes, variation of energy per neutron with density and the saturation density with hard-sphere diameter. Note that in a fermionic system, the fermions are very close to each other, and the interaction between a pair of fermions will be assumed to be a hard sphere one.

4.2: Transition Temperature, T_c, at crystallization

A gas or a liquid composed of fermions in which pairs of particles interact via hard-sphere interaction has been studied to obtain the total energy *E* of the system and to obtain the saturation density ρ_s, leading to crystallization of the system. The well-known fermion systems are ^3He, neutron matter and symmetric nuclear matter. The degrees of freedom ν for both ^3He and neutron is ν=2, but for symmetric nuclear matter

composed of equal number of neutrons and protons, ν=4. It will be assumed that each particle of diameter, *C*, is confined to move in a space with the characteristic dimension *R*, such that the mean particle spacing is *R*-*C*. Using Heisenberg's uncertainty principle, the particle spacing is given as:

$$\Delta x \Delta p = \hbar \Longrightarrow \Delta p = \frac{\hbar}{\Delta x} = \frac{\hbar}{(R-C)} \qquad (4.1)$$

The energy per particle *E/N* is given as:

$$\frac{E}{N} = \frac{(\Delta P)^2}{2m} = \frac{\hbar^2}{2m(R-C)^2} \qquad (4.2)$$

Where *m* = mass of each particle and if the ultimate particle number density in the space with characteristic dimension $R = 2.84x10^{-8}$ cm is ρ (Solis, *et.al.*, 2003), then the total number of particles *N*, in the system whose volume is *V*, can be written as

$$N = \frac{4}{3}\pi R^3 \rho \tag{4.3}$$

The number of particles on crystallization of the fermions is given, from equation (4.3) as:

$$N = \frac{4}{3}\pi C^3 \rho_0 \tag{4.4}$$

Whereρ_0 is the particle number density at crystallization.

Substituting for *R* and *C* from equations (4.3) and (4.4) in equation (4.2), yields *E/N* in a general form,

$$\frac{E}{N} = A\frac{\hbar^2}{2m}\left(\rho^{-\frac{1}{2}} - \rho_0^{-\frac{1}{2}}\right)^{-2} \tag{4.5}$$

Where $A = \frac{\pi^2}{2^{\frac{1}{2}}} \cong 7.834$ is a constant called the residue of the pole at close packing. In theory, A is predicted to lie within 1.63≤ A ≥27.0 for random close packing (*rcp*) polyhedron cell and for regular close Packing (face centered cubic) or hexagonal a = π^2 (Baker, *et. al.*, 1982). However, experimentally, the value of *A* obtained from the high pressure data of ^3He, ^4He, *H* and ^2H is A ≅ 15.7 ± 0.6 for the crystalline branch of the equation of state.

The general expression for uniform fermion hard-sphere systems with a degeneracy factor of *v* for the ground state energy per particle with a hard-core potential of range *C* (Felter and Walecka, 1971) is close pack at the same densities. The value of $v = 2$ for a fermion gas and the reduced mass of ^3He is 6.64x10^{-24} *gm*, then

$$\frac{E}{N} = \frac{\hbar^2 k_F^2}{2m}\left[\frac{3}{5} + (v-1)\left\{\frac{2k_F C}{3\pi} + \frac{4}{35\pi^2}(11 - 2log2)(k_F C)^2 + 0(k_F C)^3\right\}\right] \tag{4.6}$$

As $\frac{E}{N} \rightarrow E_0$, and introducing the thermal activation factor, $\tau = exp\left[-\frac{E_0}{k_B T}\right]$, k_F is Fermi momentum and using equation (4.6), yields,

$$E(T) = E_0 exp\left[-\frac{E_0}{k_B T}\right] \tag{4.7}$$

The transition temperature, T_c at crystallization is derived by considering the specific heat capacity of the fermions. Eqn. (4.6) gives

$$\frac{E}{N} = E_0$$

$$\frac{\partial E}{\partial T} = C_v = \frac{\partial}{\partial T}\left(E_0 e^{-E_0/k_B T}\right)$$

$$= E_0\left(-\frac{E_0}{k_B} e^{-E_0/k_B T}\right)\left(\frac{1}{T^2}\right)$$

$$C_v = \frac{E_0^2}{k_B T^2}\left(e^{-E_0/k_B T}\right) \tag{4.8}$$

The specific heat, C_V for a hard-sphere assembly of fermions, is given by:

$$C_v = \left[\frac{\partial E}{\partial T}\right]$$

At the transition temperature, $T = T_c$, and differentiating equation (4.8) with respect to temperature gives:

$$\left[\frac{\partial C_v}{\partial T}\right]_{T=T_c} = 0 = \left[\frac{\partial^2 E}{\partial T^2}\right]$$

$$\left(\frac{\partial C_v}{\partial T}\right)_{T=T_c} = 0$$

$$0 = -\frac{2E_0^2}{k_B T_c^3} + \frac{E_0^3}{k_B^2 T_c^4}$$

$$\frac{2}{1} = \frac{E_0}{k_B T_c}$$

$$T_c = \frac{E_0}{2k_B} \tag{4.9}$$

Where $\nu = 2, C$ =Particle diameter= 2.48Å,

$k_F = 1.92/r_0 \approx 2.1$Å, where r_0 =inter – particle spacing

Since E/N $\rightarrow E_0$at crystallization, and given values of m, R, C or/and A, ρ and ρ_0, eqn. (4.2) or (4.5) or (4.6) is applied to calculate E_0 and substituting the values of $E_0$and $k_B$in eqn. (4.9), the value of T_c is obtained as,

$$T_c = 19.26K \tag{4.10}$$

Thus, the transition temperature at which phase transition takes place in a system of hard-sphere gas of fermions (^3He) is 19.26 K.Thus the value of T_c obtained in this Thesis for crystallization of fermions as given in eqn. 4.9. is close to the T_c =20.3K value obtained earlier (Mishra & Rama, 1985). Note that T_c varies whenever fermion density, ρ and had-sphere diameter, C varies. An improved hard-sphere ground state equation of state for N-fermions hard-spheres (Solis, *et. al*., 2013) is given by:

$$\frac{E}{N} = \lambda_\nu \rho^{\frac{2}{3}} + \frac{(\nu-1)}{\nu}\frac{2\pi\hbar^2 C}{m}\left[\frac{1}{(\rho^{-\frac{1}{3}}-\rho^{-\frac{1}{3}})^2\left(\rho^{-\frac{1}{3}}+b(\nu)\rho_0^{-\frac{1}{3}}\right)}\right] \tag{4.11}$$

where

$$\lambda_\nu = \frac{3\hbar^2}{10m}\left(\frac{6\pi^2}{\nu}\right)^{\frac{2}{3}},\ b(\nu) = \frac{(\nu-1)}{\nu}(\gamma+1) - 1, \tag{4.12}$$

and

$$\gamma = \left(\frac{2^{\frac{2}{3}}}{\pi} - 1\right) \tag{4.13}$$

Equation (4.11) is the generalized modified London equation. In the limit $v \to \infty$,$b(v) \to \gamma$ and $\lambda_v \to 0$, then Eqn. (4.11) shows that at both low and high densities, equation (4.11) reduces to the limiting expressions.

4.3: Variation of energy per neutron, E/N with density

The variation of energy per unit neutron, *E*/*N* with density of a hard-sphere assembly starting from the ground state energy was studied for both low and high densities, and the results are presented below.

At low density, $\rho_0 \to 0$, equation (4.11) becomes

$$\frac{E}{N} = \lambda_v \rho^{\frac{2}{3}} + \frac{(v-1)}{v}\frac{2\pi\hbar^2}{m}\rho C \tag{4.14}$$

where

$$\lambda_v = \frac{3\hbar^2}{10m}\left(\frac{6\pi^2}{v}\right)^{\frac{2}{3}} \tag{4.15}$$

On the other hand, at high density, $\rho \to \rho_0$and $v \to \infty$ in equation (4.11) such that

$$\frac{E}{N} = \frac{2\pi\hbar^2}{m}\left(\rho^{\frac{-1}{2}} - \rho_0^{\frac{-1}{2}}\right)^{-2} \frac{1}{\left[\rho_0^{\frac{-1}{2}}(1-\varsigma)\right]} \tag{4.16}$$

Now using $\rho_0 \equiv \frac{\sqrt{2}}{C^3}$ and $\varsigma \equiv \left[\frac{2^{\frac{2}{3}}}{\pi} - 1\right]$then equation (4.11) becomes

$$\frac{E}{N} = \pi^2 2^{\frac{2}{3}}\frac{\hbar^2}{2m}\frac{1}{\left(\rho^{\frac{-1}{2}} - \rho_0^{\frac{-1}{2}}\right)^2} \tag{4.17}$$

Where $\pi^2\, 2^{2/3}$ =A=15.7and *m* is the reduced mass for ^3He.

Fig. 4.1 presents the results for a low density assembly, and is a plot of E/N verse density. The results indicate that the value of E/N varies linearly with density. This is due to the fact that at low density the interaction plays fewer roles in crystallization of fermions and the energy simply increases with particle number.

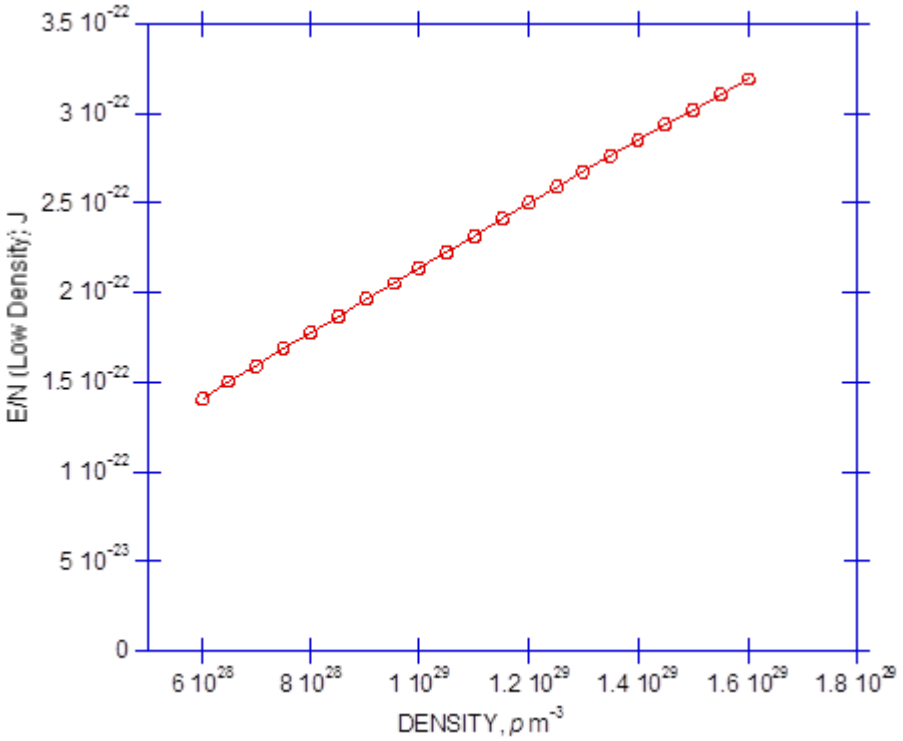

Fig. 4.1: Energy per particle for low density.

Fig. 4.2, on the other hand, presents the results for high density assembly, which is also a plot of E/N versus density. For high density assembly of fermions, there is little variation in E/N with density up to a particular density where its value suddenly rises. This is due to the fact that when the density becomes large, close to ρ_s, interactions become predominant due to the proximity of the particles at high density, and hence the energy E/N suddenly becomes large.

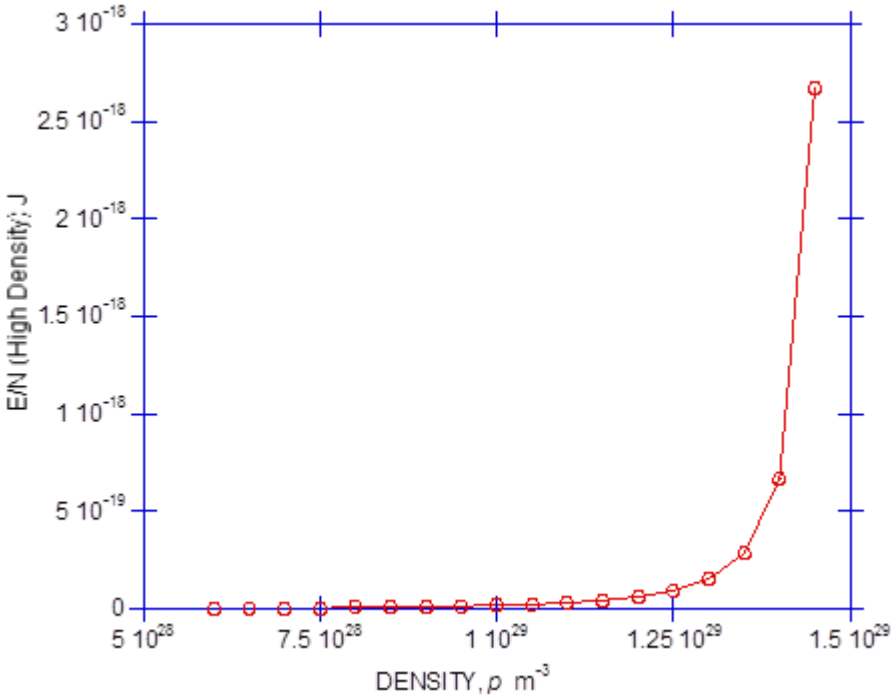

Fig. 4.2: Energy per particle for high density.

4.4: Variation of saturation density with Hard-Sphere diameter C for both low and high density fermionic system

The saturation density for an assembly of fermions will be defined as that density ρ_s, at which the hard-sphere assembly of fermions form close-pack (*cp*) crystalline structure. At this density, the total energy, *E*, of the assembly will be such that,

$$\left(\frac{\partial E}{\partial \rho}\right)_{\rho=\rho_s} = 0 \tag{4.18}$$

Now using low density value of *E/N* from equation (4.14) in equation (4.18), I can get ρ_0 as a function of *C* as,

$$\rho_s = \left(\frac{4m\lambda_v}{9\pi\hbar^2 C}\right) \tag{4.19}$$

In the high density system, the saturation density is obtained by using equation (4.17) in equation (4.19), and this calculation yields

$$\rho_s = \rho_o \equiv \frac{\sqrt{2}}{C^3} \tag{4.20}$$

Fig. 4.3 presents the results on the variation of saturation density with the hard-sphere diameter. In the case of low density, the value of ρ_s varies, on first approximation, almost linearly with C. This means that at low density the variation of ρ_s with C is insignificant since the inter-particle distance is larger than C. However, for high density assembly, the value of ρ_s decreases exponentially with C, and this is an essential condition for crystallization.

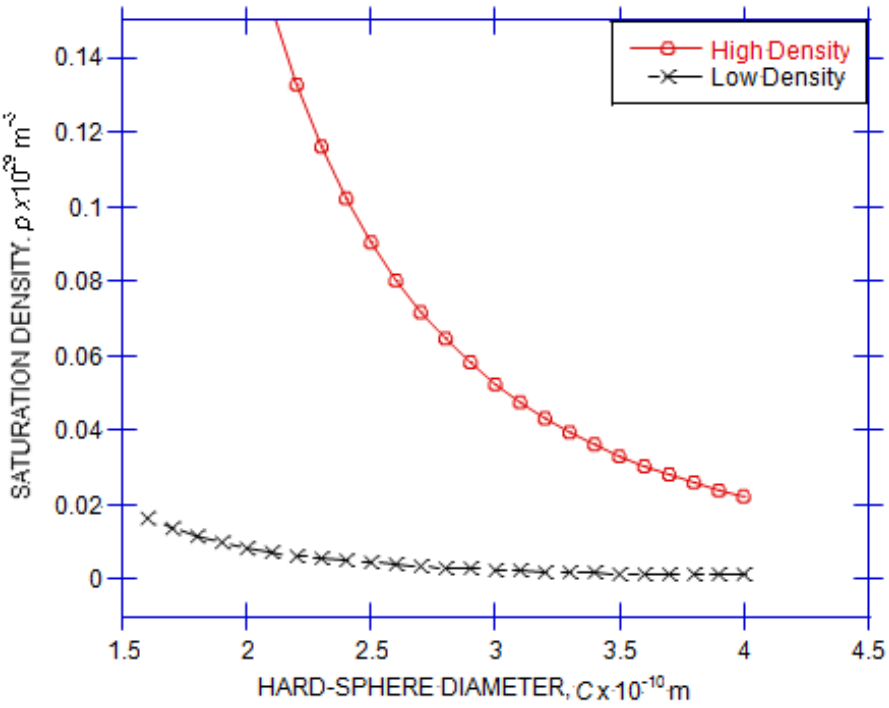

Fig. 4.3: Variation of saturation density with corresponding hard-sphere diameter for ^{3}He particles.

Table 4.1.shows variation of values of energy per particle with saturation density for both low and high densities at free particle spacing, R=2.8401Å.

Table 4.2. Energy per particle and Saturation density for low and high densities (Free-particle spacing, R =2.8401 Å).

Parameter	Density Range	
	Low	High
$\frac{E}{N} Joules$	$1.435x10^{-22}$	$3.113x10^{-21}$
$\rho_s(m^{-3})$	$7.117x10^{27}$	$1.502x10^{29}$

4.5: The Variation of Energy per particle (E/N) with Density, ρ, both for low and high density Neutron Stars

In the crystalline state of neutron matter, the nature of interaction changes drastically. A crystalline state being intrinsically restless, the particles vibrate around their position and even exchange positions. The motion is determined by the Heisenberg's uncertainty principle and gives zero-point energy. Since the particles are frozen, they almost touch each other, and the interaction between them could be treated as infinitely repulsive. Hence these two energies could constitute the equation-of-state in terms of the scattering length 'a' and density ρ

The energy, E, of an assembly of crystalline neutron matter in the low density limit will be given by (Mishra & Rama, 1985)

$$E/N = \lambda_v \rho^{2/3} + \frac{(v-1)}{v}\frac{2\pi\hbar\rho a}{m} + \frac{4\pi\hbar^2 a}{m} \quad (4.21)$$

where $\lambda_v = \frac{3\hbar^2}{10m}\left(\frac{6\pi^2}{v}\right)^{\frac{2}{3}}$, and $v = 2$, which is the intrinsic degrees of freedom for each fermion.

The energy, E, of an assembly of crystalline neutron matter in the high density limit ($v \to \infty, \lambda_v \to 0,$) will be given by (Mishra & Rama, 1985)

$$\frac{E}{N} = \pi^2 2^{2/3} \frac{\hbar^2}{2m} \left[\frac{1}{\rho^{-1/3} - \rho_0^{-1/3}} \right]^2 + \frac{4\pi\hbar^2 a}{m} \quad (4.22)$$

where $\rho_0 = \frac{\sqrt{2}}{a^3}$ and a is the scattering length.

The variation of $\frac{E}{N}$ with ρ both for low density and high density neutron stars, keeping 'a' constant, ρ may be varied between 1.4 x 10^{15} g/cm^3 and 5.237 x 10^{15} g/cm^3 and 10.85x10^{15} g/cm^3, with a difference of 0.5; and a may be varied from -18.5 fm to 1.0 fm with a difference of 0.5. One value for ρ should be 3.7x10^{15}g/cm^3 since this is supposed to be the density of neutron matter at which there may be onset of the solid phase. Also calculated was the value of $\frac{E}{N}$ for ρ = 5x10^{14} g/cm^3, since at this density under a pressure of 5x10^{27}atm, solidification of neutron matter occurs.

4.6: Low density Crystallization

Eqn.(4.20) gives the energy E/N=ε, which can be written,

$$\varepsilon = \frac{p^2}{2m} \quad (4.23)$$

$$\varepsilon = 1.435\ x\ 10^{-15} erg$$

Now, if Δp is maximum fluctuation in the momentum of the particle in the state of crystallization, then the fluctuation Δx in the displacement will be,

$$\Delta x = \frac{\hbar}{\sqrt{2m\varepsilon}}$$

(4.24)

Substituting the values of η, m and ε in equation (4.24), yields

$$\Delta x = 7.9\ x\ 10^{-9} cm$$

(4.25)

Now, using the equation,

$$\Delta x \Delta p = \eta \tag{4.26}$$

yields,

$$\Delta p = \frac{\hbar}{\Delta x} = 1.265x10^{-19} gcm/sec$$

(4.27)

4.7: High density crystallization

Similarly from eqn.(4.22) for high density condition, $\epsilon = 3.113x10^{-14} erg$, from which yields,

$$\Delta x = 1.6x10^{-9}\text{cm} \tag{4.28}$$

and

$$\Delta p = 6.25x10^{-19}\text{gcms}^{-1}$$

(4.29)

Table 4.2. shows values of energy, fluctuations in position and momentum for low and high densities.

Table 4.2: The values of energy, fluctuation in position and momentum for low and high densities

Parameter	Density Range	
	Low	High
ε	$1.435x10^{-15}$erg	$3.11x10^{-14}$erg
Δx	$7.9x10^{-9}$cm	$1.6x10^{-9}$cm
Δp	$1.265x10^{-19}$gcmsec^{-1}	$6.25x10^{-19}$gcmsec^{-1}

Table 4.3 shows variation of values of energy per particle with saturation density for a hard-core radius, $\boldsymbol{a = 2.1117}$Å

Table 4.3: Energy per particle and saturation density, (hard-core radius a=2.1117Å)

ρ_s x 10^{15} g/cm^{-3}	0.5	3.7	10.85
$E/_N x10^{-30}J$	1.3	4.8	9.8

Fig. 4.4 shows variation of energy per particle and saturation density for low and high densities at a constant radius, a=2.1117Å.

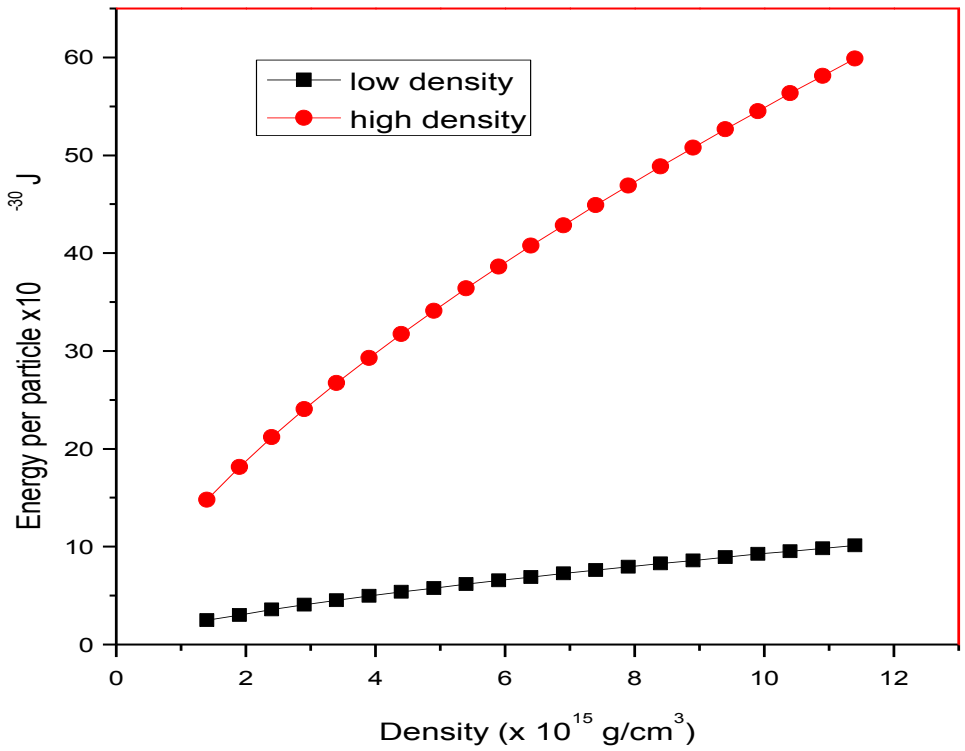

Fig. 4.4: Variation of energy per particle with density

The transition temperature T_c will vary with ρ and C. For the values of ρ and C, T_c =19.26K, but this could vary from assembly to assembly. These results show that for both low and high density; ρ_s varies as C^{-3} which means that the assembly will crystallize for some value of C irrespective of the value of ρ_s. Such results were obtained for bosons by (Khanna, et. al., 2011).

Crystallization of a hard-sphere system of fermions with densities ranging from low to high values has been studied. Saturation densities at which the total energy E, is maximum has been calculated. The values of saturation particle number densities ρ_s for low and high densities are; $7.11x10^{27}\ m^{-3}$ and $1.502x10^{29}m^{-3}$ respectively at which the fermions close pack or crystallize. Variation of ρ_s with hard-sphere diameter C is not linear and it is more or less the same for both low and high density since crystallization occurs in both the cases. The total energy, E, has been found to vary non-linearly with ρ at high densities and closely linear for low density.

Table 4.1. shows that the value of E for low density is $1.435x10^{-22}\ J$, and for high density it is $3.113x10^{-21}\ J$. These findings are consistent with experimental and computer-simulated results obtained by others.

The Table 4.3 shows that the energy E/N increases as the density increases, both for low density and high density neutron stars, keeping 'a' constant. This is exactly what it should be since increasing the density can lead to strong interactions resulting in the increase in energy of the system. This also confirms that under high pressures the system will have large density and huge amount of energy on crystallization.

Calculations have shown that the fluctuation Δx in the position for low density system is larger than the corresponding value of Δx for the high density neutron star. It should be so since the high density system is more closely packed compared to the low density system. The fluctuation Δp in the momentum in high density system is large compared to the low density system, because high density system has more energy

Fig. 4.4 shows that for low density variation in E/N is almost linear with small gradient. For high density, the variation is large with large gradient. This is because in a high density system, the energies involved are large, Δx is large, and hence the variation has to be large. The variation of $\frac{E}{N}$ with ρ shown in Figure 4.4 is very similar to what was obtained by (Grandolf, *et al*., 2012)

CHAPTER FIVE

CONCLUSIONS AND RECOMMENDATIONS

5.1: CONCLUSION

The transition temperature at which phase transition takes place in a system of hard-sphere gas of fermions (^3He) is 19.26 K.Thus the value of T_c obtained in this Thesis for crystallization of fermions as given in eqn. 4.9. is close to the T_c =20.3K value obtained earlier. Note that T_c varies whenever fermion density, ρ and had-sphere diameter, C varies.

Crystallization of a hard-sphere system of fermions with densities ranging from low to high values has been studied. Saturation densities at which the total energy E, is maximum has been calculated. The values of saturation particle number densities ρ_s for low and high densities are; $7.11x10^{27}\ m^{-3}$ and $1.502x10^{29}\ m^{-3}$, respectively, at which the fermions close pack or crystallize. Variation of ρ_s with hard-sphere diameter C is not linear and it is more or less the same for both low and high density since crystallization occurs in both the cases. The total energy, E, has been found to vary non-linearly with ρ at high densities and closely linear for low density. The value of E for low density is $1.435x10^{-22}\ J$, and for high density it is $3.113x10^{-21}\ J$. These findings are consistent with experimental and computer-simulated results obtained by others.

It is established that the energy E/N increases as the density increases, both for low density and high density neutron stars, keeping ‘a’ constant. This is exactly what it should be since increasing the density can lead to strong interactions resulting in the increase in energy of the system. This also confirms that under high pressures the system will have large density and huge amount of energy on crystallization.

It is found that the fluctuation Δx in the position for low density system is larger than the corresponding value of Δx for the high density neutron star. It should be so since the high density system is more closely packed compared to the low density system. The

fluctuation Δp in the momentum in high density system is large compared to the low density system, because high density system has more energy

Further, it has been shown that for low density variation in E/N is almost linear with small gradient. For high density, the variation is large with large gradient. This is because in a high density system, the energies involved are large, Δx is large, and hence the variation has to be large.

5.2: RECOMMENDATIONS

Since the Physics of compact neutron stars constitutes a new thriving feel of research under relativistic nuclear astrophysics which is a collection of disjointed disciplines such as high energy astrophysics, gravitational physics, nuclear and hadronic Physics, QCD, superfluid hydrodynamics, plasma Physics; the interdisciplinary nature of this study makes it a rewarding undertaking for future research studies. Neutron stars being a fascinating testbed for all sorts of extreme Physics, studying the details of their interior remains an active area of research to establish what happens to the protons and electrons and to simulate the states of matter in a neutron star on the Earth.

Cold atom trapping technique in optical lattice is an experimental tool commonly used in Condensed Matter, atomic, molecular and optical Physics, through which nano gears were made, it is recommended that further studies be undertaken in nano Science to pave way for machines or setups working on the molecular scale which could in turn lead to advances in nanotechnology. With the recent discovery of type II Weyl fermions, since quantum statistical effects fade away with decreasing particle density leading to recovery of average fermionic behaviour, their crystals could be grown in a laboratory to allow for experimental studies into their behaviour as exotic particles whose behaviour switches between electrical conductor and insulator depending on the direction of the induced current; their understanding to create highly efficient transistor components/devices in electronics and quantum computers, and could lead to more new materials with unusual transport properties.

Another promising avenue for future research is whether the very high density of a neutron star is due to the gravitational forces or nuclear forces or both.

REFERENCES

Anderson, M.H., Ensher, J. R., Mathews, M. R., Wieman, C. E., & Cornel, E. A. (1995). *Observation of Bose –Einstein condensation in a Dilute Atomic Vapour.* London: Science, 269,198-201.

Anderson, P. W, & Heine, V., (1967). *Magnetism in Transition Metals at finite temperature. I. Computational model.* Cambridge: JETP.

Anderson, P. W.& Morel, P., (1961).*Generalized Bardeen-Cooper-Schrieffer States and the Proposed Low-Temperature Phase of liquid* He^3. Phys. Rev. **123**, 1911.

Andronikashvin, E. L., (1946). *Properties of Superfluid He-4: The Two-Fluid Model.* Georgia: AIP Publishing.

Antoniadis, J., Paulo, C. C., Thomas, M., Ryan, S., Kirkwijk, V., (2013) Science 340:448.

Atkins, P. & De Paula, J., (2009). *Elements of physical chemistry.* Oxford University: Oxford University Press.

Baker G.A. Jr. Benofy, L. P., Fortes, M., Deliano, M., Peltiers, S. M., & Plastino, M., (1982). *Hard –Core Square –Well Fermions.* Journal of Physics A: Mathematical and General, vol. 21 Number 3. Fargo ND, USA: OOP Publishers.

Baker, G.A. Jr., (1971). *Singularity structure of the Perturbation Series for the Ground – state Energy of a many Fermion System.* Fargo ND, USA: OOP Publishers.

Baker, G.A., (1999). *Neutral Matter Model*. New York: Living Reviews (LR)

Balian,R. & Wertharner, N. R., (1963). *Superconductivity with pairs in a Relative P-wave.* Phys. Rev. **131**, 1553.

Bardeen, J., Cooper, L. N., & Schrieffer, J. R., (1957). *Theory of Superconductivity.* University of Illinois: APS.

Bardeen, J.,Cooper, L.N.& Shrieffer. J.R., (1957). *Microscopic Theory of Superconductivity:* University of Illinois: APS. Phys. Rev. **108**, 1175

Beguin, L. Vernier, A., Chicireanu, R., Lahaye, T., Browaeys, A., (2013). *Direct measurement of the Van der Waals interaction between Two Rydberg Atom.* Phys. Rev. Lett. **110**, 263201.

Bogoliubov, N. N, (1947). *The Theory of Superfluidity. J. Phys. (USSR),* **11,** 23

Boboliubov, N. N, et.al., (1958). *Transformations for Fermi-Bose Systems and squeezed states.* IOP Science.

Boninsegni, M., Pollet, L., Prokof'er, N., Pupillo, G., Zoller, P., (2012). *Simulated streamlines after a clear visualization of Radial Trailing Vortices between blades in a Von Karman water experiment* Phys. Rev. Lett. **109**,025302.

Bose, S. N., Theimer, D., & Ram, B., (1924). *The beginning of quantum statistics.* Zeit Schrift fur Physic, **26**,170.

Brueckner, K.A., Soda, T., Anderson, P. W., & Pierre, W., (1960). *Level structure of Nuclear matter and liquid ^{3}He.* Phys. Rev. **118**, 1442.

Buchler, H.P., Demler, E., Lukin, M., Micheli, A., Prokof'er, N., Pupillo, G., & Zoller, P., (2007). *Strongly Correlated 2D Quantum Phases with cold Polar molecules: Controlling the shape of the interaction potential.* Phys. Rev. Lett. **98**, 060404.

Bulluta, I., & Nori, F., (2009). *Quantum Simulators*. Bethesda MD: Science Publishers.

Campo, V. L., Quintanilla, J., & Betourus, J. J., (2007). *Critical bevavior driven by the confirming potential in optical Lattices with ultra-cold Fermions?* Phys. Rev. Lett. **99**, 240403.

Canuto, V. & Chitre S.M (1974). *Crystallization of dense neutron matter. Phy. Rev. D, **9**, 1587-1613*

Carr, S.T., et. al., (2009). *Deconfinement and Quantum Liquid Crystalline State of Dipolar Fermions in optical Lattices.* Int. J.Mod. Phys. **B 23**,4074.

Chaikin, P.M. & Lubensky T. C., (1995). *Principles of CMP*. Cambridge: Cambridge University Press.

Chaikin, P.M. & Lubensky T. C., (2012). *Principles of Condensed Matter Physics.* Cambridge: Cambridge University Press.

Chakraborty, T., (1999). *Quantum Dots: A Survey of the properties of Artificial Atoms*. Amsterdam; North-Holland Publishing Company.

Chen, J. Q., (2002). *Group Representation theory for Physicists.* Singapore: World Scientific.

Cinti, F., Jain, P., Boninsegni, M., Micheli, A., Zoller, P. Pupillo, G., (2010). *Super-solid Droplet crystal in a dipole-blockaded gas.* Phys. Rev. Lett. **105**, 135301

Cinti, F.F., Boninsegni, M., & Thomas, P., (2014). *Exchange-induced Crystallization of soft-core bosons.* Nat. commun. **5**,3235.

Cohen, M. L., (2008).*Essay: fifty years of CMP.* New York: American Physical Society.

Coleman, P., (2003). *Many- Body Physics: unfinished Revolution*. Rutgers University, Piscataway, USA : Annales Henri Poincare.

Coleman, P., (2011). *Introduction to Many Body Physics.* Cambridge: Rutgers University.

Committee on CMMP, (2010). *Solid State Sciences Committee; Board on physics and astronomy; Physical Sciences, national Research Council (2007). Condensed Matter and Materials physics: The Science of the World Around me.* Washington D.C: National Academies Press.

Committee on Facilities for CMP (2004). *Report of the IUPAP working group on facilities for CMP: High Magnetic Fields* (PDF): International Union of Pure and Applied physics.

Committee to Assess the current Status and Future Direction of High Magnetic Field Science in the United States; Board on physics and Astronomy; Division on Engineering and physical sciences; National Research Council, (2013). *High Magnetic Field Science and Its Application in the United States: Current Status and Future Directions.* Washington D.C: National Academies Press.

Cooper, N. R., & Shlyapnikov, G. V., (2009). *Stable Topological Superfluid Phase of Ultra-cold Polar Fermionic Molecules.* Phys. Rev. Lett. **103**, 155302.

Cornall, E.A & Wieman C.E.,(2002). *Nobel Lecture: Bose-Einstein condensation in a dilute gas, the first 70 years and some recent experiments.* Rev. Mod. Phys. **74**,875.

David, J. T., (1998). *Topological Quantum Numbers in Nonrelativistic Physics.* Washington DC: world scientific.

Davis, K. B., Mewes, M. O., Andrews, M. R., Druten, V. N. J., Durfee, D. S., Kurn, D. M., & Ketterly, W., (1995). *Bose – Einstein condensation in a Gas of Sodium Atoms*. Phys. Rev. Lett. 75, 3969-3973.

Davy, J. (ed), (1839).*The collected works of Sir Humpry Davy: vol. II*. London: Cornhill Smith Elder & Co.

De Blasio, (2014). The Astrophysical Journal. DOI: 10: 1086/176307 : May, 5, 2014.

Demarco, B., & Jin, D.S., (1999). *Onset of Fermionic Degeneracy in a trapped Atomic Gas*. London: Science 285, 1703 – 1706.

Demorest P. B., Pennuci, T., Ransom, S. M., Roberts, M. S. F., & Hessels, J. W. T., (2010). *Phenomenological QCD Equations of state for Neutron stars.* Nature 467:1081- 1083.

Dirac, P. A. M.,(1958). *The Principles of Quantum Mechanics.* Oxford: Oxford University Press

Doiron, L. N., Cyril, P., David, L., Julen, L., Jean-Baptiste, B., Liang, R., Bonn, D. A., Hardy, W. N., & Lous, T., (2007). *Quantum Oscillations and the Fermi Surface in an underdroped high – Tc Supperconductor*. London: Nature Publishing Press.

Dudin, Y. O.,& Kuzmich, A., (2012). *Strongly interacting Rydberg excitation of a cold atomic gas, Atlanta, Georgia Institute of Technology.* Science **336**, 887-9.

Dzero, V., Kai Sun, G., & Coleman, P., (2009). *Topological Kondo Insulators.* Phys. Rev. Lett. 104 (10)

Enrico, F., Inguscio, M., Stringari, S., & Wieman, C., (1999). *Bose – Einstein Condensation in atomic gases.* Amsterdam: IOS Press.

Faraday, M., (1823). *Experimental Researches in Chemistry and Physics.* England: John Murray.

Fetter, A.L., & Walecka J.D., (1971). *Quantum. Theory of Many –Particle System.* New York: Mcgraw- Hill.

Feynman, R.P. (1972). *Statistical A. Mechanics: Set of Lectures*. New York: Addison – Wesley.

Field, D., Plekan, O., Cassidy, A., Balog, R., Jones, N. C., & Dunger, J., (2013). *Spontaneous electric fields in solid films: Sponte-lectrics*. Int. Rev. Physics, Chem. 32 (3)

Fisher, M. E., (1998). *Renormalization Group Theory: Its basis and formation in statistical Physics.* Rev. Mod. Phys. 70 (2)

Fradkin, E., Steven, A. K., Vadim, O, (2007). *Electron Nematic Phase in a Transition Metal Oxide.* Science **315**, 196.

Frenkel,J., (1947).*Kinetic Theory of liquids.* Oxford: Oxford University press.

Gallagher, T. F., (1994).*Rydberg Atoms*. Cambridge: Cambridge University Press.

Gandolfi, S., Illarionov, A. Y., Fatori, S., & Schmidt, K., (2010). *Microscopic calaculation of the equation of state of Nuclear Matter and Neutron Star Structure.* Mon. Not. R. Astron. Soc, 404, L 35.

Gezerlis, A, Pethick, C. J., & Schwenk, A., (2015). *Pairing and super fluidity of Nucleons in Neutron Stars.* Oxford: Oxford University Press.

Giorgini, S., Pitaevski, L. P., Stringari, S., (2008). *Theory of Ultra-cold Atomic Fermi gases.* Rev. Mod. Phys. 80:1215

Goldstein, H., (1980). *Classical Mechanics, 2nd ed.* Boston, Massachusetts, Me: Addison-Wesley.

Grandolf S., Carlson J. & Reddy S. (2012). *Relativistic fluid Dynamics with spin*Phys.Rev.C85:032801.

Greiner, M., & Folling S., (2008). *CMP: Optical Lattices.* London: Nature.

Guillot S, & Servillat M, (2013).*Measurement of the radius of Neutron Stars with high signal-to-noise Quiescent Low mass X-ray Binaries in Globular clusters.* The Astrophysical Journal 772:7.

Hall, H.E., Viven, W.F., (1958). *The Rotation of Liquid Helium II. The Theory of mutual Friction in uniformly Rotating Helium II. Proceedings of the Royal Society A Mathematical, Physical and Engineering Science*. **238** (1213) 215

Han, J. H., (2010). *Solid State Physics* (PDF). Seoul: sung Kyun Kwan University.

Heinke C. O, Cohn, H. N., Lugger, P. M., Webb, N. A., Ho, W. C. G., Anderson, J., Campana, S., & Bogdanov, S., (2014). *Structure and Cooling of Neutron Stars: Nuclear Pairing and Superfluid effects.* Mon-not.R.Astron.Soc.444:443

Henkel, N., Nath, R., & Pohi, F., (2010). *Three-dimensional Roton-Excitations and supersolid formation in Rydberg-excited Bose-Einstein Condensate.* Phys. Rev. Lett. **104**,195302.

Henshaw, D. G.& Woods A. D. B., (1961). *Modes of Atomic motions in liquid Helium by Inelastic Scattering Neutrons.* Phys. Rev.,121, 1266.

Hoddeson, L., Braun, E., Teichemann, J., & Spencer, W., (1992). *Out of the crystal maze: chapters from the History of solid state Physics.* Oxford: Oxford University Press.

Hoffmann, D., (2013). *Fifty years of Physical Status Solid Historical Perspective*. Physical Status Solid B 250 (4).

Hofmann, C. S., Wedemuller, T., (2013). *Quantum Physics: Spooky action gets collective* Phys. Rev. Lett. **110**, 203601.

Huang, Y .P. & Wang, D. W., (2009). *Quandary phase diagrams of Fermionic dipolar gases in a planar array of one-dimensional tubes.* Phys. Rev. **A 80**, 053610.

Jaksch, D., & Zoller, P., (2005). *The cold atom Hubbard tool box.* Annals of physics 315 (1)

Jauregui, K., Hausler, W. & Kramer, B.,(1993). *Molecules in nanostructures.* Euro phys. Lett. **24**,581.

Kadanoff, L. P., (2009). *Phases of Matter and Phase Transitions; From Mean Field Theory to Critical Phenomena.* Chicago: The University of Chicago.

Kamerligh, H. O. & Dewar, J., (1908). *Liquefaction of gases and discovery of superconductivity: two very closely scientific achievements in low temperature Physics.* Cali Colombia: SCIELO Analytics.

Kapitza, P., (1938). *Viscosity of Liquid Hellium Below The* $\lambda - point$. Nature. **141** (3228): 74.

Kapitza, P., Allen, J. F., & Misener, D., (1937). *Fermionic Condensate.* Cambridge: Cambridge University Press.

Kate, L. Jones, P. & Witold, N, (2010). *Designer nuclei,* The Physics teacher, vol. 48 p38

Keating, T., Jau, Y. Y., Hankin, A. M., Deutsch, J. H., & Biedermann, G. W., (2013). *Entangling atomic spins with a Rydberg-dressed spin-flip blocade.* Phys. Rev. **A 87**,052314.

Ketterle,W., (2002). *Nobel Lecture: When atoms behave as waves: Bose Einstein condensation and the atom laser.* Rev. Mod. Phys. **74**,1131.

Khanna, K.M., & Sakwa, W.T., (2010). *Hard –Sphere Assembly of crystalline Bosons.* Moscow: African Physical Review 4:001.

Kinoslita, T., Wenger, T., Weiss S. D., (2004).*Observation of a one-dimensional Tonks-Girardeau gas.* Science .**305**, 1125.

Kirkwood, J. G., Eugene, K., & Berni, J. A., (1950). *Radial Distribution functions and the equation of state of a fluid composed of rigid Spherical molecules.* Melville, NY: American Institute of Physics.

Kittel, C. & Hoddeson, L., (1996): *Introduction to solid State Physics*. New York: John Wiley &Sons.

Kivelson, S.A., Fradkin, E., Emery, V. J., (1998). *Electronic Liquid-Crystal Phases of a doped Mott insulator.* Nature (London). **393**,550-553.

Kragh, H., (2002). *Quantum Generations: A History of Physics in the twentieth Century (reprinted).* New Jersey (USA): Princeton University press.

Ku, M. J. H., Sommer, A. T., Cheuk, L. w., Zwierlein, M. W. (2012). *Revealing the Superfluid Lambda transition in the universal Thermodynamics of a unitary Fermi Gas.* Science 335:563

Lalazissis, G. A., Niksik, T., Vretener, D & Ring, P. (2005). *New relativistic mean-field interaction with density-dependent meson-nucleon-couplin.*, Phys. Rev. C71, 024312

Landau, L .D., & Lifshitz, E. M., (1980). *Statistical Physics Part 2, 001. 9. 3rd Ed.* London: Pergamon Press.

Landau, L.D & Lifshitz, E. M., (1977).*Quantum Mechanics: Nonrelativistic theory*. London: Pergamon Press.

Landau, L.D.& Lifshlitz,E.M.,(1958).*Quantum Mechanics*. London: Pergamon.

Landau, L.D., (1999). *Theory of a Fermi liquid.* Cambridge. JETP.

Laughlin, R. B., (1981). *Quantized Hall Conductivity in 2-Dimensional.* Physical Review **B,** 23(10), 5632-5633.

Ledowski, S. & Kopietz, P., (2007). *Condensed matter theory.* Phys. Rev. **B 76**, 121403.

Lee, W. C., Giuseppe, G., & Nole, G., (2010). *Nematic phase transition in a multi-orbital hubbard model.* Phys. Rev. **B 80**, 104438.

Leggett , A.J., (1972). *Interpretation of recent results on He^3 below 3mk: a new liquid phase?* Phys. Rev. Lett . **29**, 1227.

Leggett, A.J., (1975). *Statistical CMP* Rev. Mod. Phys.**47**, 331.

Lenz, D.A., Bianca, M. M., Christos, N. L., & Blaak, R., (2012). *Thermodynamic stability and structural properties of cluster crystals formed by amphiphilic dendrimers* Phys. Rev. Lett. **109**, 228301.

Li Z. H, & Schulze H. J, (2008). *Neutron Star Structure with modern Nucleonic three-body forces.* Phys. Rev. C78:028801

Lindley, D., (2015). *Focus: Landmarks- Accidental Discovery Leads to Calibration Standard.* Virginia: American Physical Society.

Lu, M., Ho-Youn, S.,& Benjamin, L. L. (2010). *Trapping ultracold dysprosium: a highly magnetic gas for dipolar physics.* Phys. Rev. Lett **104**, 063001.

Macri, T., Boninsegni, M., & Pohl T., (2013). *Exchange-induced crystallization of soft-core bosons.* Phys. Rev. **A 87**, 061602.

Malcolm, F. C., (2003). *Magnetic Critical Scattering.* Oxford: Oxford University Press, USA.

Maths, D., (2006). *The theory of magnetism made simple.* Uttah: world scientific.

Maucher, F., Henkel, N., Saffman, M., Krolikowski, M., Skupin, S., & Pohl, T., (2011). *Rydberg-induced solitons: three-dimensional self-trapping of matter waves.* Phys.Rev. Lett. **106**, 170401.

Merali, Z., (2011). *Collaborative physics: String Theory finds a bench mate*. London: Nature.

Mercure, J.F., Goh, S. K., O'Farrell, E. C. F., Perry, R. S., (2009). *Quantum oscillations in the anomalous phase in Sr 3 Rn 2 0 7* Phys. Rev. Lett. **103**, 176401.

Micheli, A., Wang, D., Ospelkaus, S., Miranda, M. H. G., Bohn, J. L., Ye, J., (2007). *Dipolar collision of polar molecules in the quantum regime.* Phys. Rev. **A76**, 043604.,

Mishra S. G. & Rama K T V, (1985). *Statistical Mechanics of DNA Unzipping under periodic force: Scaling behaviour of Hysteresis loops.* Phys. Rev. Lett. B31 2825

Miyakawa, T., Carusotto, L., Schmiedmayer, J., & Luis V., (2008). *Focus on Bose Condensation phenomena in atomic and solid state physics.* phys. Rev. **A 77**, 061603 (R)

Modugno , G., Roat, G., Riboli, F., Ferlaino, F., Robert, J., Massino, B., (2002). *Collapse of a Degeneracy Fermionic Gas*. London: Science 297, 2240.

Moulton, W.G. & Reyes, A, P., (2006). *Nuclear Magnetic Resonance in Solids at very high Magnetic fields*. New Jersey: World Scientific.

Nambu, Y., (2008). *Spontaneous Symmetry Breaking in Particles Physics; a case of cross fertilization.* Chicago: Nobel Prize Organization.

NASA, (2017). *Origin and Evolution of Neutron Star Magnetic Fields.* USA.

Neil, W. A. & Mervin D. N., (1976). *Solid State Physics*. New York. Saunders College

Ni, K .K., Ospelkaus, S., Miranda, M. H. G., Pee'r, A., Neyenluis, B., Zirbel, J. J., Kotochigova, S,, Ye, J., (2008). *A high-phase-space-density gas of polar molecular* Science **322**, 231.

Niksik, T., Vretenar, D., Finelli, P., & Ring, P. (2002). *Relativistic Hartree- Bogoliubov model with density-depended Meson-Nucleon Couplings.* Phys. Rev. C66, 024306

Osheroff , D. D., Lee, D. M., Richardson, R. C., (1972). *Chiral ptip superfluid on a sphere.* Phys. Rev. Lett. **29**,920.

Osheroff, D. D., Richardson, R. C., & lee, D. M., (1972). *Evidence for a new phase of solid* He^3 Phys. Rev. Lett. **28**,885.

Ozel F, Bayrn. G, & Guver T, (2010). *Astrophysical Measurement of the Equation of State of Neutron Star Matter.* Phys.Rev.D82:101301.

Parigi, V., Bimbard, E., Stanojevic., J., Hillard, A. J., Nogrette, F., Tuelle-Brouri, R., DurjDumtser, A., & Grangier, P., (2012). *Observation and measurement of interaction-induced dispersive optical nonlinearities in an ensemble of cold Rydberg atoms.* Phys. Rev. Lett. **109**, 233602.

Perdew, J. P. & Ruzsinszky A., (2010). *Fourteen Easy Lessons in Density Functional Theory* (PDF). International Journal of Quantum Chemistry 110(15).

Pethick , C. J. & Ravenhall, D. G., (1995). *Matter at Large Neutron Excess and the Physics of Neutron –star Crusts.* Seattle. University of Washington.

Peyronel, T., Johnson, P. V., Watts, R. J., Stefanson, K., (2012). *A mutation in APP protects against Alzheimer`s disease and age-related cognitive decline.* Nature. **488**, 57-60.

Pomeranchulk, Y., (1958). *Effect of Fermi-liquid interaction on a phase transition of order* $2\frac{1}{2}$. Sov. Phys. JETP. **35**, 524.

Puetter, C, M., Hae-Young, K., Stroud, D., , (2010). *Transport signatures of electronic nematic stripe phases.* Phys. Rev. **B 81**, 081105 (R)

Quintanilla, J. H. C., (2012).*The Strong- correlations Puzzle.* Oxford: Physics World.

Quintanilla, J., Carr, S. T., & Betouras, J. J., (2009). *Dipole-dipole interactions in optical lattices do not follow an inverse cube power law*. Phys. Rev. **A 79**, 031601 (R)

Reimann, S.M. & Manninen, M., (2002). *Correlation-induced inhomogeneity in circular quantum dot.* Rev. Mod. Phys. **74**, 1283.

Richardson, R. C. (1998). *Experimental Techniques in CMP at low Temperatures.* New York: Addison –Wesley.

Rogers, C.A., (1964). *Packing and covering*. Cambridge: Cambridge University Press.

Roman, S., (1998). *Advanced Linear Algebra.* New York: Springer.

Schausz, P., Xiaopeng, L., & Sarma, D. S., (2012). *Exotic topological density waves in cold atomic Rydberg-dressed fermions.* Nature. **491**, 87-91.

Schempp,H., Gunter, G., Hofman, C. S., Giese, C., Saliba, S. D., Depaola, B. D., Amthor, T., Wedemuler, M., Sevincli, S., and Pohl, T., (2010). *Coherent population trapping with controlled interparticle interactions.* Phys. Rev . Lett. **104,** 173602.

Schirotzek, A., Shin, YI, Schunck, C. H., Ketterle, W., (2008). *Determination of the Superfluid Gap in Atomic Fermi Gases by Quasi particle Spectroscopy.* Phys. Rev. Lett. 101:140403

Shrieffer, J.R., (2013). *Superconductivity: Discoveries and Discovers, ed. By Kristian Fossheim.*Berlin: Springer – Verlag.

Silvera, I. F & Cole J. W., (2010). *Metallic hydrogen: the most powerful Rocket Fuel Yet to Exist*.Journal of physics 215.

Slichter C., (2012). *Introduction to the history of superconductivity; Moments of Discovery.* Illions: American Institute of Physics.

Solis, M., de Llano, M., Clark, J. W., & Baker, G. A., (2013). *Improved Hard –sphere Ground State, Equation of state cond-stat –Mech.* Seattle. University of Washington.

Solis, M.A., de Llano, M., & Clark, J. W., (2003). *Kirkwood phase Transition for Boson and Fermion Hard –sphere systems.* London. Nature.

Stefano, G.,Giezerlis, A., & Carlson, J., (2015). *Neutron matter at low and High Density.* arxiv:1501.05675v(nucl-th)

Strang, G., (2005). *Introduction to Linear Algebra.* Wellesley-Cambridge: Wellesley.

Subraanyam, S. V., & Raja, G. E. S. (1989). *High Temperature Superconductivity.* New Delhi : Wiley Eastern Ltd.

Taylor, P. L., (2002). *A Quantum Approach to CMP*. Cambridge: Cambridge university press.

Tinkham, M., (1964). *Group Theory and Quantum Mechanics*. New York: Mc Graw-Hill.

Togashi, H., Hiyama, E., Yamamoto, Y., & Takano, M.,(2016). *Equation of state for neutron stars with hyprons by the variational method*. Phys. Rev-C 93,0 35808.

Vinen, W. F., (1957). *Mixture of He-4 and He-3.* University of Birmingham: Birmingham.

Visintin, A., (1994). *Differential Models of Hysteresis*. Berlin: Springer- Verlag.

Viteau, M., Huillery, P., Bason, M. G., Malossi, N., Morsch, Oliver, M., Arimondo, E., Comparat, D., & Pierre, P., (2012). *Cooperative excitation and many-body interactions in a cold Rydberg gas.* Phys. Rev. Lett. **109**, 053002.

Viviani, M., Buendia, E., Fantoni, S., & Rosati, S., (1988). *Spin-dependent correlations in the ground state of liquid Helium -3.* London. Perganon Press.

Vollhardt, D.,& Wolfle, P. (1990). *The Superfluid phases of Helium 3*. London: Taylor and Francis.

Von, K. K., (1985). *The Quantized Hall Effect Braunschweig*. Germany: Nobel Prize Organization.

Walter, W., (1998). *Ordinary Differential Equations.* New York: Springer.

Wen, X. G., (1992). *Theory of the edge States in fractional quantum. Hall effects* (PDF). Cambridge: International Journal of Modern Physics C 6 (10).

Wentao, Z., (2012). *Photoemission spectroscopy on High Temperature Superconductor: a study of Bi_2 Sr_2 Ca Cu_2 O_8 by Laser –Based Angle –Resolved photoemission.* Virginia. Springer Science & Business Media.

Wheatley, J.C., (1975). *Progress in low temperature physics.* Rev. Mod. Phys. **47**,415.

Wigner, E.P.,(1934). *On the interaction of electrons in metals.* Phys. Rev. **46**, 1002.

Yamase, H., (2009). *Effect of disorder on a pomeranchuk instability.* Phys. Rev. Lett. **102,** 116404.

Yeh, N. C., (2008). *A perspective of Frontiers in Modern CMP*. Carlifonia: AAPS Bulletin.

Zdunik, J. L., Fortin, M. & Haema, P. A., (2017). *Neutron star properties and equations of state for the core*. 599, A 119.

Zhang, T., & Van Sciver, S. W., (2005). *Journal of low Temperature Physics.* Springer.

Zhizhong, H. M., de, L., Buenda, E., & Guardiala, R., (1991). *AZiZ Fermions and liquid ^{3}He*. Liverpool: University of Liverpool.

APPENDICES

i) Table A1: Energy per particle for low density; corresponds to Fig. 4.1.

E/N(J)	$\rho(M^{-3})$
1.411	0.6
1.500	0.658
1.577	0.716
1.660	0.774
1.743	0.800
1.826	0.861
1.992	0.919
2.000	0.977
2.075	1.000
2.158	1.064
2.241	1.122
2.324	1.180
2.407	1.200

2.532	1.267
2.656	1.325
2.718	1.383
2.801	1.400
2.905	1.470
3.030	1.528
3.154	1.600

ii) Table A2: Energy particle for high density; corresponds to Fig. 4.2.

E/N(J)	$\rho(M^{-3})$
0.000	0.605
0.000	0647
0.000	0.689
0.000	0.750
0.000	0.794
0.000	0.845
0.000	0.889
0.000	0.941
0.058	1.000

0.062	1.046
0.068	1.088
0.071	1.130
0.107	1.188
0.142	1.250
0.284	1.282
0.639	1.324
1.500	1.382
2.414	1.424

iii) Table A3: Variation of saturation density with corresponding Hard-Sphere diameter for ^{3}He particles; corresponds to Fig. 4.3.

Hard-Sphere diameter, $CX10^{-10}m$	Low Density ρ X $10^{29}m^{-3}$	High Density ρ $X10^{2}m^{-3}$
1.625	0.016	
1.750	0.014	
1.813	0.012	
1.938	0.010	
2.000	0.008	0.

2.125	0.007	0.148
2.250	0.006	0.132
2.313	0.006	0.114
2.438	0.006	0.100
2.500	0.005	0.088
2.625	0.005	0.080
2.750	0.004	0.068
2.813	0.004	0.064
2.938	0.004	0.060
3.000	0.002	0.052
3.125	0.002	0.046
3.250	0.002	0.042
3.313	0.002	0.040
3.438	0.002	0.036
3.500	0.001	0.032
3.625	0.001	0.030
3.750	0.001	0.026
3.813	0.001	0.022
3.938	0.001	0.020

4.000	0.001	0.016

iv) Table A4: Energy per particle and saturation density for low and high densities at a constant hard-core radius, a=2.1117Å; Corresponds to Fig. 4.4

Density, ρ in terms of 10^{15}gcm^{-3}	Low density a = constant	High density a=constant
	$E/_N \, x10^{-30} J$	$E/_N \, x10^{-30} J$
1.4	2.5014	14.8
1.9	3.0019	18.1354
2.4	3.5874	21.1917
2.9	4.0699	24.0412
3.4	4.5254	26.7307
3.9	4.9589	29.2910
4.4	5.3739	31.7438
4.9	5.7749	34.1053
5.4	6.1614	36.3876
5.9	6.5359	38.6004
6.4	6.9004	40.7516
6.9	7.2559	42.8473

7.4	7.6024	44.8930
7.9	7.9409	46.8931
8.4	8.2729	48.8514
8.9	8.5982	50.7712
9.4	8.9174	52.6554
9.9	9.2410	54.5064
10.4	9.5301	56.3266
10.9	9.8332	58.1177
11.4	10.1317	59.8817

A5: PUBLISHED RESEARCH ARTICLES

1. **Murunga, G.S., Tonui, J. K., & Khanna, K. M. Crystallization of Neutron Matter (Neutron Stars):** *International Journal of Latest Engineering Research and Applications (IJLERA) ISSN: 2455-7137 Volume-02, Issue-06, June-2017, PP-110-114.*